$CuInS_2$ thin films using chemical methods for the fabrication of $CuInS_2$/CdS solar cells

Thesis submitted to
Cochin University of Science and Technology
for the award of the degree of

Doctor of Philosophy

By

Bini.S

Department of Physics
Cochin University of Science and Technology
Kochi-682 022, India.

2003

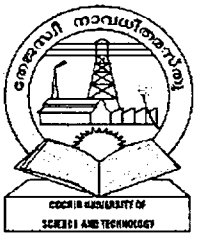

Department of Physics

Cochin University of Science and Technology

Cochin – 682 022

CERTIFICATE

Certified that the work presented in this thesis entitled "**$CuInS_2$ thin films using chemical methods for the fabrication of $CuInS_2$/CdS solar cells**" is based on the bonafide research work done by Ms. Bini S under my guidance, at the Department of Physics, Cochin University of Science and Technology, Cochin – 682 022, and has not been included in any other thesis submitted previously for the award of any degree.

Cochin - 22

08.05.2003

Prof. K. P. Vijayakumar

(Supervising Guide)

DECLARATION

Certified that the work presented in this thesis entitled **"$CuInS_2$ thin films using chemical methods for the fabrication of $CuInS_2$/CdS solar cells "** is based on the original research work done by me under the guidance and supervision of Prof. K. P. Vijayakumar, Department of Physics, Cochin University of Science and Technology, Cochin - 22 and has not been included in any other thesis submitted previously for the award of any degree.

Cochin – 22
08.05.2003

Bini S.

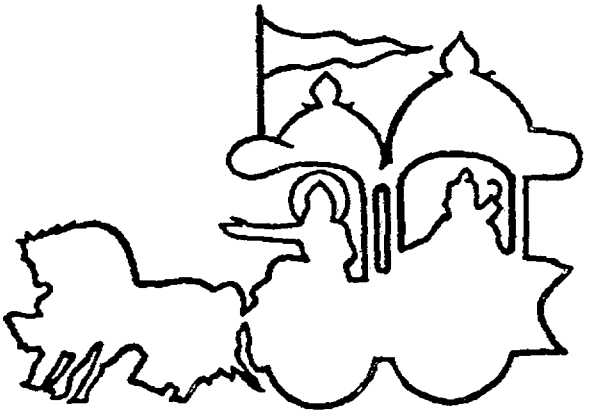

" Your right is to work only, but never to the fruit of that.
Let not the fruit of action be your object,
nor let your attachment be to inaction "

(Bhagavadgita 2/47)

Acknowledgement

At the outset may I express my sincere and heartfelt gratitude to Dr.K.P.Vijayakumar, my supervising guide for his smart guidance and timely motivations. Moreover, being the Head of the department, he was kind enough to provide all the facilities available at the Department.

Next I would like to thank Dr.C.Sudha Kartha whose encouragements and valuable advices were equally important for the timely completion of this work.

I am also thankful to Dr.N.Unnikrishnan Nair, Vice chancellor of CUSAT for providing necessary facilities and financial assistance in the form of fellowship.

I remember with gratitude the facilities provided by Prof. Elizabeth Mathai, Prof. K. P Rajappan Nair, Prof. M. Sabir and Prof. K. Babu Joseph, former Heads of the department of Physics, CUSAT.

During present work, a part of sample characterisation was done at Iwate University, Morioka, Japan, through our collaboration with Prof.Y. Kashiwaba. I take this chance to express my deep gratitude to Prof. Y. Kashiwaba. Also, I express my sincere thanks to Dr.T.Abe for carrying out XPS measurement, and Dr. Yasuhiro Kashiwaba , Sendai National College of Technology, Japan for thickness measurement. I am thankful to

Director, Sree Chitra Tirunal Institute of Medical Science & Technology for granting me permission for SEM analysis.

I acknowledge the assistance from UGC through DSA-COSIST scheme. Supports from Ministry of Non-conventional Energy Sources, DST, and ANERT are also gratefully acknowledged.

Words are insufficient to express my gratitude to my colleagues Ms. Bindu K, Ms. Teny Teresa John , Mr. Ram Kumar. S, Mrs. Syamala S.B, Mr. Paulraj M, Mrs.Rupa R. Pai, Mr. Wilson K.C, Mr. Ratheesh Kumar P.M, Ms. Beena Mary John, Mr.Arun B, and Mr.Sreekumar. I am thankful to my seniors and other research Scholars of this department for their moral support.

I am highly indebted to Sri. Chulliparambil Balakrishnan, Manager, National H S S, Engandiyoor for his fatherly advices and motivations in the hour of need. Also I would be grateful to our principal Mr.V Premlal for his inspirations, and management committee for the support. I shall always remember with pleasure the help and co-operation extended by my colleagues.

I thank every members of my family for being always a source of inspiration. I appreciate their patience and understanding. They were the chief force behind the successful completion of this work.

Dedicated
to
my Parents, Teachers, Husband & Daughter

Contents

Preface

List of publications

Chapter 1
Solar cells:An introduction 1

Chapter 2
Review on copper indium sulfide films and cells 45

Chapter 3
Preparation of $CuInS_2$ thin films starting from
CBD Cu_xS and CBD CdS.....90

Chapter 4
Studies on $CuInS_2$ thin films prepared using
chemical spray pyrolysis technique 141

Chapter 5
Fabrication and characterisation of all-sprayed
$CuInS_2$/CdS solar cells.....192

Chapter 6
Summery and conclusion 218

Preface

Today, in this time of scarcity of conventional energy sources, photovoltaics is viewed as an ideal way to produce eco-friendly power from a virtually inexhaustible source without noise or pollution. Based on semiconductor technology, solar cells operate on the principle that electricity will flow between two p and n type semiconductors when they are put in contact with each other and exposed to light (photons). When photons strike a solar cell, electrons are set free from the semiconductor atoms. These free electrons can be channeled to flow through the solar cell's built-in circuit, producing electricity. By linking a number of solar cells together, a useful flow of direct current (DC) electricity can be generated. Photovoltaic-generated electricity can be used as is, or stored in a battery for consumption in a later time, or converted to alternating current (AC) by an inverter.

In general, PV materials are categorized as either *crystalline* or *thin film* and are judged on two basic factors viz, efficiency (how much of the sun's light they transform into usable electricity) and economics (how difficult and how expensive they are to manufacture). The cost of PV systems is a key factor affecting large-scale applications and improvements in conversion efficiency will help to reduce the cost. Since the first photovoltaic panel was developed in 1954, the efficiency of solar cells has risen steadily. Because of the continuing improvements in PV technology, declining prices and new markets, the PV business is likely to grow by 20%-30% annually in the next few decades.

Lowering the cost of solar cell production is one of the most important intentions in photovoltaic research. To achieve this, it is necessary to develop new or improved thin-film materials with good photovoltaic properties and appropriate band gaps, that can be deposited rapidly and uniformly over large areas.

Semiconductor materials most frequently used in thin film technology are silicon, copper indium diselenide, or cadmium telluride. Amorphous silicon is the only thin-film technology that already has a substantial market share (15%), and it is generally believed to be the first thin-film technology that can compete with crystalline silicon. However, thin film silicon cells lack the ordered structure and inherent photovoltaic properties of crystalline silicon, and its present efficiency is 13.5%. CdTe is close to an ideal photovoltaic material with respect to its physical properties with a bandgap close to the optimum. Laboratory cells have already reached efficiencies over 16%. One major drawback is the high content of cadmium which gives rise to environmental concerns. Copper indium diselenide (CIS) is one of the most promising thin film materials today. With the incorporation of gallium, $Cu(In,Ga)Se_2$ has reached the highest efficiencies of all thin film cells. The record laboratory efficiency recently announced by ENREL is an impressive 18.8%, small modules are at 14% and large modules at 11%-12%. This has motivated several research groups to carryover extensive research in CIS based cells. However, the optical bandgap of CIS (1.02 eV) is quite small. Moreover, selenium raises apprehension for consumers for ecological reasons. Therefore, elimination of selenium in the compound used is viewed as a major contribution to mitigate the negative environmental perception. One possibility is to substitute S to Se and prepare $CuInS_2$ thin films.

$CuInS_2$, which is the material for the present study has great potential for photovoltaic applications due to its optimum direct bandgap of 1.53eV and high absorption coefficient. $CuInS_2$ can be obtained in both n and p-type so that fabrication of homojunction solar cells is possible. When they are paired with CdS, they are found to have a compatible lattice structure with acceptable lattice mismatches and differences in electron

affinities favorable for the formation of heterojunctions. The material has a number of additional potential advantages in comparison with CIS. These include the significantly reduced toxicity and abundance of its constituents, which makes it suitable for terrestrial as well as space applications. The highest conversion efficiency reported recently for $CuInS_2$ based solar cells is 12.5%

$CuInS_2$ films have been prepared using different techniques such a vacuum evaporation, chemical vapor deposition, flash evaporation, rf sputtering, sulfuration of CuIn alloys, electrodeposition, chemical bath deposition and chemical spay pyrolysis (CSP). For economic reasons, it will be very interesting to deposit this film using a low-cost deposition technique. In our lab, we prepared $CuInS_2$ thin films using chemical bath deposited (CBD) Cu_xS for the first time. This is quite new technique and has the potential of being low in cost, as the preparation of Cu_xS film is carried out by the simple and low cost chemical bath deposition technique at room temperature itself. This is a zero energy process as no substantial amount of energy is required for the process. Also we used spray pyrolysis, which is another low cost deposition technique, for preparing device quality $CuInS_2$ thin films with good photo response. We could fabricate $CuInS_2$/CdS solar cells using these films.

This thesis contains results of the work done in the Thin Film Photovoltaic Division of the Dept. of Physics, CUSAT and is organized into six chapters, with introduction, conclusion and references. The chapter- wise description of the contents is given below.

Chapter-1 is a general introduction to solar cells. It starts with a brief history of solar cells and describes principle and theory of solar cell operation. Later description of different solar cell structures and the various factors affecting its efficiency are also

included. Some important thin film solar cells are also mentioned in this chapter. The chapter ends mentioning the scope and importance of present work.

Chapter-2 presents an exhaustive review on Copper indium sulfide films and $CuInS_2$ based solar cells.

Chapter-3 has two parts. The first part deals with the preparation of copper indium sulfide films using CBD copper sulfide films and advantages of this deposition technique are hinted. Experimental details and characterization of the films using XRD, absorption and transmission studies, XPS along with brief description of the different characterization techniques are also included.

Second part of this chapter describes an attempt to prepare copper indium sulfide films using copper sulfide films, which are prepared through the conversion of cadmium sulfide films. The important results, advantages and drawback of this method are highlighted.

Chapter-4 mainly deals with the preparation and characterization of copper indium sulfide films using chemical spray pyrolysis. This technique is essentially suitable for the solar cell production, because large-area deposition of thin films with low cost is possible and it is one of the chemical techniques suitable for a molecular level design of thin films. Many groups were successful in preparing $CuInS_2$ films using this technique. We prepared films by systematically varying the copper to indium ratio and copper to chalcogen ratio in the initial spray solution, at different substrate temperatures. Structural, electrical and optical characterization of all the films obtained was carried out. It is found that the chemical composition of the solution controls the film resistivity and photo response very much as it affects the stoichiometry of the film. We could optimize the composition of the solution to get good values of film resistivity and photo- response. We have selected the

best film in terms of photo response and electrical resistivity to fabricate solar cell structure with CdS.

Chapter-5 describes the fabrication of $CuInS_2$/CdS solar cells by an "all-spray" method. The bottom electrode SnO_2 is deposited at a temperature of 450^0C. Over this, the absorber layer $CuInS_2$ is deposited at a temperature of 300^0C and finally the window layer CdS is sprayed at the same temperature. Cells were fabricated by varying the thickness of both the window and absorber layer. The current-voltage characteristics of the cells fabricated are discussed and the cell conversion efficiencies are calculated.

Chapter-6 is a summary of whole work done. The important results are highlighted. The chapter ends with a note on the environmental and safety aspects of the materials and the thin film deposition techniques used in the present work

LIST OF PUBLICATIONS

Journal/ conference papers

1. Preparation of $CuInS_2$ thin films using CBD Cu_xS films.
   S.Bini, K.Bindu, M.lakshmi, C Sudha Kartha, K P Vijayakumar, Y.Kashiwaba,T.Abe
   Renewable Energy , 20(2000) 405

2. $CuInS_2$ thin films using a new technique
   S.Bini, K.Bindu, M.lakshmi, C Sudha Kartha, K P Vijayakumar,T.Abe, Y.Kashiwaba,
   Proceedings of the DAE Solid State Physics Symposium, Kurukshetra University, Kurukshetra, 41 Dec 27-31,(1998),489
   [Also presented at the 53rd meeting of the Tohoku branch of The Japan Society of Applied Physics, Dec, 1998, Sendai ,Tohaku University,Japan]

3. Electrical and structural characterisation of spray pyrolysed $CuInS_2$ thin films
   S.Bini, K.Bindu, M.lakshmi, C Sudha Kartha, K P Vijayakumar
   Workshop on Complete Cycle Charaterisation of Materials, Organised by MRSI, IGCAR Kalpakkam, Sep. 12-14, 2001

4. Characterisation of spray pyrolysed indium sulfide thin films
   Teny Theresa John, **S Bini**, Y Kashiwaba, T Abe, Y Yasuhiro, C Sudha Kartha, K P Vijayakumar
   (Accepted for publication in Semiconductor Science and Technology)

5. Amorphous Selenium thin films prepared using CBD:Optimization of the deposition process and Characterization
   Bindu. K, Lakshmi. M, **Bini. S**, Sudha Kartha. C, Vijayakumar. K.P, Abe. T and Kashiwaba.Y
   Semiconductor Science and Technology, 17(2002)270

6. Chemical bath deposition of different phases of copper selenide thin films by controlling bath parameters
   M.lakshmi. K.Bindu, **S.Bini**, K P Vijayakumar, C Sudha Kartha,T.Abe, Y.Kashiwaba.
   Thin Solid Films, 370 (2000) 89

7. Reversible $Cu_{2-x}Se \leftrightarrow Cu_3Se_2$ phase transformation in copper selenide thin films prepared by chemical bath deposition
   M. Lakshmi, K. Bindu, **S.Bini**, K.P. Vijayakumar, C. Sudha Kartha, T.Abe, Y.Kashiwaba
   Thin Solid Films,386(2001)127

8. Structural and Optical absorption changes of chemically prepared Cu2-x Se due to Indium diffusion
   K. Bindu, M. Lakshmi, **S. Bini,** C Sudha Kartha and K. P.Vijayakumar.
   DAE, Solid State Physics Symposium, IGCAR, Kalpakkam, Dec 20 –24,1998

9. CBD – A technique to prepare different phases of Copper Selenide
   K. Bindu, M. Lakshmi, **S. Bini**, C Sudha Kartha and K. P.Vijayakumar.
   Proceedings of the DAE Solid State Physics Symposium, Kurukshetra University, Kurukshetra,41(1998) Dec 27 –31,487

10. Preparation of Pyrite (FeS_2) Thin Films Using Chemical Bath Deposition Technique: An attempt
    M.Lakshmi, K.Bindu, **S.Bini**, C.Sudha Kartha, and K.P.Vijayakumar,
    ANERT National Conference , Trivandrum ,Feb 1999.

Chapter-1

SOLAR CELLS: AN INTRODUCTION

1.1 Introduction 3
1.1.1 Brief history of solar cells 5
1.2 Principle of solar cell operation 6
1.3 Solar Cell Structures 6
1.3.1 Semiconductor- semiconductor homojunctions 7
1.3.2 Semiconductor- Semiconductor heterojunctions 8
1.3.3 Schottky Barriers (Metal- Semiconductor heterojunctions) 9
1.3.4 Buried or heteroface junctions 11
1.3.5 Alternative device structures 12
1.4 Theory of semiconductor solar cell structures 13
1.4.1 Semiconducor-Semiconductor Homojunctions 13
1.4.1.1 Electrostatics of p-n junction 13
1.4.1.2 Junction Capacitance 15
1.4.1.4 More realistic photovoltaic model 21
1.4.2 Theory of Heterojunctions 23
1.4.2.1 Energy-band diagram and static characteristics 23
1.4.2.2 Current Transport 24
1.4.3 Solar cell output parameters 26
1.4.4 Spectral response 28
1.5 Factors influencing efficiency of Solar cells 28
1.6 Efficiency Measurement 31
1.7 Thin Film Solar cells 32
1.8 Scope of present work 39

1.9 Conclusion.....40
References.....41

Chapter-1

SOLAR CELLS: AN INTRODUCTION

1.1 Introduction

Solar electricity, produced by photovoltaic devices, is one of the most promising options whose capabilities and potentials are yet to be identified for sustainably providing the world's future energy requirements. Photovoltaics (PV) involve direct conversion of sunlight into electricity using thin layers of material known as 'semiconductors', which are having electrical properties intermediate between those of metals and insulators. Basic energy supply for a solar cell is photons of the solar spectrum and product is usable electrical energy.

This conversion has the advantage that it introduces no direct contamination to environment. PV cells have an important feature that the voltage of the cell does not depend on its size, and remains fairly constant with changing light intensity. However, the current in a device is almost directly proportional to light intensity and size.

Global annual production of PV devices has about 18-20% growth per year during the last 20 years. This is mainly because of its increasing penetration into remote applications for telecommunications, water pumping, telemetry etc. Worldwide PV shipments show a continuous growth over the last two decades. Assuming an average growth rate of 25%, it is expected that PV production would increase to 65GWp/yr in year 2025 (Fig.1.1) [1].

Ever since the first solar cell was developed, PV was dominated by silicon. However, because of its indirect bandgap and low absorption coefficient, silicon is not the ideal material for PV conversion. In spite of this, crystalline silicon today has a market share of 86%, which is almost equally distributed between single crystal and cast

silicon. Main reason for this dominating position is that silicon technology had already been highly developed and good quality material is being produced in large quantities for the popular semiconductor market, especially consumer electronics and telecommunication.

Manufacturing cost for PV systems is dominated by cost of materials used as well as that of the technology for device fabrication. This favors development of thin-film solar cells on low-cost substrates. While thin film cells achieve lower efficiencies than crystalline cells, production process is considerably less expensive. Moreover, as thin film cells can be extremely light and flexible, they can meet a variety of needs for which crystalline solar cells are too big or too rigid. Also a large number of techniques are available for the deposition of different thin films. The challenge is to develop new or improved thin-film materials with good photovoltaic properties and appropriate band gaps that can be deposited rapidly and uniformly over large areas.

Although the technology in the past has been based on silicon wafers, a transition is in progress to a second generation of a potentially low cost thin film technology.

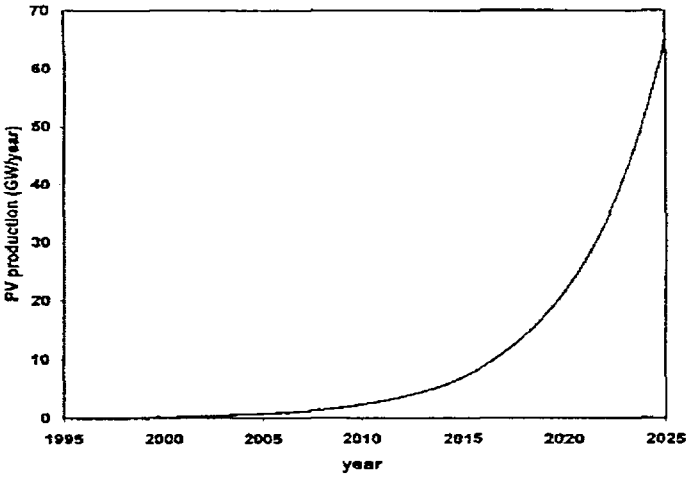

Fig.1.1 Projected annual PV production assuming 25% growth rate

1.1.1 Brief history of solar cells

Origin of solar cells can be traced back to the discovery of Becquerel in 1839 that a photo voltage resulted from the action of light on an electrode in an electrolyte solution [2]. Later, Adams and Day (1877) observed a similar effect in the solid material selenium shortly after Smith (1873) had demonstrated the phenomenon of photoconductivity in selenium [3]. This was followed by the development of photocells based on both these materials and cuprous oxide. Russel Ohl discovered the first silicon solar cell accidently in 1940. He was surprised to measure a large electrical voltage from a rod of silicon when he shone a flashlight on it [4]. However, the first efficient silicon solar cell was announced only in 1954 [5].

These cells found application as power sources in space craft as early as 1958. By the early 1960s, design of cells for space application was more or less stabilized [6]. More than thousand satellites using solar cells were launched between 1960and 1970. However, in the mid 70s efforts were initiated to make solar cells for terrestrial applications and there was a reawakening of interest in terrestrial use of these devices, especially due to oil shortage. In the 1980s, there was a large improvement in technologies resulting in reduction in cost of cells. This opened a new horizon for solar cells in commercial applications [7].

In 1914, solar conversion efficiency of the selenium cell was just 1%. With improved technology, silicon cell efficiency under terrestrial sunlight reached 14% in 1958. Cuprous sulphide/ cadmium sulphide hetero junction was the first all-thin-film photovoltaic system to receive significant attention. First cell of this type, with an efficiency of 6%, was reported in 1954 by Reynolds et al. [8].

At present, a host of new materials are being studied for thin film solar cells and due to the progress of new technologies in material processing and device fabrication, there is considerable improvement in cell efficiency and cost reduction.

1.2 Principle of solar cell operation

The most common solar cells are formed by making a junction between n-type and p-type semiconductors and the basic device requirement for photovoltaic energy conversion is an electronic asymmetry in the semiconductor structure. Three major processes are involved in the conversion of sunlight into electrical energy. These are,

a) Absorption of sun light (photon) in the semiconductor material

Absorption depends on the intensity of the sunlight, the amount of light reflected from the front surface of the solar cell, the semiconductor band gap energy and thickness of the layer.

b) Generation of electron –hole pairs

When light is absorbed in the semiconductor, a negatively charged electron and a positively charged hole are created.

c) Separation of charge carriers

Light generated charge carriers are separated by the built-in field existing at the junction. n-type region has large electron densities but low hole densities. Hence, electrons flow readily through such a material while holes find it very difficult. Exactly the same is true for holes in p-type material. The generated electrons flow from p-type region to n-type and hole in the opposite direction. When the illuminated p-n junction is electrically shorted, a current will flow through the short-circuiting lead (Fig.2.2).

1.3 Solar Cell Structures

Interfaces between dissimilar materials are important to solar cell devices because they can give rise to built-in fields. Field regions are inherent to solar cell structures and are required for photovoltaic action. There are four principal ways to obtain the internal

field in a semiconducting structure needed to produce photovoltaic behavior: homojunctions, heterojunctions, buried or heteroface junctions, and Schottky barriers. We can classify cells according to the type of inter face structure used to develop the principal field region [9].

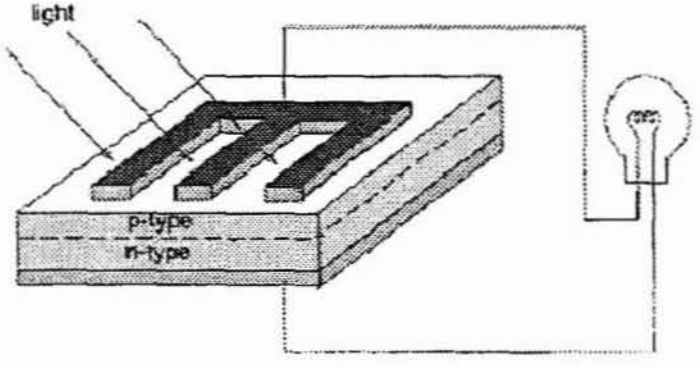

Fig.2.2 Incoming sunlight is converted to an electrical current flow in a load connected between the cell contacts

1.3.1 Semiconductor- semiconductor homojunctions

A junction between n and p type layers of same semiconductor material is called "homojunction". Usually p-n homojunctions are made by diffusing or implanting one dopant into oppositely doped material. Consequently there are no interface states at the metallurgical junction. Energy band diagram of a p-n abrupt junction is shown in Fig.1.3.

In Semiconductor p-i-n homojunction structure, an intrinsic layer of semiconductor is interjected between two heavily doped regions, which will enhance the built-in electric field, and hence the carrier collection will improve [10].

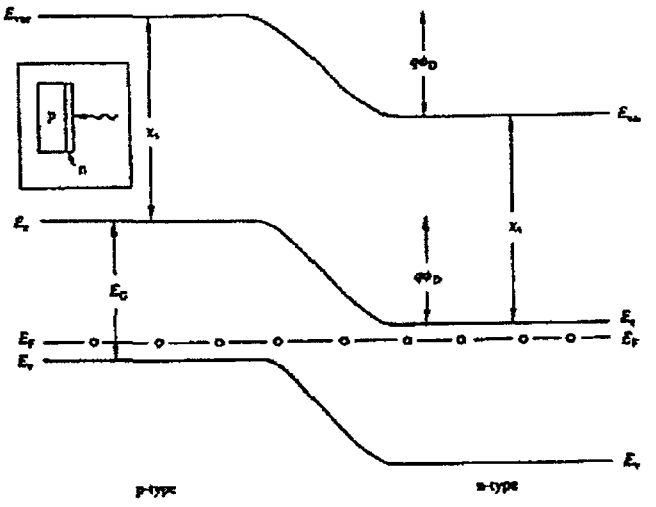

Fig. 1.3 Energy band diagram of a p-n homojunction

1.3.2 Semiconductor- Semiconductor heterojunctions

A junction formed between a large bandgap (window) material and a low bandgap (absorber) material is known as a "heterojunction". If conductivity type of these two semiconductors is the same, the junction is called isotype heterojunction and if the conductivity type is different, the junction is called anisotype heterojunction. Energy band diagram of an anisotype heterojunction is represented in Fig.1.4. Brief theory of anisotype heterojunction structure, which is the structure fabricated in the present work, is discussed in the following section.

Main advantages of heterojunction cells are

i) They allow use of semiconductors, which can only be doped either n-type or p-type

ii) These have attractive electrical and optical properties and are good from low cost point of view. iii) Heterojunctions having window/absorber structure can be formed that protects minority carriers from top surface or bulk recombination sinks. iv) These

heterojunction cells are capable of higher efficiencies than homojunction cells due to a better match to the solar spectrum, as there are two band gaps.

However, there are some notable drawbacks and these are listed below. i) If electron affinities and doping levels of the two materials differ very much, these give rise to 'spikes' in the conduction band, which are undesirable for photovoltaic operations. ii)With an ideal case having either small spikes or no spikes at all, the maximum efficiency of a heterojunction cell is limited by the ideal efficiency of the smaller bandgap material. iii) Mismatch between lattice structures of the two materials will give rise to energy levels within forbidden gap, which act as very efficient recombination centers. Hence to produce heterojunctions with nearly ideal properties, it is essential to use semiconductors with nearly identical lattice structures.

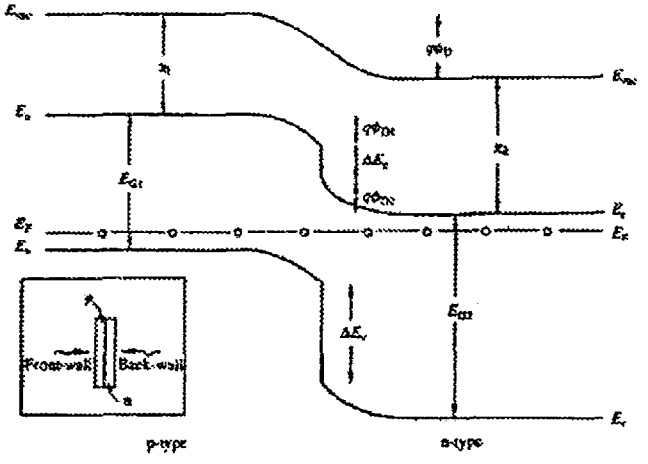

Fig.1.4. Energy band diagram of an anisotype heterojunction

1.3.3 Schottky Barriers (Metal- Semiconductor heterojunctions)

When a metal and a semiconductor are brought into contact, because of the differences in the availability of the charge carriers in the metal and semiconductor, all this potential drop occurs on the semiconductor side of the junction. This can give rise

to a depletion region at the interface as in the case of a p-n junction. This type of Schottky diodes has both rectifying and photovoltaic properties. A typical energy band diagram is given in Fig.1.5 [9].

In this type of junctions, it is experimentally observed that since there are a very large number of interface states at the metal-semiconductor interface due to lattice mismatch, the height of the induced barrier at the junction is independent of the work function of the metal. The larger the height of the barrier induced at the junction, the better is the photovoltaic performance of the junction [11].

The main advantage of the Schottky barrier solar cell is that it does not require any high temperature processing and is easy to fabricate. This reduces cost of production considerably. Eventhough dark current in a Schottky barrier diode is of a few orders of magnitude higher than that in the pn junction diode with the same area, open circuit voltage (V_{oc}) is low and this reduces the efficiency. However, V_{oc} can be increased by inserting a thin insulating layer between the metal and the semiconductor, forming metal-insulator-semiconductor (MIS) structure. But when the insulating layer is thick (>2nm), the short circuit current density will be reduced considerably [12].

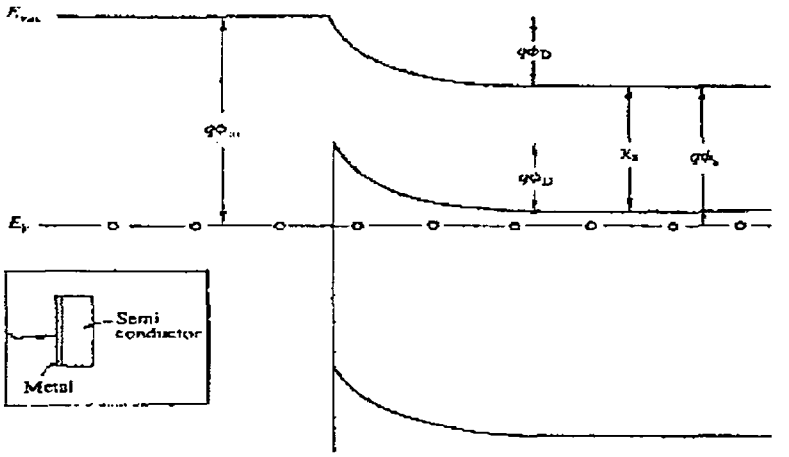

Fig.1.5 Energy band diagram of metal-semiconductor junction

1.3.4 Buried or heteroface junctions

Fig1.6 shows a representative energy band diagram for a buried p-n homojunction with a heavily doped p^+-p heterojunction. The structure is actually that of a p^+-p-n junction. This structure retains the advantages of a p-n junction while at the same time it provides a different front surface interface for the p-type region of the junction. This will decrease the surface losses.

This device differs from ordinary pn junction in the sense that that here the junction is much deeper and the doping density is moderate on the topside of the junction. A front surface field is used at the top of the device. This approach overcomes limitations imposed on the open circuit voltage by diffused top layer of normal cell structure. Substantial improvement in open circuit voltage was reported using this approach [13]. Carrier collection is not optimum. So current output tends to be less than that of other devices.

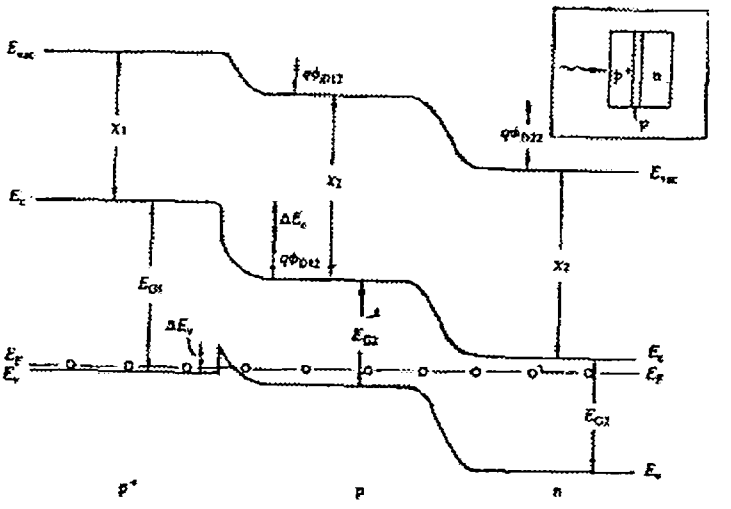

Fig. 1.6. Energy band diagram of a heteroface junction

1.3.5 Alternative device structures

There is a wide range of possibilities for photovoltaic possibilities with different structures apart from the above mentioned ones. Some such devices are briefly mentioned below. In addition to these, there are some special approaches specifically made to improve the cell efficiency. These include violet cell, BSF cell, Black cell, Grooved cell, point contact cell, passivated emitter cell, MIS cells and multijunction or tandem cells.

a) Back-Surface Field (BSF) cells

This type of cell introduced the concept of shielding photo generated minority carriers from high recombination plane of back surface by employing electric field of a low-high junction. A reduced recombination at the back surface can increase short circuit current and hence reduce saturation current, resulting in an overall increase of efficiency [14]. Devices having BSF structure were having efficiencies approaching 19-20% range for silicon single crystal and 21% for GaAs under terrestrial conditions [15].

b) Front surface field cell

The second one in this list is the 'front surface field cell'. With this approach, it is possible to bring both contacts to the rear of the cell. This eliminates losses due to shadow associated with normal top contact and would make cells easier to inter-connect. This cell has to be thin compared to minority carrier diffusion length to get full current output. However these cells had handling difficulties in the case of large area cells.

c) Vertical Multi Junction cells

Here junctions are perpendicular to the illuminated surface of the cell. Deep groves are etched into the cell using anisotropic etch. These vertical junctions ensure that even carriers generated deep in the absorber layer can be collected. In order to make

this effective, distance between the vertical junctions must be of the order of a diffusion length apart.

Heterojunctions formed between liquids and semiconductors also possess interesting photovoltaic properties.

1.4 Theory of semiconductor solar cell structures

1.4.1 Semiconducor-Semiconductor Homojunctions

1.4.1.1 Electrostatics of p-n junction

When a p-n junction is formed between two semiconductors, at the interface between n-type and p-type, both carrier concentrations have a strong gradient. Electrons diffuse from the n-type to the p-type part where they recombine with holes. At the same time, holes go over from the p to the n-type region and they recombine with electrons. This results in the production of ionized, immobile and uncompensated impurities near the interface, which remains with negative charge in p-type part and positive charges in n-type part. These space charges produce an electric field and thus a potential difference (step) at the p-n junction. Formation of a potential step means that p and n type semiconductors are shifted with respect to one another until their Fermi energies have reached the same value. Constant Fermi level required at thermal equilibrium, results in a unique space charge distribution at the junction. The space charge density ρ is given by

$$\rho = q(p - n + N_D^+ - N_A^-) \quad \text{.....(1)}$$

where p and n are the densities of holes and electrons N_D^+ and N_A^- are the densities of ionized donors and acceptors. Unique space charge distribution and electrostatic potential ψ are given by Poisson's equation: [16]

$$\frac{d^2\psi}{dx^2} \equiv -\frac{d\xi}{dx} = -\frac{\rho_S}{\varepsilon} = -\frac{q}{\varepsilon}(N_D - N_A + p - n) \ldots\ldots(2)$$

In regions far away from the metallurgical junction, the total charge density is zero. For p-type neutral region, we assume $N_D = 0$ and p>>*n*. The electrostatic potential of the p-type neutral region with respect to the Fermi level is given by

$$\psi_p = -\frac{kT}{q}\ln\frac{N_A}{n_i} \ldots\ldots\ldots\ldots\ldots\ldots\ldots\ldots\ldots\ldots\ldots\ldots(3)$$

Similarly, electrostatic potential of the n-type neutral region with respect to the Fermi level :

$$\psi_n = \frac{kT}{q}\ln\frac{N_D}{n_i} \ldots\ldots\ldots\ldots\ldots\ldots\ldots\ldots\ldots\ldots\ldots\ldots\ldots(4)$$

Total electrostatic potential difference between p-side and n-side neutral regions at thermal equilibrium is called built-in potential (V_{bi}):

$$V_{bi} = \psi_n - \psi_p = \frac{kT}{q}\ln\frac{N_A N_D}{n_i^2} \ldots\ldots\ldots\ldots\ldots\ldots\ldots\ldots(5)$$

An applied voltage V_a will change the potential difference between the two sides of the diode by V_a. Hence the potential across the transition region will become ($V_{bi} - V_a$).

In depletion approximation, a solar cell device is divided into two regions: quasi-neutral region where the space charge density is assumed to be zero throughout and a depletion region where the carrier concentration is assumed so small that only space charge from ionized dopants is considered.

Electric field strength can be obtained by integrating the space charge distribution. The maximum field strength in the depletion region can be calculated using the expression [11],

$$\xi_{\max} = -\left[\frac{2q}{\varepsilon}(V_{bi} - V_a)/(\frac{1}{N_A} + \frac{1}{N_D})\right]^{1/2} \quad \text{.....(6)}$$

Width of the depletion region is given by the expression [11],

$$W = l_n + l_p = \left[\frac{2\varepsilon}{q}(V_{bi} - V_a)(\frac{1}{N_A} + \frac{1}{N_D})\right]^{1/2} \quad \text{.....(7)}$$

where l_n and l_p are the distances up to which the depletion region extends on either side of the junction.

1.4.1.2 Junction Capacitance

In the depletion approximation, a change in the applied voltage will cause a change in stored charge right at the edges of the region. This is identical to the situation of a parallel plate capacitor of plate separation w, where w is the width of the depletion region. Hence depletion region capacitance C per unit area is given by

$$C = \frac{\varepsilon}{W} \quad \text{.....(8)}$$

where ε is the dielectric constant

For a two-sided abrupt junction, capacitance per unit area is expressed as [17]

$$C = \left[\frac{qN_D N_A \varepsilon_n \varepsilon_p \varepsilon_0}{2(\varepsilon_n N_D + \varepsilon_p N_A)(V_{bi} \pm V)}\right]^{1/2} \quad \text{.....(9)}$$

where ε_n and ε_p are dielectric constants on the n and p regions respectively, and ε_0 is the permittivity of free space, V is the applied reverse bias voltage to the junction, and V_{bi} is the built in potential.

Under reverse bias, depletion region capacitance dominates the total diode capacitance. Hence measuring C as a function of reverse bias to the solar cell and plotting $1/C^2$ vs. V

will allow determining the junction related parameters like depletion layer width and doping profile near junction.

1.4.1.3 Current-Voltage characteristics

Current-voltage characteristics of a solar cell help to understand the device function. In the following section, dark and illuminated characteristics of a solar cell are discussed.

A. Dark characteristics

It has been found that when a forward voltage is applied to a diode, minority carrier concentration at the edge of the depletion region depends exponentially on the voltage applied to the diode [18]. When quasi-neutral regions are uniformly doped and majority carrier currents small, minority carriers flow primarily by diffusion.

On n-type side of the diode, minority current is given by the expression

$$J_h = -qD_h \frac{dp}{dx} \quad \text{.....(3)}$$

where D_h is the diffusion coefficient for holes, J_h is the hole current density and dp/dx is the hole concentration gradient.

According to continuity equation,

$$\frac{1}{q}\frac{dJ_h}{dx} = \text{-(U-G)} \quad \text{.....(4)}$$

where G is the generation rate and U is the recombination rate, in n-type region and can be expressed as

$$U = \frac{\Delta p}{\tau_h} \quad \text{.....(5)}$$

Where τ_h is the minority carrier life time which can be regarded as constant at least for small disturbances from equilibrium and Δp is the excess concentration of holes.

$$\Delta p = p_n - p_{n0} \quad \text{.....(6)}$$

Where p_n is the total concentration of holes and p_{n0} is the equilibrium concentration of holes.

Combining the above equations,

$$D_h \frac{d^2 p_n}{dx^2} = \frac{p_n - p_{n0}}{\tau_h} - G \quad \text{.....(7)}$$

In the dark, G = 0. Also,

$$\frac{d^2 p_{n0}}{dx^2} = 0, \text{ as } p_{n0} \text{ is equilibrium concentration of holes.}$$

$\therefore$ eqn (7) becomes,

$$D_h \frac{d^2 \Delta p}{dx^2} = \frac{\Delta p}{\tau_h}$$

$$\frac{d^2 \Delta p}{dx^2} = \frac{\Delta p}{L_h^2} \quad \text{.....(8)}$$

where $L_h = \sqrt{D_h \tau_h}$

L_h has the dimensions of length and is known as diffusion length. This diffusion length is an important parameter in the case of solar cells.

General solution to eqn. (8) is

$$\Delta p = Ae^{x/L_h} + Be^{-x/L_h} \quad \text{.....(9)}$$

Constants A and B can be found by applying following boundary conditions.

1. At $x = 0$, $p_n = p_{n0} e^{qV/kT}$
2. P_n is finite as $x \to \infty$

These boundary conditions lead to the following solution:

$$\left.\begin{aligned} p_n(x) &= p_{n0} + p_{n0}[e^{qV/kT} - 1]e^{-x/L_h} \\ n_p(x') &= n_{p0} + n_{p0}[e^{qV/kT} - 1]e^{-x'/l_e} \end{aligned}\right\} \quad \text{.....(10)}$$

where x′ is defined in Fig.1.7. Semi logarithmic plot of distributions of carriers throughout the p-n junction diode under forward bias is shown in Fig.1.7.

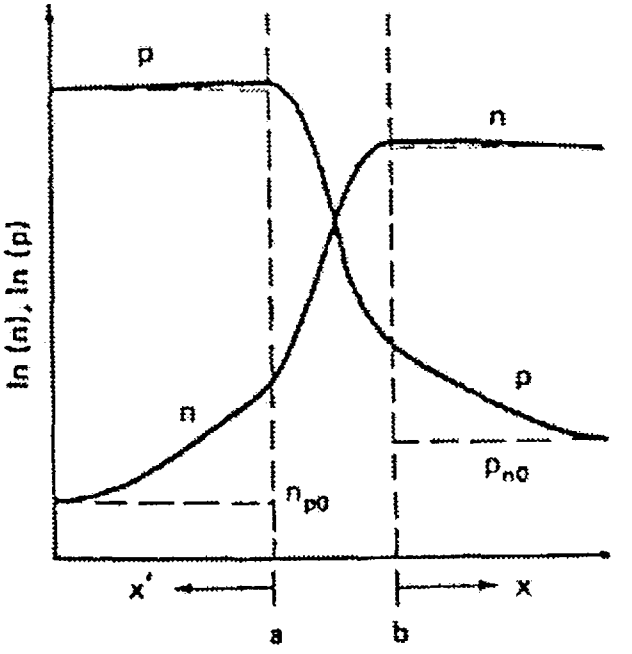

Fig.1.7. Semi logarithmic plot of distributions of carriers throughout the p-n junction diode under forward bias

Once carrier distributions are known, minority current can be calculated by substituting eqn.10 in eqn.3 gives,

$$J_h(x) = \frac{qD_h p_{n0}}{L_h}(e^{qV/kT} - 1)e^{-x/L_h} \quad \text{.....(11)}$$

similarly, in the p-type region,

$$J_e(x') = \frac{qD_e n_{p0}}{L_e}(e^{qV/kT} - 1)e^{-x'/L_e} \quad \text{.....(12)}$$

Considering the total current flow in the depletion region, the continuity equations give

$$\frac{1}{q}\frac{dJ_e}{dx} = U - G = -\frac{1}{q}\frac{dJ_h}{dx} \quad \text{.....(13)}$$

Magnitude of the change in current across depletion region is

$$\delta J_e = |\delta J_h| = q\int_{-w}^{0}(U - G)dx \quad \text{.....(14)}$$

Since w is small, it is reasonable to assume that the integral involved in eqn(14) is negligible. Hence total current is obtained as,

$$J_{total} = J_e|_{x'=0} + J_h|_{x=0}$$

$$= \left(\frac{qD_e n_{p0}}{L_e} + \frac{qD_h p_{n0}}{L_h}\right)(e^{qV/kT} - 1) \quad \text{.....(15)}$$

Eqn.15 can be written as

$$I = I_0(e^{qV/kT} - 1) \quad \text{.....(16)}$$

where I_o is the reverse saturation current. Equation (16) is "ideal diode law". Here,

$$I_0 = A\left(\frac{qD_e n_i^2}{L_e N_A} + \frac{qD_h n_i^2}{L_h N_D}\right)$$

where A is the cross sectional area of the diode.

B.Illuminated characteristics

Here for mathematical simplicity, it is assumed that the generation rate of electron-hole pairs due to illumination, is constant throughout the device. This would correspond to a specific physical situation where the cell is illuminated by long wavelength light consisting of photons of energy close to that of the semiconductor

band gap. Current-voltage characteristics of the junction when illuminated can be derived following the same method as the one used to find current-voltage characteristics of the junction kept in darkness.

Since generation rate G is not zero (but a constant), eqn.8 in the former section, can be rewritten as

$$\frac{d^2\Delta p}{dx^2} = \frac{\Delta p}{L_h^{\,2}} - \frac{G}{D_h} \quad \text{.....(17)}$$

Since G/D_h is constant, corresponding general solution is obtained as

$$\Delta p = G\tau_h + Ce^{x/L_h} + De^{-x/L_h} \quad \text{.....(18)}$$

Boundary conditions used for analysis of the diode in darkness remain unchanged. Hence this gives the solution as

$$p_n(x) = p_{n0} + G\tau_h + [p_{n0}(e^{qV/kT} - 1) - G\tau_h]e^{-x/L_h} \quad \text{.....(19)}$$

with a similar expression for $n_p(x')$

Corresponding current density is given by the following equation,

$$J_h(x) = \frac{qD_h p_{n0}}{L_h}(e^{qV/kT} - 1)e^{-x/L_h} - qGL_h e^{-x/L_h} \quad \text{.....(20)}$$

with a similar expression for $J_e(x')$.

Neglecting the effect of recombination in depletion region and including effect of generation in this region, change in the current density across this region can be written as

$$|\delta J_e| = |\delta J_h| = qGw \quad \text{.....(21)}$$

Proceeding as before, we get the following result for current-voltage characteristics:

$$I = I_0(e^{qV/kT} - 1) - I_L \quad \text{.....(22)}$$

where I_L is light generated current, and

$$I_L = qAG(L_e + W + L_h) \quad \text{.....(23)}$$

The current-voltage characteristics of a p-n junction in darkness and when illuminated are shown in Fig.1.8. Illuminated characteristics are merely the dark characteristics shifted down by a current I_L. This gives a region in the forth quadrant where power can be extracted from the diode.

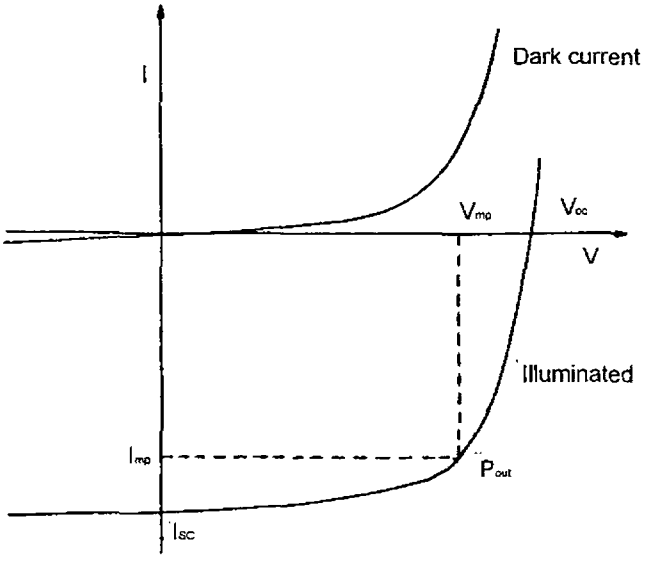

Fig.1.8 current-voltage characteristics of a p-n junction – with and without illumination

1.4.1.4 More realistic photovoltaic model

Solar cells generally have a parasitic series and shunt resistance associated with them. There are several physical mechanisms responsible for these resistances. Bulk resistance of semiconductor material of the cell, resistance of the metallic contacts and interconnections and contact resistance between metallic contact and semiconductor are the main contributors to the series resistance (R_s). Shunt resistance, (R_{sh}) is caused by leakage across the pn junction around the edge of the cell and in nonperipheral regions

in the presence of crystal defects and precipitates of foreign impurities in the junction region.

In a real solar cell, we have to consider effects of non-zero R_s and non-finite R_{sh}, voltage depended collection effects that makes the actual light-generated current less than I_L and the possibility for a change in major parameters I_0, n, Rs and R_{sh} between the dark and light conditions [9].

In general, junction current (in dark) can be expressed as

$$I^d = \gamma^d \{I_0^d \exp[\alpha^d (V - I^d R_s^d)] + V / R_p^d - I_0^d\} \quad \text{.....(24)}$$

where $\gamma^d = \dfrac{1}{(1 + R_s^d / R_p^d)}$ and $\alpha^d = q / n^d kT$ for transport mechanisms not involving tunneling. In the light, $I^l = \gamma^l \{I_0^l \exp[\alpha^l (V - I^l R_s^l)] + V / R_p^l - I_0^l - H(V) I_L\}$ ...(25)

where H(V) is a voltage dependent collection function, describing fraction of the light generated carriers that actually contribute to the light generated current.

$H(V) = g(V)h(V)$ where $g(V)$ describes loss of carriers by recombination in bulk and h(V) describes loss of carriers by recombination at the junction interface due to interface states. Equivalent circuit of a solar cell indicating series resistance R_s and Shunt resistance R_{sh} are shown in Fig.1.9.

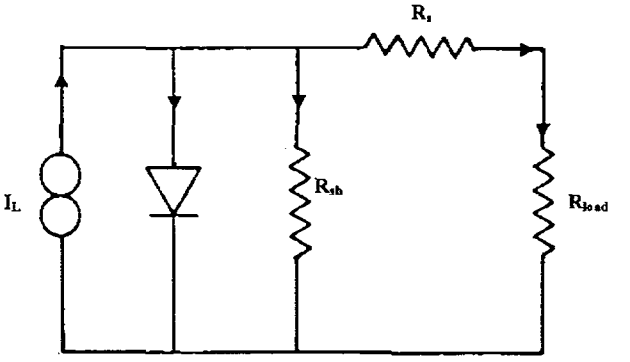

Fig.1.9.Equivalent circuit of a solar cell

1.4.2 Theory of Heterojunctions

1.4.2.1 Energy-band diagram and static characteristics

Consider two semiconductors 1 and 2 with band gaps E_{g1} and E_{g2}, permitivities ε_{s1} and ε_{s2}, work functions ϕ_1 and ϕ_2 and electron affinities χ_1 and χ_2. Let ΔE_c be the electron affinity difference and ΔE_v be the hole affinity difference. At thermal equilibrium, Fermi level coincides on both sides of the junction. Total built-in potential (V_{bi}) is given by

$$V_{bi} = \phi_1 - \phi_2 = V_{d1} + V_{d2}$$
$$= E_{g2} - (E_f - E_{v2}) + \chi_2 - \chi_1 - (E_{c1} - E_f) \ldots\ldots\ldots (29)$$
$$V_{bi} = V_{d2} + \Delta E_c \ldots\ldots\ldots (30)$$

Capacitance and depletion widths can be obtained by solving Poisson's equation, as in the case of homojunction, [19]

$$C = \left[\frac{qN_{D1}N_{A2}\varepsilon_1\varepsilon_2\varepsilon_0}{2(\varepsilon_1 N_{D1} + \varepsilon_2 N_{A2})(V_{bi} \pm V)} \right]^{1/2} \ldots\ldots\ldots\ldots\ldots\ldots (30)$$

$$x_1 = \left[\frac{2N_{A2}\varepsilon_1\varepsilon_2\varepsilon_0(V_{bi} - V)}{qN_{D1}(\varepsilon_1 N_{D1} + \varepsilon_2 N_{A2})} \right]^{1/2} \ldots\ldots\ldots\ldots\ldots\ldots (31)$$

and

$$x_2 = \left[\frac{2N_{D1}\varepsilon_1\varepsilon_2\varepsilon_0(V_{bi} - V)}{qN_{A2}(\varepsilon_1 N_{D1} + \varepsilon_2 N_{A2})} \right]^{1/2} \ldots\ldots\ldots\ldots\ldots\ldots (32)$$

Maximum electric field existing in the interface region is seen to occur at x = 0 and is given by

$$\xi_{\max} = \frac{qN_A x_1}{2\varepsilon_1} \quad \text{or} \quad \xi_{\max} = \frac{qN_D x_2}{2\varepsilon_2} \ldots\ldots\ldots\ldots(33)$$

1.4.2.2 Current Transport

Carrier transport properties of heterojunctions are generally dominated by the phenomena in interface region. Several transport mechanisms may be operative at the interface. These include i) ideal diffusion or emission currents for electrons, ii) recombination-generation currents, iii) recombination through interface states, iv) tunneling from band states to localized defect states in the gap, across the interface, and v) band to band tunneling. Several authors have proposed different models based on experimental data as well as theoretical considerations. The model of Anderson forms basis and starting point for most other heterojunction theories [20]. In this section, three main models for abrupt anisotype heterojunctions (viz, i)Anderson's model,ii) tunneling model and iii) interface recombination model) are discussed.

i) Anderson's model:

In this model, effects of dipoles and interface states are neglected. Further it is assumed that, owing to discontinuities in the band edges at the interface, diffusion current consists of only electrons or holes. Current voltage relation, in the absence of generation recombination currents is given by

$$J = A\exp(-qV_{d2}/kT)[\exp(qV_2/kT) - \exp(-qV_1/kT)] \ldots..(37)$$

where

$$A = aqXN_{d2}(D_{n1}/\tau_{n1})^{1/2} \ldots\ldots\ldots\ldots\ldots\ldots\ldots\ldots\ldots\ldots\ldots\ldots(38)$$

X – transmission coefficient for electrons across the interface

A is junction area, D_{n1} and τ_{n1} are diffusion coefficient and lifetime of minority carriers respectively, in the p-type material.

Perlman and Feucht included the effects owing to a spike in the conduction band edges in emission model. Current-voltage relation, neglecting generation and recombination within the space charge region is expressed as [19]

$$I = \frac{I_s[\exp(qV/kT)-1]}{(I + I_s/I_d)} \quad \text{.....(39)}$$

where $$I_s = aqN_{D1}(D_{n_1}/\tau_{n1})^{1/2} \quad \text{.....(40)}$$

ii) Tunneling model:

In tunneling model, electrons have to tunnel through potential barrier in the n-type wide bandgap material in order to flow from n-type to p-type or vice versa. If tunneling through the barrier greatly exceeds thermal emission through the barrier, then $I = I_s(T)\exp(V/V_0)$ where V_0 is a constant and $I_s(T)$ is a weakly increasing function of temperature.

iii) Interface recombination model:

Current density for interface recombination case, when the smaller bandgap p-type material is degenerate, has the form

$$J = qN_{c2}S_I \exp\left[\frac{-(qV_{d2}+\delta_2)}{kT}\right]\left\{\exp\left[\frac{q(V-JR_sA_\perp)}{kT}\right]-1\right\} \quad \text{.....(41)}$$

where N_{c2} is effective density of states in n-type wide bandgap semiconductor, V_{d2} is the diffusion voltage , δ_2 is equal to E_{c2}-E_f, R_s is series resistance, $A_\perp$ is normal area of the diode and S_I is effective interface recombination velocity

$$S_I = v_{th}\sigma N_I^* \quad \text{.....(42)}$$

where v_{th} is the thermal velocity of electrons, σ is capture cross-section of the interface states, and N_I^* is density of the empty interface states.

S_I can also be written as

$$S_I = v_{th}\sigma\Delta a / a^3 \quad \text{.....(43)}$$

where Δa is difference in lattice constant between the two materials and a is average lattice constant in the plane of the junction.

1.4.3 Solar cell output parameters

Following parameters are used to characterize performance of a p-n junction solar cell.

i) Short circuit current (Isc) : This is the maximum current that can be extracted from the device by connecting upper and lower electrodes of the cell to an ammeter with negligible internal resistance. Ideally this is equal to the light generated current I_L. Low energy band gap and high diffusion length of the minority carriers are favorable for high short circuit current.

$$I_{sc} = I_0[e^{qV_{oc}/nkT} - 1] \text{.....(44)}$$

ii) Open circuit voltage:- This is the maximum voltage generated by the device while drawing negligible current.

$$V_{0c} = \frac{nkT}{q}\ln(\frac{I_L}{I_0} + 1) \text{ .....(45) where n is diode quality}$$

factor and its value lies between 1 and 2.

In order to get high open circuit voltage, saturation current of the diode must be as small as possible and for this high band gap is essential. But this is contrary to the requirements for high photocurrent. Maximum conversion efficiency is obtained for semiconductors with an energy band gap between 1.2 and 1.5 eV

iii). Maximum power output: - Power output of any operating point in the fourth quadrant is equal to area of the rectangle indicated in Fig1.8. One particular operating point (V_{mp}, I_{mp}) will maximize this power output.

$$P_{mp} = V_{mp} \times I_{mp} \quad \text{.....(46)}$$

iii) Fill factor (FF):- Fill factor is a measure of the flatness of output characteristics. For cells of reasonable efficiency, FF has a value in the range 0.7 to 0.85.

$$FF = \frac{V_{mp} \times I_{mp}}{V_{oc} \times I_{sc}} = \frac{P_m}{V_{oc} \times I_{sc}} \quad \text{.....(47)}$$

Energy conversion efficiency(η) is then given by

$$\eta = \frac{V_{mp} \times I_{mp}}{P_{in}} = \frac{V_{oc} \times I_{sc} \times FF}{P_{in}} \quad \text{.....(48)}$$

where P_{in} is total power in the light incident on the cell.

$$P_{in} = A\int_0^\infty F(\lambda)(hc/\lambda)d\lambda \quad \text{.....(49)}$$

where A is the total device area, $F(\lambda)$ is the number of photons per cm^2 per sec per unit bandwidth incident on the device at wavelength λ and (hc/λ) is the energy carried by each photon [21].

Ideally, FF is a function of the open circuit voltage (V_{oc}) alone. Defining normalized voltage V_{oc} as $\frac{V_{oc}}{(kT/q)}$, an empirical expression describing this relationship can be expressed as,

$$FF = \frac{V_{oc} - \ln(V_{oc} + 0.72)}{V_{oc} + 1} \quad \text{.....(50)}$$

Efficiency becomes large when fill factor, short circuit current and open circuit voltage are as high as possible.

1.4.4 Spectral response

Photocurrent collected at each wavelength, relative to the number of photons incident on the surface at that wavelength determines "spectral response" of the device. "Internal spectral response" is defined as the number of electron- hole pairs collected at short circuit conditions relative to number of photons entering the material.

$$SR(\lambda) = \frac{J_p(\lambda)}{qF(\lambda)(1-R(\lambda))} + \frac{J_n(\lambda)}{qF(\lambda)(1-R(\lambda))} + \frac{J_{dr}(\lambda)}{qF(\lambda)(1-R(\lambda))} \quad \text{.....(51)}$$

where J_p,J_n and J_{dr} are hole diffusion, electron diffusion and drift contributions respectively to the total photocurrent density J_L.

External response is internal one modified by reflection of light from the surface of the device.

$$SR(\lambda)_{ext} = SR(\lambda)[1-R(\lambda)] \quad \text{.....(52)}$$

1.5 Factors influencing efficiency of Solar cells

A major reason for low efficiency of a solar cell is the fact that each photon irrespective of its high energy, generates one electron- hole pair. The electron and hole quickly relax back to the edges of the respective carrier bands emitting phonons, which has low energy but relatively high momentum than a photon. Energy thus wasted is dissipated as heat. This effect alone limits the maximum available efficiency to about 44% [22].

Excessive recombination of carriers taking place in the bulk of the semiconductor and at the surfaces reduces the efficiency. Only the electron-hole pair generated near the junction contributes to light generated current.

A part of the generated free carriers do not reach the junction because of their low diffusion length or due to recombination at the surface or in the bulk. Loss occurs

due to the reflection of the incident light too. In the case of silicon, about 30% of the light is reflected at the surface. But this loss can be minimized to nearly 0% if an appropriate anti reflection coating is used or the surface is so prepared that the cell appears black [23].

Top electrode of cell reduces active surface area of the semiconductor exposed to sunlight. This blocks 5 to 15 per cent of the incoming light. If the cell is not thick enough, a part of the incident light will not be absorbed, and it passes out at the back.

Short circuit current of solar cells is not strongly temperature-dependent. It tends to increase slightly with increasing temperature. But other cell parameters like open-circuit voltage and the fill factor, both decrease. Power output and efficiency decrease with increasing operating temperature. For silicon, the power output decreases by 0.4 to 0.5% per ^{0}C.

Diffusion length is the parameter most directly controlling short circuit current of a cell, and it can also influence open-circuit voltage if the diode current is controlled by the diffusion length of the material [24]. Generally, diffusion length should be as long as possible and certainly equal to the thickness of the absorber layer.

Power loss factor L_S due to series resistance (R_S) is calculated using the following expression

$$L_s = \frac{J_m \times R_s}{V_{oc}} \quad \text{.....(53)}$$

and impact of the shunt resistance(R_{Sh}) in the power factor is calculated using the expression

$$L_p = \frac{V_m}{J_m \times R_{sh}} \quad \text{.....(54)}$$

Effect of parasitic resistance on the output characteristics of solar cells is indicated in Fig.1.10.

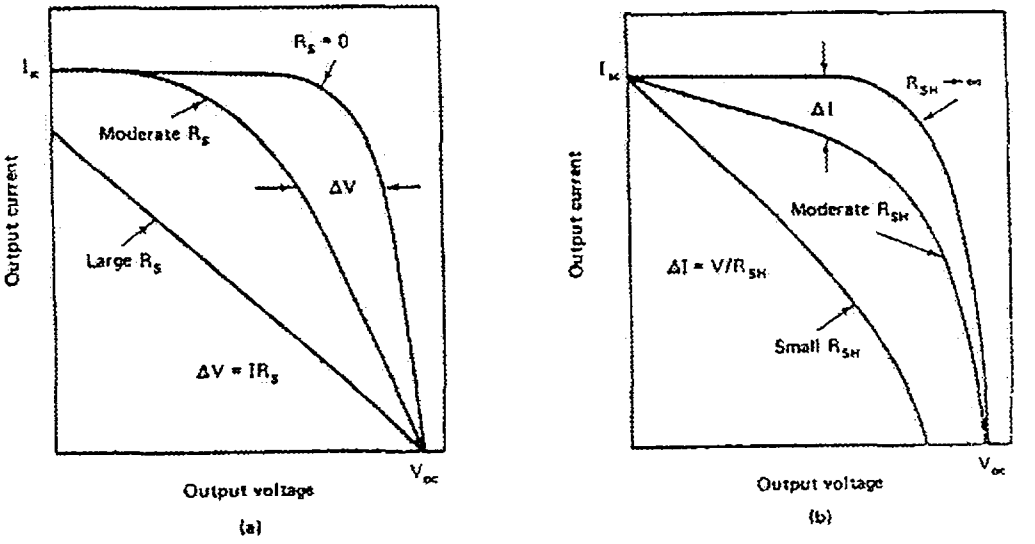

Fig.1.10 Effect of Rs and Rsh on output characteristics of a solar cell
a) Effect of series resistance(Rs), b) Effect of Shunt resistance

Magnitude of effect of R_S and R_{Sh} on fill factor can be found by comparing their values to the characteristic resistance of the solar cell defined as

$$R_{CH} = V_{oc}/I_{sc} \quad \text{.....(55)}$$

If R_S is a lot less than this quantity, there will be little effect upon the fill factor. An approximate expression for the fill factor in the presence of series resistance can be written as

$FF = FF_o\ (1\text{-}r_S)$ .....(36) where $r_S = R_S/R_{CH}$ and FF_o is the ideal FF in the absence of parasitic resistance.

From Fig.1.10, it is also evident that both R_s and R_{sh} act to reduce fill factor.

Apart from these, there are certain material and structural characteristics affecting cell performance. They are, stoichiometry, grain size, surface properties, grain boundary properties, bulk lifetime, energy band profiles, impurities, dislocations and interface states. Each of these properties is discussed in detail by L L Kazmerski [24].

1.6 Efficiency Measurement

Solar cell efficiency can be measured by measuring power of incident sunlight using a pyranometer and electrical power generated at the maximum power point. However, performance of the cell measured in this way will depend greatly on the precise spectral content of the sunlight, which varies with air mass, water-vapor content, turbidity etc. Hence this approach would make comparison difficult between the performance of devices measured at other than the same time and place. An alternative approach is a method using calibrated reference cells. A central test authority calibrates reference cells under standard illumination conditions. Performance of the cell under test is then measured relative to the reference cell. For this technique to be accurate, reference and test cells must be made from the same semiconductor material using a similar processing technique. Three methods that are approved by NASA – Lewis under the direction of the Department of Energy for the testing of solar cells are summarized in Fig.1.11 [25].

A four point contacting scheme is desirable in which voltage and current leads to the cell under test are kept separate. This eliminates effects due to series resistance of the test leads and associated contact resistances. Cells are mounted on a temperature-controlled block. 25 °C and 28 °C are standard temperature for solar cell measurements. Lamp intensity is adjusted to give desired intensity as measured by a reference cell. By varying load resistances, characteristics of the test cell can be measured.

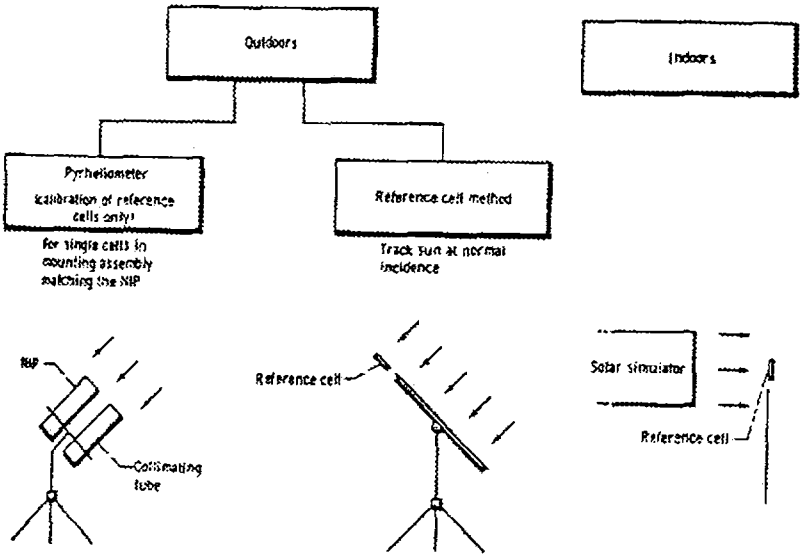

Fig.1.11 DOE/NASA solar cell testing methods

Spectral Response is the output current under short-circuit condition per unit incident power in monochromatic light as a function of wavelength. Measurement of spectral response can provide detailed information about design parameters of any particular solar cell.

Spectral response of a test cell can also be measured by direct comparison with the output of a cell having calibrated spectral response. The simplest technique is to use a steady-state source of monochromatic light from a monochromater.

1.7 Thin Film Solar cells

During the energy crisis of early 1970s, both public and private sectors became interested in terrestrial applications of photovoltaic energy generation. Initial efforts focused on lowering the cost of single crystal silicon (sc-Si) solar cell modules. Parallel

efforts were also initiated to find alternative materials that could be processed in thin film form.

Thin film cells are produced by depositing thin layers of semiconductor material onto a supporting substrate such as glass, plastic or stainless steel. Generally speaking, single crystal solar cell is the most efficient in terms of electrical output, but it is also the most expensive. While thin film cells achieve lower efficiencies than crystalline cells, their production cost is considerably less. Moreover thin film cells can be extremely light and flexible, and hence they can meet a variety of needs for which crystalline solar cells are too big or too rigid [26]. Reduced material use is another main advantage. In thin film cells, only one or two micron thickness of semiconductor material is required, which is 100-1000 times less than the thickness of silicon wafer [4]. Because of low consumption of active solar cell material, even rare and expensive elements can be considered here. Further advantage is that such cells have relatively high tolerance for impurities and crystalline imperfections because the diffusion length scales with film thickness [27].

Requirements of ideal solar cell material are: 1) Bandgap between 1.1 and 1.7 eV, 2) Direct band structure, 3) Consisting of readily available, non toxic materials,4) Easy, reproducible deposition technique, suitable for large area production, 5) Good photovoltaic conversion efficiency and 8) Long-term stability.

Out of a large number of experimentally tested thin film materials, only a handful of materials have emerged as good solar cell absorber layers. One reason is that many chemical, physical and practical conditions have to be fulfilled simultaneously. Most compound semiconductors, when formed in polycrystalline form, have poor electronic properties due to the activity at grain boundaries [28]. Grain boundaries provide recombination surfaces for minority carriers and thus degrade performance of the device. Further it affects device operation by creating shorting paths [29]. However, a few materials maintain good performance in polycrystalline form.

Initially, research was concentrated on thin film solar cells of polycrystalline Cu_2S/CdS. But due to severe stability problems, this work was discontinued by the early 1980s. Presently, amorphous silicon, copper indium diselenide, and cadmium telluride are the most popular semiconductors in the field of thin film solar cells. All these materials have shown continuous improvement of laboratory efficiency over the years as indicated in Fig.1.13. Each of these technologies has its own strength and weaknesses. Brief descriptions of all these cells are given below.

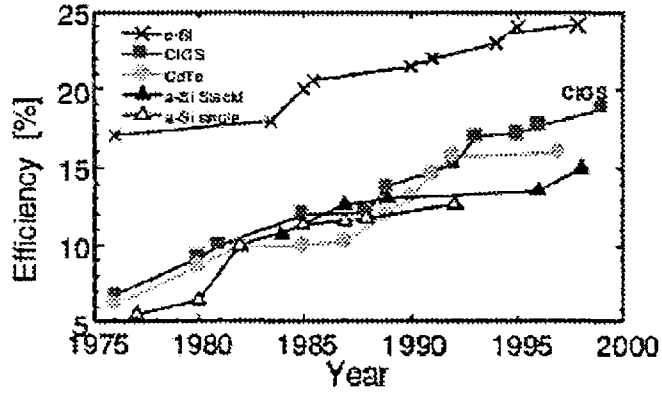

Fig. 1.13 Improvement of efficiency over time for prominent solar cell materials

i)Amorphous silicon cell (a-Si:H)

The best known thin film material is amorphous silicon (a-Si), which has been in production for about 15 years [30]. First amorphous silicon cell was produced in 1976 by Carlson [31]. By 1994, its efficiency became 10.2%. Today more than 15% of cells and modules produced worldwide are based on a-Si [4].

This material is actually a-Si-hydrogen alloy, containing 20-30% hydrogen. a-Si is produced by decomposing the silane (SiH_4) gas, at low temperature and it is found that incorporation of hydrogen improves the material quality. It can also be prepared using Glow discharge [32] and chemical vapor deposition techniques [33]. It has high

optical absorption coefficient($>10^5 cm^{-1}$) and can be easily doped using boron and phosphorous for p and n-type respectively. Bandgap of a-Si can be tailored from 1.1eV to 2eV with addition of carbon or germanium [27].

Major problem of this cell is linked with outdoor usage. Some of the beneficial effects of hydrogen become undone under bright sunshine and the cell performance degrades (Staebler-Wronski effect) and these cells show initially some degradation of efficiency because of this. Stabilized efficiency is only 6-7% for the best commercial modules. However, since the film deposition temperature is low, they can be deposited onto low-temperature substrates such as plastics. This makes them especially suitable for consumer products.

As thinner cells exhibit higher stability, stalked cells have been designed to utilize this effect. Multijunction solar cells have reached 13.7% efficiency and an efficiency of 18.7% has been reported for the hybrid structure a-Si:H/Si [34].

ii) Thin film crystalline silicon solar cells (f-Si)

Early attempts to develop thin-film solar cells based on the polycrystalline silicon did not give encouraging results since the silicon layers had to be quite thick to absorb most of the available light. However, it is now well recognized that its poor absorption is no longer an issue provided light trapping is introduced whereby the light is confined to regions where the photogenerated carriers have high collection probabilities [35]. Optically a cell can appear about 50 times thicker than its actual thickness if this happens.

Thin-film crystalline silicon (f-Si) covers a broad technological field, which is usually divided in two main routes:

- High-temperature- replacement of thick, expensive, silicon by a thin (< 50 μm) silicon film on a low-cost substrate
- Low-temperature- the use of micro crystalline silicon < 5 μm in an amorphous silicon-like or amorphous silicon-based structure [36].

In low temperature approach, silicon is deposited in amorphous form and then heated for prolonged periods at intermediate temperatures to crystallize it. In another approach, a nanocrystalline phase of silicon is produced by changing the amorphous silicon deposition conditions.

More recently, cell efficiency above 10% has been confirmed with this approach. 19.2% efficiency has been reported for a CVD-epi-Si p^+/p structure on SIMOX wafer substrate [4]. Tandems are often made with both microcrystalline and amorphous silicon. Presently crystalline thin film technology is being characterized using a wide range of laboratory activities, but considerable work is necessary to put this into production lines. Probably only thin Si-cell concept, which is about to be a commercially available product, is the Silicon Film TM technology developed by Astropower [37].

iii) Cadmium Telluride Cells (CdTe)

CdTe is one of the most promising photovoltaic materials for use as low-cost, high-efficiency thin film solar cells due to the near optimum bandgap (1.5eV at room temperature), high absorption coefficient (around $5\times10^4 cm^{-1)}$ and manufacturability. CdTe based solar cells have a theoretical conversion efficiency of the order of 28% [38].

A variety of techniques had been used for the deposition of CdTe thin films. The most widely used techniques are electrodeposition, physical vapor deposition (PVD), close-space sublimation (CSS), screen-printing and spray pyrolysis. Heterojunction devices with n-type cadmium sulfide (CdS) films show very low minority carrier recombination at the absorber grain boundaries and at the metallurgical interface, which results in high quantum efficiencies.

Recently, ~16% efficiency (which is the current world record for CdTe solar cells), was reported by Aramoto et al. [39]. This cell structure is antireflection coat/glass/ITO/CdS/CdTe/Cu-doped carbon/Ag, where CdS and CdTe films were

deposited by chemical vapor deposition (CVD) and close-spaces sublimation (CSS) method respectively. The National Renewable Energy Laboratory [NREL] developed a modified CdTe device structure and fabricated a CdS/CdTe polycrystalline thin film solar cell demonstrating efficiency of 16.4% [40].

Photovoltaic performance of the CdS/CdTe device in the as deposited state is poor. $CdCl_2$ treatment after CdTe deposition and heat treatment after screen printing of the Cu doped carbon electrode upgrades device performance [41].

One major issue is the high content of cadmium in CdTe solar cells. Cd metal, which is classified as a toxic/ carcinogen is, present both in the window and absorber layers, which gives rise to environmental hazards. Another issue is regarding the electrical contacts.

iv) Copper Indium Diselenide ($CuInSe_2$) solar cells

A promising thin film technology at the moment is the one based on ternary chalcopyrite $CuInSe_2$ (CIS). Direct bandgap of 1.04 eV is near the optimal value for terrestrial conditions. By substituting Ga for In and S for Se, the bandgap can be modified continuously over a wide range. This material has its absorption coefficient larger than $5X10^4cm^{-1}$.CIS forms an ideal heterojunction with CdS, since the lattice mismatch between chalcopyrite $CuInSe_2$ and hexagonal CdS is only about 1.2%. No interfacial spikes are formed in conduction band, as the electron affinities of the two materials are very close [19].

This compound is often alloyed with copper gallium diselenide ($CuGaSe_2$) and copper indium disulphide ($CuInS_2$), giving CIGS material with up to five elements involved [42,28]. There are two different approaches for CIGS film deposition. The first is the coevaporation of elements onto a heated substrate and the second process; selenization of stacked layers / metal alloys is more suitable for industrial production.

Conversion efficiencies are now approaching 19% for CIS/CdS/ZnO-based devices [43,44]. In these devices CIS (2 μm) and ZnO (0.5 μm) layers are deposited

using high vacuum physical deposition techniques (coevaporation and sputtering) but the CdS films (20–50 nm) are prepared using chemical bath deposition (CBD) in aqueous solutions [45]. This is a recent and innovative combination between vacuum and solution deposition approaches. The record lab efficiency recently announced by ENREL is an impressive 18.8% for cells. Small modules are having 14% and large modules are having 11-12%. Seimens is now marketing the first products of a pilot line production with efficiencies above 10% [46,47].

Our research group at 'Thin Film Photovoltaic Division' of Cochin University of Science and Technology is also seriously involved in the fabrication of $CuInSe_2$ based solar cells. Fabrication of the first $CuInSe_2$/CdS thin film heterojunction entirely using chemical bath deposition belongs to our credit [48]. Efficiency of the best cell fabricated was 3.1%, with an open circuit voltage 365mV and short circuit current density $12mA/cm^2$. Thus it was demonstrated for the first time that a simple, low-cost process like CBD could be used for the fabrication of a complete $CuInSe_2$/CdS solar cell. Details of this work are presented in reference [49].

Also we are successful in preparing $CuInSe_2$ films through a new selenization process developed in our lab, which avoids usage of poisonous gases or Se vapor [50]. For this, amorphous selenium films were prepared from an acidified solution of Na_2SeSO_3 using CBD at room temperature. $CuInSe_2$ films were prepared using two methods: One method is selenization of multilayer having structure In/Cu and the second is thermal diffusion of Cu into In_2Se_3 film, prepared using selenization of In film. Research is in progress to fabricate solar cells using these films.

Apart from the use of cadmium, there is another difficulty related due to the limited known resources of indium, often-quoted limitation of this technology viz, 'manufacturability'. It is usually difficult to diagnose problems in production of this material, since the difference between good and bad material is not sufficiently well understood to allow differentiation and control during the various manufacturing steps.

1.8 Scope of present work

Although solar cells based on CIGS films have shown good conversion efficiencies, mismatch in the electron affinity and hence band offset at the junction between their absorber layer and the window layer (CdS) is considered to be one of the major limiting factors towards furthering the efficiency value [51]. Use of selenium in synthesizing this material is not favored due to its toxicity. Conventional selenization processes involve usage of selenium vapor or H_2Se gas which are extremely toxic. In this regard, $CuInS_2$ films have an edge over the above material since this does not contain any toxic constituent.

$CuInS_2$, which is the material selected for the present work, possesses several exceptional material properties, which make it potentially well suited for photovoltaic applications. Its direct bandgap of 1.53eV is nearly optimum for solar energy conversion. Absorption coefficient is high. This material can be prepared both in p-type and n-type form so that homojunction is possible. Heterojunction can be fabricated with n-type CdS which is the most commonly used window layer. Its electron affinity is such that there is no spike in conduction band when junction is formed with n-type CdS. Since radiation hardness is high, cells based on this material can also be used for space applications.

Messe et al. predicted theoretical efficiencies between 27% and 32% for the $CuInS_2$ homojunction and this is the highest figure for any photovoltaic device [52]. Many groups have already reported the possibilities of synthesizing $CuInS_2$ films leading to the fabrication of solar cells with efficiencies ~12% [53-55]. The best cell efficiencies to date for this ternary material is 12.5% [56]. As the next stage of development, efforts are to be made to produce this absorber layer with simple and cost-effective processes.

In the present work, we developed a new method for the preparation of p-type $CuInS_2$ using chemical bath deposited (CBD) Cu_xS thin film. This is a low cost and very convenient process as the preparation of Cu_xS film is carried out using simple and inexpensive CBD technique at room temperature itself. No substantial amount of energy is required in this process. Also we used chemical spray pyrolysis (CSP), which is another low cost deposition technique for preparing device quality films with good photoresponse. We obtained further information about the dependence of film resistivity and photoresponse as a function of composition in the spray solution. This information is useful for designing solar cells using this material. We could fabricate an 'all sprayed' $CuInS_2$/ CdS solar cell with efficiency 1.7% in the present work as a preliminary step. Even though the efficiency is low, we feel that this is the beginning of a challenging work.

1.9 Conclusion

After discussing basic theory and principle of solar cell operation, different solar cell structures and factors affecting efficiency of the cells are mentioned. It is obvious that low-cost thin film solar cells fabricated using compound semiconductors are good options. These have potential for developing a highly efficient cell, and they will become important and sustainable resource for our energy needs in the near future. A brief review of the important thin film solar cells is included and the significance of $CuInS_2$ thin film as a photovoltaic material is highlighted.

References

[1] G.H.Lin and D.E Carlson, *International Journal of Hydrogen Energy*, 25 (2000) 807

[2] Becquerel.E, C.R. Hebd. Seances Acad. Sci, 9 (1839) p-561

[3] Alan L. Fahrenbruch and Richard H. Bube, Fundamentals of solar cells, Academic press, New York (1983) p- 9

[4] M.A.Green, Energy Policy, 28 (2000) 989

[5] D. M. Chapin, C. S. Fuller, and G. L. Pearson, J. *Appl. Phys.*, 25 (1954) 676

[6] M.A.Green, Solar cells, Prentice-Hall, Inc, Englewood Cliffs, (1992) p-2

[7] Rathindra Nath Biswas, Electronics for You, Feb (1998) p- 45

[8] D.C Reynolds, G. Leies, L L Antes, and R.E Marburger, *Phys. Rev.*, 96 (1954) 533

[9] Richard H Bube, Photoelectronic properties of semiconductors, Press Syndicate of the University of Cambridge, New York, USA, 1992

[10] K.W.Boer, Survey of semiconductor Physics, Vol.II, Van Nostrand Reinhold, NewYork (1992) p-820

[11] M.A.Green, Solar cells, Prentice-Hall, Inc, Englewood Cliffs, (1992) p-175

[12] M. S. Thyagi, Semiconductor Materials and Devices, John Wiley & Sons, (1991) p-348

[13] M.A.Green, Solar cells, Prentice-Hall, Inc, Englewood Cliffs, (1992) p-171

[14] Hans Joachim Moller, Semiconductors for solar cells, Artech House, Boston, (1993)p-52

[15] S.J.Fonash, Solar Cell Device Physics, Academic Press, (1981)

[16] S.M Sze, Semiconductor devices, Physics and technology, John Wiley &sons, New York, (1985) p-73

[17] K L Chopra and S R Das, Thin film solar cells, Plenum press, New York, (1983 p-75

[18] M.A.Green, Solar cells, Prentice-Hall, Inc, (1992) p-70

[19] K.L.Chopra and S. R. Das, Thin film solar cells, Plenum press, New York (1983)

[20] Alan L. Fahrenbruch and Richard H. Bube, Fundamentals of solar cells Academic press, New York (1983) p- 130

[21] Harold J.Hovel, Semiconductors and semimetals, Vol-II Solar cells, Academi Press, New York, (1975) p-72

[22] M.A.Green, Solar cells, Prentice-Hall, Inc, Englewood Cliffs, (1992) p- 90

[23] Krishan Lal (Editor), Synthesis Crystal Growth and characterization, North Holland (1982) p-491

[24] Lawrence L Kazmerski (Ed) Polycrystalline and Amorphous thin films an devices, Academic press, (1980)

[25] Alan to Fahrenbruch, R.H.Bube, Fundamentals of solar cells, Academic press New York (1983)p-36

[26] "An over view of Photovoltaic technology", Perihelion's Watts Up article, Winte 2001

[27] Adolf Goetzberger and Christopher Hebling, *Solar Energy Materials and Sola Cells*; 62 (2000) 1

[28] Kazmerski L, Photovoltaics: a review of cell and module technologies Renewable and sustainable energy reviews.1 (1997) p-71

[29] K. L. Chopra and Inderjeet Kaur, Thin Film Device Applications, Plenum Press New York, (1983) p-109

[30] Nancy B Solomon, AIA article "Architectural Record"- continuing educatio Series

[31] D.E.Carlson, C R Wronski, *Appl. Phys. Lett.*28; (1976) 671

[32] C. Yang Jeffry; *Prog. Photovolt. Res. Appl., 6 (1998) 181*

[33] V. M Fthenakis and Moskowitz; *Prog. Photovolt.: Res. Appl*; 3 (1995) 295

[34] W. H Bloss, F. Pfisterer, Schubert. M and T.Walter; *Prog. Photovolt. Res. Appl*; 3 (1995) 3

[35] S.R Wenham, MA Green, S Edmiston, P Campbell, L Koschier, C B Honsberg, A.B.Sproul, D.Thorpe, Z.Shi, G.Heiser, *Solar Energy Materials and Solar Cells;* 41/42 (1996) 3

[36] R.H.Bossert, C.J.J.Tool, J.A.M.van Roosmalen, C.H.M.Wentink, M.J.M. de Vaan, Thin film solar cells-technology Evaluation and Perspectives, May 2000, NOVEM, The Netherlands

[37] A.M. Barnett, D.H. Ford, J.C. Checchi, J.S. Culik, R.B. Hall, E.L. Jackson, C.L. Kendall, J.A. Rand, Very-large-Area silicon-film TM solar cells, Proceedings of the 14th European Photovoltaic Solar Energy Conference, Barcelona, (1997) p-317

[38] Robert W. Birkmire and Erten Eser, *Annu. Rev. Mater. Sci*; 27 (1997) 625

[39] T.Aramoto, S.Kumazawa, H.Higuchi, T.Arita, S.Shibutani, T.Nishio, J.Nakajima, M.Tsuji, A.Hanafusa, T.Hibino, K.Omura, H.Ohyama and M.Murozono, Jpn.J.Appl.Phys.36 (1997) 6304]

[40] [http://www.ecomall.com/greenshopping/newsolar.htm].

[41] Tamotsu Okamoto, Yuichi Matsuzaki, owshad Amin, Akira Yamada and Makoto Konagai, *Jpn.J.Appl.Phys*; 37(1998) 3894

[42] Brian Pamplin and R.S Feigelson, *Thin Solid Films*, 60 (1979) 141

[43] J.R. Tuttle, J.S. Ward, A. Duda, T.A. Berens, M.A. Contreras,K.R. Ramanathan, A.L. Tennant, J. Keane, K. Emery,R. Noufi, Mater. Res. Symp. Proc. 426 (1996) 123

[44] Photovoltaic Insider's Report , February,1999, page-2

[45] M.J. Furlong, M. Froment, M.C. Bernard, R. Cortes, A.N. Tiwari, M. Krejci, H. Zogg, D. Lincot, *Journal of crystal growth*; 193 (1998) 114

[46] C J Oswald, The PV industry moving into the solar century, Proceedings of the 2nd World conference on Photovoltaic solar energy conversion, Vienna, 1998

[47] H W Shock, A Shah, Proceedings of the 14th European PV Solar Energy Conference, Barcelona, 1997, p-2000

[48] P. K. Vidyadharan Pillai and K. P. Vijayakumar, *Sol. Energy Mat. Sol. Cells*; 51 (1998) 47

[49] P. K. Vidyadharan Pillai, Ph.D Thesis, Cochin University of Science and Technology, 1997

[50] K. Bindu, M. Lakshmi, S. Bini, C. Sudha Kartha, K.P. Vijayakumar, T.Abe and Y. Kashiwaba, Semicon.Sci.technol., 17 (2002) 270]

[51] S.Bandyopadhyaya, S Chaudhuri, A K Pal, *Solar Energy Materials & solar cells* 60 (2000) 323

[52] J M Meese, J C Manturuthil and D R Locker, *Bull. Am. Phys. Soc;* 20 (1975) 696

[53] T Walter, R Menner, ch.Koble, H W Shock; Proc.12th EC Photovoltaic Solar Energy Conf., Amsterdam,1994,1775

[54] T Watanabe, M.Matsui, *Jpn. J. Apl. Phys*; 35 (1996) 1681

[55] D.Braunger, D.Hariskos, T Walter, H W Shock, *Solar Energy Materials & solar cells*; 40 (1996) 97

[56] Robert W. Birkmire, Compound Polycrystalline Solar Cells: Recent Progress and Y2K perspective, p-4

Chapter 2

REVIEW ON COPPER INDIUM SULFIDE FILMS AND CELLS

2.1 Introduction 46
2.2 $CuInS_2$ Thin Films 49
2.2.1 Preparation 49
2.2.2 Optical Properties 55
2.2.3 Electrical properties of $CuInS_2$ 58
2.2.4 Different studies on $CuInS_2$ thin films 59
2.2.5 Study of defects in $CuInS_2$ 64
2.2.6 Effect of incorporation of Na 65
2.2.7 Etching of $CuInS_2$ films using KCN 66
2.3 $CuInS_2$ based solar cells 67
2.4 Significance of present study 81
2.5 Conclusion 82
References 83

Chapter 2

REVIEW ON COPPER INDIUM SULFIDE FILMS AND CELLS

2.1 Introduction

$CuInS_2$ belongs to the group of I-III-VI_2 compounds which are probably the most interesting ternary members in the tetrahedral family. These compounds, usually have chalcopyrite structure [1]. In I-III-VI compounds, if I and III atoms are replaced by II atoms, cubic zincblende structure would result. Chalcopyrite structure is the simplest, noncubic ternary analogue of the well-understood binary Zincblende structure, with c/a ratio approximately equal to 2. Lattice parameters of this compound are given in table-2.1.

All Cu-In-dichalcogenides can have ordered, chalcopyrite structure, with a tetragonal unit cell in which Cu and In atoms sit on distinct lattice sites or the disordered, zincblende structure, with a cubic unit cell in which the Cu and In atoms are distributed randomly on the lattice sites occupied by Zn in cubic ZnS [2].

$CuInS_2$ has body centered tetragonal structure as represented in Fig.2.1. Chalcopyrite is the most stable phase at 0K. At high temperatures (above 1200 K), the most thermodynamically stable phase is sphalerite, where Cu and In atoms are randomly distributed in the tetragonal cation sub- lattice [3].

Although sphalerite lattice structure is unusual for the bulk material, such lattice structure has been observed in thin films of $CuInS_2$ obtained by the method of the sulfurization of CuIn in H_2S at 300 °C [4]. For $CuInS_2$ nanocrystals in a glass matrix also, the sphalerite lattice has been observed [5].

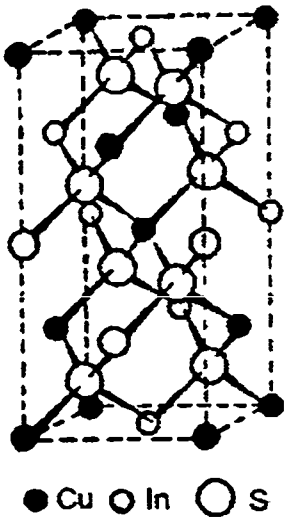

Fig.1 The tetragonal chalcopyrite structure of $CuInS_2$

Table-1

Chemical Formula:	$CuInS_2$
Composition:	Molecular Weight = 242.50gm
	Indium 47.35 % In
	Copper 26.20 % Cu
	Sulfur 26.45 % S
	100.00 %
Empirical Formula:	$CuInS_2$
Lattice Parameters:	a = 5.52 Å,c = 11.13 Å
	c/a = 2.01
Melting temperature:	1000-1050 °C [11]
Bandgap	1.55 eV

The optical absorption of $CuInS_2$ is very high with optical absorption coefficient nearly $10^5 cm^{-1}$ in the visible and near-IR regions [5-6]. A comparison of the absorption length of different semiconducting materials is represented in Fig.2.2

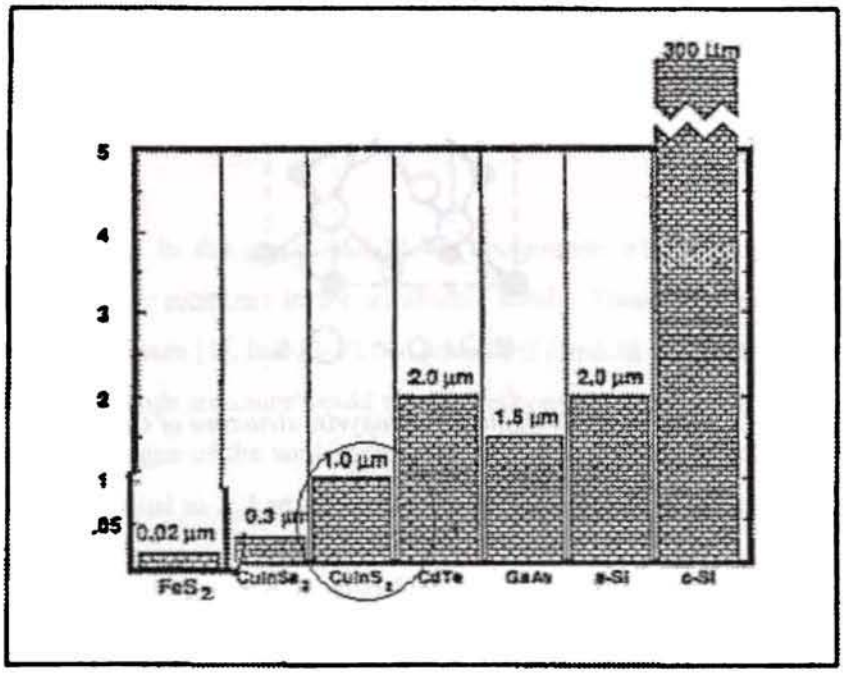

Fig.2.2 Comparison of the absorption length for different semiconductor materials

There are four major techniques for the synthesis and subsequent crystal growth of $CuInS_2$. They are, 1) direct synthesis from stoichiometric amounts of the constituent elements, 2) direct synthesis involving binary compounds of the constituent elements, 3) Vapor transport of the constituent elements and 4) solution or flux growth [7]

2.2 $CuInS_2$ Thin Films

2.2.1 Preparation

During mid 1970s, the chalcopyrite ternary compounds received considerable attention and attempts were made to prepare these compounds in thin film form. In 1975, two deposition schemes for producing $CuInS_2$ thin films (viz., single and double source methods), were reported for the first time by Kazmerski et al.[8]. For the single–source method, single-phase $CuInS_2$ was used as the starting material. The second, and more controllable and reproducible scheme involved a two-source arrangement. First, the single-phase $CuInS_2$ powder was evaporated from a resistive –heated alumina crucible, and a second sulfur source was utilized to vary the amount of sulfur in the system [8].

Since then, $CuInS_2$ thin films have been prepared by a variety of methods, including the three source evaporation [3,6,9] rf sputtering [10,11], close spaced chemical transport [12], chemical deposition [13,14], electrodeposition [15-17], flash evaporation [18,19], painting [20], sparay pyrolysis [21-23], stacked elemental layer deposition technique [24] and two-stage process causing chalcogenization of the Cu-In alloy or Cu/In layer with S vapor/H_2S gas at high temperature [4,25,26]. Among these, the two-stage process was found to be the best method for producing thin films of large area.

However, it has also been found that it is difficult to obtain high-grade single-phase $CuInS_2$ thin films by using conventionally available two-stage processes, because various impurity phases such as $Cu_{2-x}S$, InS, In_2S_3, or $CuIn_5S_8$ are inevitably introduced in the sulfurized $CuInS_2$ film [4]. On the other hand, a single phase $CuInS_2$ film can be prepared through sulfurization of homogeneous Cu-In thin film. But the preparation of Cu-In thin film by applying a simple annealing on Cu-In alloy or Cu/In layer is nearly

impossible because, an alloy or intermetallic compound containing Cu and In at a ratio of 1:1 does not exist in the Cu-In binary system [27].

Hwang et al. prepared $CuInS_2$ thin films using flash evaporation [11]. XRD analysis showed that the films prepared at the source temperatures in the range of 1100-1450^{0}C contained In and InS phases. $CuInS_2$ peaks became more distinct at higher source temperatures. At high temperature range, the incongruent dissociation of $CuInS_2$ in vacuum could happen like this:

$$2CuInS_2 \rightarrow Cu_2S + In(I) + InS(g)\uparrow + S_2(g)\uparrow \quad [11]$$

Since $CuInS_2$ dissociates incongruently, it is very difficult to deposit single phase $CuInS_2$ thin film by the flash evaporation method. However, Agarwal et al. reported successful preparation of single-phase n-type $CuInS_2$ thin films in the year 1998 [5]. Influence of substrate temperature on the crystallinity, conductivity activation energy and optical bandgap were investigated. An increase in the conductivity activation energy was observed with increase of substrate temperature, due to the improvement in the crystallite size and crystallinity. Neumann et al. reported optical properties of $CuInS_2$ thin films prepared using flash evaporation [19].

Hwang et al. used RF sputtering for preparing $CuInS_2$ films. Stoichiometric $CuInS_2$ powder was pressed into a 1½" diameter disk under high pressure and this disk was used as the sputtering target and frequency was in the range 12 to 14 MHz [11].

Bhattacharya et al., tried to prepare copper indium sulfide films on Ti substrates using elctrodeposition [15]. Plating solution contained 6.2mM $InCl_3$, 6.2mM CuCl, 0.125M thiourea, 0.2%(v/v) Triethanolamine and 0.25%(v/v) ammonia in water. pH of the solution was kept at 2 by adding dilute HCl. Plating was carried out using a calomel reference and a platinum auxiliary electrode. As-deposited layers were annealed in Ar. A subsequent heat treatment in H_2S further improved the photoresponse. Films heated

in S vapor showed some tendency to be p-type. It was found that heating p-type layers in H_2 changed them to n-type [28].

$CuInS_2$ thin films prepared using electrodeposition from aqueous solution of Cu^+ and In^{3+} ions and thiourea with subsequent annealing in H_2S atmosphere, were characterized using photo electrochemical measurements in polysulfide electrolyte [16]. Laser scanning of photo current together with microprobe analysis correlated n-and p-type behavior with In rich and Cu rich areas respectively. p-type layers were readily prepared using this method by increasing copper to indium ratio to more than unity. They prepared $CuInS_2$ layers through electro deposition of a Cu-In alloy and subsequent sulfurization in H_2S. They also electrodeposited Cu-In alloys from cyanide electrolytes and obtained $CuInS_2$ after H_2S treatment [29].

In 1990, there is another report on elctrodeposition of Cu-In alloys for preparing $CuInS_2$ thin films [30]. In this case, Cu-In alloy was prepared using electroplating from less toxic aqueous solution containing low toxicity complexes of copper and indium with citric acid. As-deposited layers were then heated in H_2S. They noticed that Cu/In ratio in the bath had a great influence on the composition of the film.

Two mechanisms for the formation of $CuInS_2$ were proposed: one of them is direct formation from reaction between the alloy and H_2S gas while the other is formation via interdiffusion of the binary sulfides, which can be obtained at low temperatures in H_2S atmospheres.

Binsma et al. prepared $CuInS_2$ thin films via a two-stage process, with reproducible results [4]. Double layer consisting of copper covered with indium could be converted into single phase $CuInS_2$ at T>325 °C in the presence of liquid sulfur.

p-$CuInS_2$ films were deposited using spray pyrolysis in 1985 by Tiwari et al. [31]. Vijaya Lakshmi et al. prepared Mn doped p-$CuInS_2$ films using spray pyrolysis and observed an increase in band gap with Mn content in the film [32]. Later, X-ray, kinetic and optical properties of $CuInS_2$ films prepared using spray pyrolysis were

investigated by Hernandez et al. [33]. Evolution of properties of spray-deposited CuInS films with post-annealing treatment was reported very recently [34].

Samaan et al. prepared $CuInS_2$ thin films using rf sputtering in argon atmosphe ($3X10^{-2}$ Torr) with a frequency of 13.56 MHz supplied from a crystal-controlle generator via a matching unit [10]. The loose powder sputter target was prepared from p-type polycrystalline material. Rutherford Back Scattering (RBS) analysis indicate that films had an overall sulfur deficiency. They found that this deficiency was function of dc bias voltage induced on the target surface and increasing the dc bi could increase the S content of the films. $CuInS_2$ samples prepared on water-coole substrates showed presence of Ar impurities, which had been trapped during the sputte deposition process.

In 1986, Padam et al. reported for the first time, chemical deposition of CuInS thin films from a bath containing 10ml $CuCl_2.21/2H_2O$ (0.5M), 5.5ml $InCl_3$ (0.5M) 40ml thiourea (0.5M), 6ml triethanolamine (0.5M) and 20 ml ammonia (13.4M). The studied the effect of deposition parameters on the structural and electrical properties o these films [13].

Chemical bath deposition is based on slow reaction between the slowly release Cu^+, In^+ and S^- ions from their complexes, according to the following steps: [14]

$$CuCl_2 + NH_3 \rightarrow [Cu(NH_3)_4]^{2+} \quad \text{.....i}$$

$$InCl_3 + TEA \rightarrow [In(TEA)]^{2+} \quad \text{.....ii}$$

$$CS(NH_2)_2 + OH^- \rightarrow CH_2N_2 + H_2O + HS^- \quad \text{.....iii}$$

$$HS^- + OH^- \rightarrow S^{2-} + H_2O \quad \text{.....iv}$$

The overall reaction is represented in the following equation,

$$[Cu(NH_3)_4]^{2+} + [In(TEA)]^{2+} + S^{2-} \rightarrow CuInS_2 + solution \quad \text{.....v}$$

Surface topography of the films was studied using scanning electron microscope. On increasing the film thickness, grain size increased and grain boundary became better and an increase in the grain size was observed.

Tembhurkar et al. prepared $CuInS_2$ thin films using aqueous solutions of cupric chloride, indium tri chloride and thiourea [35]. Molarity of each solution was 0.003 M and were mixed in the ratio 1:1:3.2 by volume. Lattice parameters of films were calculated from X-ray diffraction measurements and the values obtained are a = 0.5524 nm, c = 1.1105nm. The tetragonal distortion $\Delta(=2-c/a)$ was -0.01031.

Polycrystalline $CuInS_2$ thin films were prepared through sulfurization of Cu-In-O films deposited from a sintered $Cu_2In_2O_5$ target by using a pulsed laser deposition (PLD) method [36]. Subsequent annealing in H_2S gas atmosphere produced $CuInS_2$ films. Films with chalcopyrite structure were obtained when Cu-In-O films were sulfurized at a temperature higher than 400°C.

Takahiro et al. reported a two-stage process in which Cu-In-O films are prepared from a $Cu_2In_2O_5$ target by pulsed laser deposition, during the first process. In the second process, these Cu-In-O films were transformed into $CuInS_2$ by annealing in H_2S atmosphere [27]

Polycrystalline thin films of single phase $CuInS_2$ were prepared from copper/ indium/ sulfide stacked layer through various heat-treatments in the nitrogen atmosphere [24]. Stacked layers were converted to single phase $CuInS_2$ at optimum heat-treatment temperature of 500 °C. Post deposition heat treatments were carried out to investigate how the as-deposited films were affected by heat treatment.

Yamamoto et al. prepared $CuInS_2$ thin films using RF sputtering from binary compounds Cu_2S and In_2S_3 [37].

One-step electrodeposition of Cu-In-S thin films using $Na_2S_2O_3$ as sulfur source was carried out for the preparation of $CuInS_2$ films [17]. Sulfur content in the film was sufficient compared with the films deposited using $CS(NH_2)_2$. These films did not show

a 'waste thread 'like morphology which is characteristic of electrodeposited Cu-In precursors.

Yukawa et al reported electrodeposited Cu_2S thin films as first step for the preparation of $CuInS_2$ films by two-stage electrodeposition [17].

$CuInS_2$ thin films were also grown through a two-step process without H_2S. Here they used elemental sulfur for sulfurization of sequentially evaporated Cu/In stalks [38].

Another method for the preparation of $CuInS_2$ absorber layers was developed by J.Penndorf et al. in 1998 [39]. This technique is called "CIS on copper tape" or "CISCuT". In a continuous roll-to–roll process, a copper tape is first electrochemically plated with In layer. This tape undergoes rapid sulfurization process in the second step at 600°C in atmospheric pressure. Different analyses reveal that in this high-speed and highly productive process, photoactive $CuInS_2$ is formed.

Miles et al. prepared Polycrystalline thin films of $CuInS_2$ using a two-step process [25]. Magnetron sputtering of alternate ultra thin layers of Cu and In resulted in the formation of $Cu_{1.1}In_9$ precursor layer. This was converted into chalcopyrite $CuInS_2$ by annealing in a closed graphite box containing elemental sulfur, at temperature around 350 °C. $CuInS_2$ thin films were grown using close-spaced vapor transport in a vertical reactor closed under vacuum. Solid iodine was used to act as the reagent. Electrical, optical and structural characterizations of the films were done. Samples grown at the low temperatures (360 °C & 370 °C) showed very high Hall mobilities that could be due to CuI, which is present in these films [12].

In 2001, there is another report on the electrical properties of Cu-In-S absorber prepared by CISCuT technique [40]. When sulfurized under special transient conditions, an internal structure with at least four different semiconducting layers was found, and this structure has a rectifying I-V characteristic without any buffer layer. Electron beam induced current (EBIC) investigation and thermo power measurement revealed pnp

structure with the n-type layer being the In-rich one. The lower part of the film contained a short- circuited p-n junction, switched in series in the opposite direction.

In the same year, another new technique, ion-layer gas reaction (ILGAR) for the deposition of $CuInS_2$ was developed by Moller et al. [41]. This technique involved chemical bath deposition of Cu(I) and In(I) salts by dipping porous substrates in appropriate precursor solutions. In a subsequent gas phase reaction with pre-heated H_2S vapor, deposited ion salts were converted into $CuInS_2$. Typical layer thickness after a single ILGAR cycle was 10-20Å, and thicker layers were obtained by repeating the process.

$CuInS_2$ and $CuIn_{(1-x)}Al_xS_2$ thin films were prepared on various substrates using the chemical spray pyrolysis technique (CSP) [42]. It was found that the nature of the substrate and the presence of Al atoms in the material noticeably affect growth and structure of the film. Annealing of $CuInS_2$ film deposited on SnO_2 resulted in best composition.

In order to get information on work function (Φ) of the film (deposited over pyrex), Kelvin method was used, which allows to determine contact potential difference $(\Phi_1 - \Phi_2)/q$ between the surface of these samples. Work function difference ($\Phi_{material} - \Phi_{probe}$) for $CuInS_2$ was -350meV. But by introducing Al atoms in the film, this was increased to -400 meV.

2.2.2 Optical Properties

Optical properties of $CuInS_2$ near fundamental edge were studied using measurements of absorption, reflectivity, electroreflectance, photoreflectance, wavelength-derivative reflectance, photovoltage and photoconductivity.

Sun et al. measured absorption coefficient of vacuum- deposited $CuInS_2$ thin films at room temperature [43]. Absorption edge corresponding to direct bandgap transition (1.54±0.02 eV) is observed in the α vs. hv graph. In p-type $CuInS_2$ thin films,

another edge is evident at lower energies (1.41-1.42eV) and is attributed to transition from a copper vacancy level to the conduction band.

Annealing a vacuum deposited p-type $CuInS_2$ film in H_2S/Ar, results in increase of magnitude of α for $h\nu>1.54$eV and sharpening of the absorption edge. In addition, the structure associated with the Cu-vacancy band diminishes. Improvement in absorption characteristics is attributed to the grain growth, resulting from the annealing procedure and reduction of copper vacancies in the film. This is probably due to two mechanisms. First is migration of copper interstitials to the lattice sites and the second is filling of sites with excess sulfur during annealing [43].

Neumann et al. studied optical absorption of flash evaporated $CuInS_2$ thin films in the photon energy range from 0.5- 4.2 eV [19]. Band gap was found to be 1.524± 0.005 eV at room temperature. Ground state energy of exciton was found to be 8± 2meV. An indirect allowed transition was observed at 1.565± 0.005 eV and was ascribed to an optical transmission from the valence band maxima at the boundary of the Brillouin zone to the lowest conduction band minimum at the zone center. Three further transitions (which were probably due to the copper d states in the valence band) were found at energies well above the fundamental edge.

$CuInS_2$ has positive temperature coefficient of energy gap below 120 K, which has been explained as the result of thermal expansion, whereas, the negative temperature coefficient above 120 K is considered to be the result of electron- phonon interaction. Contribution of electron-phonon interaction to energy gap in $CuInS_2$ was studied using photocurrents of Schottky barrier diode in the temperature range 10 to 300K [44]. Experiments done by Hsu et al. show that electron- phonon interaction for the band transition is dominated by the highest energy phonons. Wada et al. observed an increase in the bandgap of the films with annealing temperature [27].

Optical properties of sprayed $CuInS_2$ thin films in fundamental absorption region was studied by Ghafor et al. [45].

Evaporated films demonstrated two optical direct transitions of 1.5 eV and 1.72eV [14]. It was concluded that the higher gap might be due to optical transitions from the copper d states in the valance band to the lowest conduction band minimum, which disappeared due to heating. This result was confirmed by Neumann et al. [19].

2.2.2.1 Luminescence studies of $CuInS_2$

First observation of homojunction electroluminescence in $CuInS_2$ was reported by P M Bridenbaugh et al. [46]. Two peaks at 1.48 and 1.40eV were present in the 300K spectrum, whereas a deep emission at 1.42eV dominates the 77K electroluminescence spectrum.

In low temperature photoluminescence spectrum of $CuInS_2$, Emission peak at 8075Å is attributed to radiative recombination of free excitons associated with the lowest direct energy gap and is based on the observation of exciton reflection anomalies at approximately the same wavelength.

A number of investigators detected emissions at 1.446eV and 1.406eV and attributed these to the transitions between donor (V_s, In_i) and acceptor (V_{cu}) levels [47]. Characteristic emission near 1.44 eV , could be particularly promoted by sulfur annealing. Wu et al. found that 1.425eV emission was only observed in sulfur-rich thin film samples (p-type) [9].

In the case of nanoparticles of $CuInS_2$ in a glass matrix, luminescence signal was observed in the region of 700-1100 nm, corresponding to long-wavelength tail of the optical absorption [5]. Investigation of the photoluminescence at liquid nitrogen temperature revealed two maxima in the region of 870nm (1.43eV) and 960nm (1.29eV). Since ratio of their intensities is not constant, Gurinovich et al. suggested a possibility of two different channels of luminescence.

2.2.3 Electrical properties of $CuInS_2$

It is observed that electrical properties of I-III-VI compounds containing S or Se can readily be controlled by suitable annealing conditions [48]. Electrical characteristics of $CuInS_2$, which has been annealed under maximum or minimum sulfur pressures, is given in table-2. Significant changes in resistivity and mobility can be obtained by annealing at different temperatures.

Table-2

Room temperature electrical properties of annealed $CuInS_2$

Sample specificarions	Type	ρ(Ω-cm)	Carrier density (cm^{-3})	μ (cm^2/V-s)	Refere
Crystals,Annealed under maximum S pressure	P	5	1×10^{17}	15	[Ref.1; 188]
Annealed under minimum S pressure	N	1	3×10^{16}	200	[Ref.1; 188]
$CuInS_2$ thin films prepared using two-source evaporation	P	0.8-400	10^{13}-10^{16}	0.2, 3.2[c]	[(8)]
$CuInS_2$ thin films prepared using two-source evaporation	N	0.1-800	10^{14}-10^{19}	1-10, 28[c]	[(8)]

[c]Recrystallized in H_2S, initially n type.

$CuInS_2$ is readily made p-type by annealing at temperatures in the range 600-800°C for 24hr under maximum S pressure, and quenching to room temperature. On the other hand, annealing under minimum S pressure at a temperature of 650 °C for a time as short as 15 minutes results in n-type conductivity [49].

Electrical resistivity was reduced in the case of RF sputtered films by annealing the samples in argon atmosphere (10^{-2} torr) for 10 minutes at 410 °C [10]. Similar behaviour was observed by Pamplin et al. for films annealed in air at 500 °C [21].

Electrical conductivity of n-type $CuInS_2$ is governed by sulfur vacancies, copper vacancies and indium interstitials while that of p-type is controlled by interaction of sulfur and copper vacancies. Masse et al. attributed n-type conduction to the creation of sulfur vacancies and the p-type conduction to the creation of copper vacancies [50]. Wu et al further reported the existence of indium interstitials as donors in undoped $CuInS_2$ [9].

2.2.4 Different studies on $CuInS_2$ thin films

Scheer et al. studied microstructure and phase chemistry of $CuInS_2$ thin films prepared using coevaporation [6]. They found that morphology of evaporated single-layer $CuInS_2$ films depends on stoichiometry, mainly the Cu/In ratio. In- rich films had gray-black shiny region while Cu-rich regions had gray-blue and dull appearance.

Compositional relations in the ternary phase diagram of Cu-In-S can be expressed by the parameters "melecularity deviation (Δm)" and "stoichiometric deviation (Δs)".

$$\Delta m = \frac{[Cu]}{[In]} - 1 \ , \quad \text{and} \quad \Delta s = \frac{2[S]}{[Cu] + 3[In]} - 1$$

Formation of Cu chalcogenide secondary phases in films prepared using three different preparation techniques with positive non-molecularity (Δm>1) was studied by Scheer et al.[46] Using X-ray diffraction and electron spectroscopy, they found that the films prepared by coevapoaration and sulphurization has a CuS overlayer at the front surface. Segregation of CuS is not found in films prepared using spray pyrolysis [51].

Migge et al. performed a thermochemical analysis in Cu-In-S system at 298 K t estimate free energies of the compounds In_6S_7, $In_{2.8}S_4$, $CuInS_2$, $CuIn_5S_8$ and the recent discovered $CuIn_2$. They reported that free energy of $CuInS_2$ is -315 ± 54 kJ/mol [52].

Influence of post deposition annealing of coevaporated $CuInS_2$ films i hydrogen and oxygen atmosphere is studied using photoluminescence (PL) and nuclea reaction analysis (NRA) techniques [53]. Intensity of the PL peak at 1.445 eV can b drastically influenced by post-deposition treatments. This transition is ascribed to th donor-acceptor pair recombination between a sulfur vacancy and a copper vacancy They found that sulfur vacancy can be activated by hydrogen annealing and passivate by oxygen annealing.

Grzanna et al. studied chemical stability of $CuInS_2$ in oxygen at 298 K [54] b performing thermochemical analysis in the quartenary system Cu-In-S-O. They foun 12 quartenary two-phase equilibria for Cu-In-S-O system. From the predominance are diagram of Cu-In-S-O for different partial pressures of oxygen, they found that the are of existence of $CuInS_2$ become smaller and those of In_2O_3 and $In_2(SO_4)_3$ larger wit increasing oxygen pressure. The field of $CuInS_2$ just vanishes if the oxygen pressur becomes -51.5 Pascal. This pressure corresponds to the equilibrium,

$$2CuInS_2 + 6O_2 = In_2(SO_4)_3 + Cu_2S$$

Thus for oxygen pressures larger than this value, $CuInS_2$ is unstable and will b transformed into Cu_2S and $In_2(SO_4)_3$.

C.Dzionk et al. investigated reactive annealing of Cu-In precursors in H_2S atmosphere for preparing $CuInS_2$ thin films [26]. They used a combination of XRD an complementary Perturbed Angular Correlation (PAC) measurements. It is found tha $CuInS_2$ films having chalcopyrite structure can be obtained at 400 °C and 500 °C. A higher temperature, a significant loss of indium due to the formation of the volatile In compound occurs resulting in copper sulfide precipitation.

Based on these measurements they derived a model for the phase formation during reactive annealing process. In the first step, Cu-In precursors undergo a phase transformation. In the second step, In contained in the stoichiometric or In-rich precursors, is transformed into In_2S_3. Then remaining Cu-In phase reacts to form $CuInS_2$ and CuS. The binary sulfides in the third step react to form $CuInS_2$. Later reaction is incomplete in the case of In rich precursors. So In_2S_3 remains and slowly combines with $CuInS_2$ to form $CuIn_5S_8$. In Cu-rich samples, there is no In_2S_3. Hence the third reaction does not apply and CuS remains as the minor phase.

Hydrogen diffusion in $CuInS_2$ thin films was studied by measuring the spreading of implantation profiles upon annealing [55]. Hydrogen diffusion observed was too slow and was attributed to the intrinsic diffusion of hydrogen in these materials. It is found that in poly crystalline $CuInS_2$ films, hydrogen leaves the samples through pores between grains.

Interaction of atomic hydrogen with the surface of Cu-III-VI_2 chalcopyrite semiconductors was studied by Lippold et al.[56]. Technique of low energy broad beam ion implantaion into heated targets was used to introduce atomic hydrogen. They found that for temperatures above 150 °C, surface layer becomes rich in indium. Based on the results of micro Raman analysis and EDAX, they proposed a model for this effect: copper in-diffusion, caused by the filling of Cu vacancies and possible substitution of Cu by hydrogen. They also suggested that incorporation of atomic hydrogen at elevated temperatures could be a tool for controlled post growth stoichiometry variation of Cu chalcopyrite surfaces

Otte et al. implanted H^{3+} at 300eV into Cu-chalcopyrite semiconductors at temperatures between 50 °C and 300°C [57]. They found an increase of radiative recombination, which has been attributed to defect passivation due to hydrogen incorporation.

Ordering of Cu and In atoms in near stoichiometric $CuInS_2$ epitaxial films wa studied using transmission electron microscopy by Su et al. Nonchalcopyrite ordering o metal atoms was observed, which was identified as CuAu-type ordering. It was foun that the CuAu-ordered structure coexists with chalcopyrite ordered structure [58].

Matsushita et al investigated formation process of $CuInS_2$ phase from bot Cu+In+2S and CuIn+2S mixtures using Differential Thermal Analysis (DTA) an powder x-ray diffraction measurement [59]. In the chemical reaction process of forme mixture, an explosive endothermic reaction occurs at 640 °C, which is ascribed t formation of In-S materials. In the latter case, an explosive sulfurization reaction occu at about 700°C, leading to the complete formation of the $CuInS_2$ phase.

Electronic switching in thin films received much attention due to its potentia applications in electronic industry. Recently, Kanzari et al. observed current controlle electronic switching effect in amorphous p-$CuInS_2$ thin films, when sandwiche between gold and copper electrodes [60].

In solar cells made of amorphous silicon or Indium phosphide, hydrogen i either an essential part of the system or is used to improve the performance of the cells Effect of hydrogen in the chalcopyrite materials is now beginning to receive attentio Gil et al. performed muon spin rotation (μSR) experiments on $CuInS_2$ to study the effe and behavior of hydrogen in the material [61]. Muon spin rotation can provid information on the local structure and electronic configuration of isolated hydroge because; muon can be regarded as a proton analogue or 'light isotope' of hydrogen.

Recently, there was a report on microstructure and secondary phases i coevaporated $CuInS_2$ films on Mo coated glass and soda lime glass, using Rama scattering, Auger electron spectroscopy (AES), transmission electron microscopy, an x-ray diffraction techniques. Using combination of micro-Raman and AES techniques they identified that major secondary phases in Cu rich films are CuS at the surface o the as-grown layers and MoS_2 at $CuInS_2$/Mo interface. Raman spectrum of $CuInS_2$ i

characterized by the presence of dominant A_1 mode, at about 290cm^{-1}. This corresponds to vibrations of S anions in X-Y crystallographic directions of the tetragonal cell. Position and width of this peak are very sensitive to structural features [3].

Effect of post-deposition thermal treatments on properties of sprayed $CuInS_2$ was reported by Krunks et al. [62] They found that vacuum annealing at 500 °C and hydrogen treatment at 400-500 °C purify the films from secondary phases, reduced chlorine content and improved crystallinity. Vacuum annealing resulted in n-type films due to the formation of In_2O_3 phase while treatment in hydrogen reduced oxygen-containing residues resulting in p-type $CuInS_2$ films with resistivity close to 10Ω-cm.

Removal of a deleterious CuS phase in $CuInS_2$ through KCN etching is considered to be problematic. Aggour et al. developed a novel electrochemical treatment for $CuInS_2$ films, to remove the segregated CuS phase [63]. Electrochemical treatments were carried out in a glass cell having three electrode potentiostatic arrangement with a Pt counter and a saturated calomel electrode as the reference. They were able to remove CuS phase and photo effect observed using this method was as good as that obtained after the KCN etch.

Electric and magnetic properties of Mn and Fe doped $CuInS_2$ compounds were studied by Tsujii et al. [64]. Electrical conductivity changes drastically with increasing Mn concentration, indicating an increase of carrier density. It is found that susceptibility is reduced due to increase in Mn concentration, which indicates enhancement of antiferromagnetic interaction. However, magnetic ordering is not observed in these systems. For Mn doped samples, magnetization shows a step like increase around the field B_{step} = 25 T. This phenomenon was well explained by assuming the presence of Mn-Mn pairs or clusters, within which antiferromagnetic exchange interaction couples Mn ions. In the case of samples doped with Fe, magnetization increases monotonically

without any step, as antiferromagnetic interaction of Fe ions is weak since Fe-I distance is much larger than that of Mn-Mn.

Non-stoichiometric $CuInS_2$ is a novel material for thin film solar cells. Electr energy loss spectrometry analysis revealed that there are considerable late inhomogeneities on a scale of less than 100nm [65]. It is yet unknown whether Cu or surplus comes in nano precipitates irregularly distributed in the otherwise stoichiomet matrix, or forms super cells where particular atoms are replaced by their complements

2.2.5 Study of defects in $CuInS_2$

Sulfur deficient $CuInS_2$ thin films prepared using rf sputtering exhibited p-ty conductivity. This behavior in thin films is not well understood. Two different mod to identify the electrically active intrinsic defects in ternary compounds, free of a secondary phase, were proposed.

According to Neumann, one should use covalent bonding model instead of ion model to assign electrical nature of cation and anion vacancies and interstitials [66 Based on this model, group VI vacancies should act as acceptors, contrary to t assumption of ionic model, which predicts donor behavior for group VI vacancies. Th was observed in both $CuInS_2$ and $CuInSe_2$ samples, which have overall anion deficien and p-type conductivity. However, this model fails to be totally consistent, since t decreasing the anion deficiency, one should observe a decrease in the net ho concentration and not an increase as observed by Samaan et al. [10].

Noufi et al. suggest that p-type conductivity in selenium deficient CuInS accounted for, if one assigns to In a valance charge state of In^{2+} and/or In^{+} instead In^{3+}. This could also result in the creation of acceptor states. However, there is no dire experimental evidence on the different charge states of In in $CuInS_2$ or $CuinSe_2$ single crystals. Hence it seems that origin of p-type conductivity in sulfur deficie $CuInS_2$ is still an open question. Sulfur vacancies for bulk single crystal $CuInS_2$ c

form a shallow acceptor level (ΔE_A = 0.15 eV) that disappears after annealing in sulfur vapor [5].

2.2.6 Effect of incorporation of Na

Sodium incorporation into $CuInS_2$ is of great interest because controlled incorporation of Na into this material has improved cell performance remarkably. In 1997, Watanabe et al. investigated characteristics of Na-incorporated $CuInS_2$ films by intentional addition and diffusion from a soda-lime glass [67]. They observed a striking difference in the film morphology between the Na containing and Na-free $CuInS_2$ films in the size and shape of the grains. SEM micrographs revealed that Na-free $CuInS_2$ films had needle like grains on the surface. However, with sodium, grains changed significantly to large and coarse. Also the full width at half maximum (FWHM) of the (112) peak for sodium containing $CuInS_2$ films was much narrower than that of sodium free films. Enhancements in conductivity, crystallite quality and device performance is also reported in controlled Na- incorporated $CuInS_2$.

In 1998, they investigated effects of intentional Na incorporation on electrical conductivity of Cu-poor $CuInS_2$ thin films [68]. These films were deposited through sulfurization of In-S/Cu/Na_2S/In precursors. Sodium incorporation resulted in a remarkable increase in conductivity and cell efficiency of $CuInS_2$-based solar cells. Photoluminescence measurements revealed that enhancements were due to annihilation of donor states, (most likely In interstitials) by sodium incorporation.

Changes in the electronic structure of $CuInS_2$ thin films due to Na incorporation were studied by Fukuzaki et al. [69]. XPS spectra were recorded for Na free Cu deficient $CuInS_2$ and Na incorporated films. Peaks corresponding to Cu 2p, In 4d and S 2p of $CuInS_2$ films were shifted by –0.5 eV, due to Na incorporation. They suggested formation of a new (Na,Cu)InS_2 phase on the film surface. Electron density of states increased by Na incorporation and increments were larger for films with larger Cu

deficiency. They propose that the electrons were delivered from Na_{Cu} into the valen band of the Cu-deficient p-$CuInS_2$.

Yamamoto et al. investigated electronic structures of Na-incorporated In-ric $CuInS_2$, based on *ab initio* electronic band structure calculations. They found th formation of ionic Na_{Cu}-S bond decreases Madelung energy, resulting in a shift i energy levels of S 3p orbitals, in the vicinity of Na atoms, towards lower ener regions [70]. Mobile Na will act as a passivator of donor states such as In_{Cu} an interstitial In.

2.2.7 Etching of $CuInS_2$ films using KCN

Dissolution of metal chalcogenides in cyanide solutions is established since lo before and was applied in surface treatment of solar cells. KCN is known to dissol copper selenides and copper sulfides and was used successfully to prepare CuGaS based solar cells from very Cu-rich material [71]. Post deposition stoichiometr adjustment can be done using chemical etching step, using KCN. Complexing of copp by cyanide results in soluble species allowing to remove a variety of electronicall deleterious copper chalcogenides [51].

In order to remove quasi-metallic CuS layer, which predominantly precipitat at the front surface of the Cu-rich films, Scheer et al. chemically treated the samples in XCN solution with X = Na, K [72].

Ogawa et al. have also applied KCN treatment on the $CuInS_2$ film [73]. For thi $CuInS_2$ film was dipped in aqueous solution of 10% KCN for 3 minutes at roo temperature and rinsed in deionized water. They found that after KCN treatment, Cu/ ratio was lowered to ~1 and is almost independent of the ratio existing before treatmer Resistivity increased by a factor of ~100, mainly due to a reduction of excess carri concentration.

Hashimoto et al. found that KCN treatment adjusted the conduction band offsets from –0.7eV to –0.05eV. It also changed the interface Cu/ In ratio at the interface. KCN treatment removed Cu_xS phase or corrected structurally poor interface and made the band offsets close to the theoretical estimation [74].

2.3 $CuInS_2$ based solar cells

For economical reasons as well as because of the possibility of large-scale production, thin-film photovoltaic technology had been identified as an effective method, during the 1970s itself. But if the thin-film device is to be cost effective, substantial increase in device efficiency must be attained.

In 1977, Kazmerski et al. reported fabrication and characterization of vacuum deposited thin-film heterojunctions of several ternary compounds, including $CuInS_2$ [75]. $CuInS_2$ films were grown by dual source deposition technique and CdS window layer was evaporated from a Ta- baffled source. Substrates were polished alumina with a Zn-Au-metallization for back contact. Efficiency of the $CuInS_2$/CdS cell was 2.55%.

First ternary thin film homojunction device (n-p $CuInS_2$) solar cell was also reported in the same year by Kazmerski et al.[76]. Here also, $CuInS_2$ films were grown using dual source deposition technique, employing a resistive-heated quartz crucible for single-phase ternary powder and a Ta boat for sulfur. Purpose of second chalcogen source was to alter S content in the film during the growth and hence, to control carrier type. Device with efficiency η= 3.33% was reported and the best efficiency obtained was 3.62%.

In 1979, Gorska et al. reported an attempt to prepare solar cells using spray pyrolysed $CuInS_2$ thin films [77]. They prepared heterojunction by spraying $CuInS_2$ onto heated CdS single crystals. However, photoactivirty was very poor. They also

prepared an all-thin- film heterojunction device, by spraying CdS over the $CuInS_2$ laye In this case also, voltage and current values obtained were very low. (Voc ≈ 0.25V an Isc ≈ 0.004mA/cm^2 respectively).

Totally sprayed $CuInS_2$/Cd(Zn)S cell with an efficiency of 2.66% was reporte by Ram et al., in 1985 [78].

Heterojunctions of hydrogenated a-Si films prepared by R.F.sputtering, wi spray pyrolysed $CuInS_2$ films have been reported by Kumar et al., in 1986 [79 Capacitance- voltage measurements showed the formation of a abrupt heterojunctio exhibiting photovoltaic behavior with Voc = 220mV and Isc = 0.20mA/ cm^2.

In 1992, Walter et al. investigated heterojunctions formed with coevaporate $CuInS_2$ and $CuIn(Se,S)_2$, an alloy of $CuInS_2$ with $CuInSe_2$ [71] . During spectr response measurements, he observed reversal of photocurrent for certain wavelengt range even at zero bias condition. This was attributed to the presence of quasi-metalli CuS phase, because the reversed photocurrent could not be observed in samples etche using KCN. They could get efficiency of 6.1% for a (Zn,Cd)S / $CuInS_2$ solar cell and a efficiency of 10.1% ZnO / CdS/ $CuIn(Se,S)_2$ structure.

In 1993, Scheer et al. prepared heterojunctions having structure glass/ Mo/ p $CuInS_2$/ n-CdS/ n^+-ZnO/ Al with an efficiency of 10.2% [72]. Absorber layer wa deposited using the technique of coevaporation of the elements and over this, CdS laye was deposited from a chemical bath. Sputtered ZnO:Al layers served as transparen conductive window layer. Although they attempted to fabricate a configuration o $CuInS_2$ / ZnO also, without the bath-deposited CdS, those cells exhibited much lowe photovoltages than in the previous case. Mitchel et al. reported 7.3% efficiency for ZnO/ CdS/ $CuInS_2$ thin-film cell [80].

In 1994, an efficient thin-film photovoltaic cell was fabricated using th heterostructure consisting of $CuInS_2$ film obtained by sulfurization of a metalli precursor, a chemical bath deposited CdS layer and an atom-beam-sputtered In_2O_3 fil

[73]. A preceding KCN treatment of the Cu-rich $CuInS_2$ film lowered the Cu/In ratio and raised the resistivity. Conversion efficiency obtained was 9.7%.

In the same year, 3.1% efficient solar cell was reported by Uenishi et al [81]. This heterojunction had atom beam sputtered ZnO film, chemical bath deposited CdS layer, and $CuInS_2$ film prepared using sulfurization of metallic precursor. Cells prepared with Cu/In ratio 1.68 had an efficiency of 1.2%, while cells having Cu/In ratio 1.85 exhibited an efficiency of 2.75%. But an efficiency of 3.15% was obtained for a film with Cu/In ratio 1.21 after annealing in vacuum at 150^0C for 30 minutes.

According to Hovel, for a heterojunction solar cell, the best photovoltaic out put will be obtained, when conduction band offset (ΔE_c) is small [82]. If ΔE_c is positive, a notch is found in the absorber. But if ΔE_c is negative, open circuit voltage is limited by the built in potential, which is smaller than the bandgap of the absorber layer material by $-\Delta E_c$.

In 1995,Hashimoto et al. reported the band offsets at the $CuInS_2$/ CdS interface, determined by XPS [74]. In order to accurately calculate the band offsets, they measured $Cd4_d$ and $In4_d$ core levels as well as the valence band maximum (VBM). Then the band offsets are given by

$$\Delta E_v = E_{v-In4d} - E_{v-Cd4d} - \Delta E_{CL} \text{ , and}$$

$$\Delta E_c = -\Delta E_v - E_g(CuInS_2) + E_g(CdS)$$

ΔE_{CL} is the energy difference between Cd4d and In4d levels of CdS/ $CuInS_2$ heterojunction and the values were, $\Delta E_v = 1.8 \pm 0.3$eV and $\Delta E_c = -0.7 \pm 0.4$eV

After KCN treatment for removing degeneracy in carrier concentration, band offset changed to $\Delta E_v = 1.08 \pm 0.1$eV and $\Delta E_c = -0.05 \pm 0.15$eV. KCN treatment not only reduced carrier concentration of the $CuInS_2$ film, but also improved the interface to establish alignment of conduction band minima.

In 1996, Braunger et al. showed that in $CuInS_2$ based heterojunctions, CdS can be replaced by $In_x(OH,S)_y$, which is Cd free buffer layer [83]. For the fabrication of this, $CuInS_2$ thin layer was formed using thermal coevaporation of the three elements and the secondary CuS phase was removed by KCN etching. Cd-free buffer layer was deposited from aqueous solution of thioacetamide (CH_3CSNH_2) and $InCl_3$ at room temperature as well as temperature up to 70 °C. The highest efficiency of this Cd-free, Se-free thin film chalcopyrite cell was 11.4%.

In almost all solar cells made from Cu-rich $CuInS_2$ films, KCN treatment was essential to remove the secondary CuS phase, and to improve efficiency of the cell. Watanabe et al. tried to prepare high efficiency $CuInS_2$ solar cell without using poisonous KCN treatment [84]. For this, $CuInS_2$ films were prepared using a two-stage process in which Cu-In-S precursors were sputtered in H_2S/Ar and then annealed in H_2S atmosphere. They felt that reduction of secondary phases in In-rich samples is very important to obtain high efficiency without using poisonous KCN. They achieved an efficiency of 6.3% for the ITO/ CdS/ $CuInS_2$ structure, without KCN treatment.

CdS has been successfully used as buffer layer for Cu-III-VI_2 thin film absorbers for a long time. However from the point of view of environmental safety, the development of a Cd-free material is highly desirable. Finding out an alternative for CdS to produce Cd-free solar cells has been one of the most important intentions of several research groups working in this field. Several new n-type layers have been used to fabricate heterojunction with $CuInS_2$ films.

Crystalline silicon (c-Si) is one such material. Lattice mismatch of 2% between c-Si and $CuInS_2$ is quite moderate. First epitaxial Si / $CuInS_2$ heterojunctuion device was reported in the year 1997 by Metzner et al [85]. They deposited slightly Cu-rich $CuInS_2$ epilayers on sulfur terminated Si-(111) surfaces of n-type wafer. The heterojunction was completed by the deposition of indium tin oxide (ITO) layer and Ga

metallic back contacts. However, photoactivity of the device was very low. AM 1.5 illumination yielded a photocurrent of only 1.2mA.

Ennaoui et al. used ZnO, a material having band gap higher than that of CdS, as buffer layer for $CuInS_2$ solar cells [86]. ZnO films were prepared using chemical bath deposition or successive ionic layer adsorption and reaction (SILAR) method. Due to the large bandgap of the ZnO buffer layer, an enhanced response in the short wavelength of the spectrum was observed. However, the cells had lower efficiency (~ 3.8%).

Solar cells were fabricated using $CuInS_2$ thin-films prepared through sulfurization of Cu-In-O precursors in H_2S gas in H_2 atmosphere [87]. The cell having structure ITO/ ZnO/ CdS/ $CuInS_2$/ Mo/ glass, was fabricated after KCN treatment. Performance of these cells was studied as a function of the H_2 gas pressure during sulfurization and found that open-circuit voltage, short circuit current and fill factor increased with increasing the H_2 gas pressure. Conversion efficiency of the cell was strongly affected by the reduction of Cu-In-O precursors and the best cell had an efficiency of 7.5%.

Cells were also fabricated using $CuInS_2$ thin films through sulfurization of sequentially deposited Cu/In stacks with elemental sulfur. The window layer CdS/ZnO was deposited after removal of CuS secondary phase segregated at the surface by KCN etch and could get an efficiency of 10.4% [38]

In 1997, there was an interesting report by Scheer et al. They found that annealing of Cu-poor coevaporated films in S atmosphere during an extended cool-down period enhanced the lateral conductivity at room temperature [88]. They also observed an improvement of solar cell parameters of the $CuInS_2$/ CdS/ ZnO cells fabricated using films subjected to the cool-down process. This influence was explained by the saturation of S vacancies during the cool-down period. By reducing the cooling

rate from 10K/min to 2K/min, efficiency increased from 3% to 8.3%, under AM 1.
simulations.

Without toxic KCN treatment, conversion efficiencies of over 6% was achieve by using $CuInS_2$ films prepared by sulfurization of precursors containing Na, while th cells using Na-free absorber layers showed poor cell performance of about 1%. N incorporation was carried out deliberately by adding layer of a sodium compoun between the precursor and the Mo electrode. The enhancement of V_{oc} (from 0.235V t 0.665V) and FF (from 0.270 to 0.526) is striking compared with J_{sc}. However, high concentrations of Na reduced cell efficiency [67]. They speculate that this must be du to the formation of $NaInS_2$ phase, which is highly resistive.

Nature of substrates has very much influence on the properties of the fil deposited over it. In the case of $CuInS_2$ films prepared by sulfurization of metall precursors deposited on Mo coated soda lime glass, it was observed that Cu-rich film often peeled off from the substrate. Film's adhesion to the substrate was significantl improved by introducing a very thin Ga layer between the Mo surface and the stacke Cu/In precursor layer [89]. An efficiency of 10.5% was obtained using this adheren thin film. Comparable efficiency was obtained for cells prepared on Pt substrates.

An 8.25% efficient $CuInS_2$ solar cell having a four-layer structure (low ρ $CuInS_2$/ high ρ-$CuInS_2$/ high ρ-CdS/ low ρ-CdS) was fabricated by Park et al.[90]. The found that lattice mismatch between $CuInS_2$/ CdS has reduced to 2.8%.

The highest efficiency reported so far for $CuInS_2$ based solar cells is 11.1% (total area efficiency) or 12.5% (active area efficiency) for a $CuInS_2$/ CdS/ ZnO structure with MgF_2 antireflection coating [91]. In this work, they used a sequentia process; at first the metal layers were deposited using DC magnetron sputtering an later this was sulfurized using elemental sulfur vapor. Heterojunctions were the prepared using chemical bath deposited CdS and a sputtered transparent conductin

ZnO window layer. The best cell with lowest defects was made from copper rich precursor layer having Cu/In ratio 1.8.

Gal et al. electrodeposited films of size quantized CdS as buffer layer on the $CuInS_2$ [92]. The resulting $CuInS_2$/CdS thin film solar cells exhibited higher photocurrents and conversion efficiency (11.4%) than those made with conventional non-quantized CdS films. This was mainly due to the increased band gap of quantized CdS, allowing more light to reach the active $CuInS_2$ layer.

$CuInS_2$ thin films prepared through the new 'CISCuT' technique mentioned earlier [39] was also been used for preparing solar cells. Attempts to prepare conventional p-$CuInS_2$/ n-CdS heterojunction failed all the time. Surprisingly, only a structure of $CuInS_2$/ p-type semiconductor leads to a diode characteristic. ZnTe, Cu_2O, $Cu_{2-x}S$ and Cu(S,O) have successfully been used to form such devices. First solar cell made from this material {$CuInS_2$/ Cu(S,O)} had an efficiency of 6.1%.

As incorporation of Na increases conductivity of $CuInS_2$, Watanabe et al. prepared solar cells using Na incorporated $CuInS_2$ [68]. These films were prepared through sulfurization of In-S/ Cu/ Na_2S/ In precursors. The cell structure was ITO/ CdS/ $CuInS_2$/ Mo/ SiO_2/ SLG, and efficiency was 8.8%.

In order to have further improvement in efficiency of the cells fabricated using Na-incorporated $CuInS_2$ thin films, it was felt that there should be an increase in the open circuit voltage and hence the band gap has to be increased. Gallium (Ga) is commonly used as isovalent substitute for In, in order to increase the band gap. Watanabe et al. could attain higher open circuit voltage (exceeding 0.80V) by adding Ga to Na-incorporated $CuInS_2$ thin films [93]. $Cu(In,Ga)S_2$ films were prepared through the sulfurization of Na-containing Cu-In-Ga precursors in H_2S atmosphere. The cell structure was ITO/ ZnO/ CdS/ $Cu(In,Ga)S_2$/ Mo/ Ti/ SiO_2/ SLG and the efficiency was 11.2% which is the highest efficiency reported for $CuInS_2$ solar cells fabricated without KCN treatment

Until recently, there have been a few studies to elucidate conversion losses, which limit performance of the thin film $CuInS_2$ solar cells. Device or material parameters involved in its performance remain still unknown. Kneisel et al. applied thermal admittance spectroscopy to characterize trap properties of high efficiency $CuInS_2$/ CdS/ ZnO thin film solar cells. Defect spectra revealed that there is no dependence on the buffer layer. Two pronounced trap levels were found at 0.3 eV and 0.5 eV [94]. Both were identified as majority carrier traps in bulk p-$CuInS_2$ space charge region. The trap at 0.5 eV is correlated with a decrease in open circuit voltage of the cell.

Hashimoto et al. analyzed CdS/ $CuInS_2$ heterostructure using XPS [74]. Band offsets at CdS/ $CuInS_2$ interfaces formed on untreated $CuInS_2$ as well as those formed on KCN treated $CuInS_2$ were precisely determined by measuring core-level binding energies. They found that KCN treatment reduced conduction band offset (ΔE_c) from ~0.7 eV to a very small value of 0.05 eV and correspondingly, cell efficiency increased from 3.01% to 9.67%.

Performance of $CuInS_2$ solar cell, consisting of a transparent conductive oxide/ CdS/ $CuInS_2$ heterostructure have been analyzed by Ito et al. [95]. A theoretical model, in which a very thin n-type $CuInS_2$ layer is assumed to exist at the interface between the p-type $CuInS_2$ and the n-type CdS buffer layer, was developed to explain the characteristics. In this case, an n-n heterojunction was formed between n-type CdS buffer layer and n-type $CuInS_2$ layer. Two types of junctions(an abrupt junction and a graded junction) were theoretically discussed.

$CuInS_2$ solar cells were prepared by "rapid thermal process (RTP)" using a sequential preparation in which metallic layers of Cu and In are rapidly heated in presence of elemental sulfur vapor [96]. It is found that RTP improved crystal growth at

detrimental phases can be avoided by passing intermediate temperatures rapidly. Cells prepared from these films could reach 11.4% (total area) efficiency.

Recently, Klaer et al reported development of $CuInS_2$ based mini-module on 5x5 cm^2 glass substrate with 9.2% efficiency [97]. It consisted of 7 integrated series connected cells, with a total area of 16.2cm^2. Absorber layer was grown using a sequential process, consisting of deposition of metallic films using sputtering followed by sulfurization in elemental sulfur vapor. Layer structure of the complete module was Mo/ $CuInS_2$/ CdS/ ZnO.

It is well known that for polycrystalline cells, grain size must be large compared with the absorbing layer thickness, if an appreciable fraction of short circuit current potentially available is to be realized in practice. Onama et al. developed a process to fabricate higher efficiency solar cells using large grain $CuInS_2$ thin film synthesized from sulfur precursor [98]. They could prepare films with a maximum thickness of 9μm, having very large grains. To prevent peeling from substrate, a very thin Pt or Pd layer was deposited between the Mo and $CuInS_2$. They characterized $CuInS_2$ absorbers having different film thicknesses varying from 2-9μm and related this to the performance of the photovoltaic device. The higher limit of film thickness for high efficiency device was found to be about 4 μm. Devices using thick films (>4 μm) gradually showed low efficiency and low stability in spite of high quality of the film. It is worth noting that device with very thick absorber layer (9 μm) showed a low efficiency. However, when the layer was thinned by chemical etching process, the cells showed an efficiency of ≈ 12%.

For CISCuT cells, commonly used p-type buffer layer is Cu(O,S), with a band gap of 2.6 eV. To increase the cell performance, CuI buffer layer with a higher band gap of 3.1 eV has been used. This lead to an improvement in performance of CISCuT cell from 3.89% to 5.2% [99].

Luck et al. investigated influence of different Na concentrations on $CuInS_2$ fil and corresponding $CuInS_2$/CdS/ZnO thin-film solar cells [100]. While morphology the absorbers seemed to be not affected by this variation, corresponding PL spec differed significantly. Properties of the cells, however, showed no dependence on concentration. This implies that even though the defect chemistry of $CuInS_2$ is chan by the presence of Na, this influence has no impact on properties of corresponding sc cells.

Preliminary results of a new cell designed using an extremely thin Cul absorber (eta-solar cell) has been reported recently [101]. Absorber is embedded i porous and transparent structure in order to increase effective path length of light in absorbing material and to attain high absorption. For this, nano-porous /micro-por TiO_2 films were deposited over SnO_2/glass substrates using screen-printing /sp pyrolysis and $CuInS_2$ layer was deposited using ion layer gas reaction (ILGA Heterojunction was completed with electrodeposited p-type CuSCN layer. Multi scattering within porous structure and effective separation of charge carriers within depletion layer were obtained using an absorber layer of thickness 540nm.

Solar cell parameters, structure, and preparation methods of some of the repor cells are tabulated in Table-2.3

Table-2.3

Cell structure	Method of fabrication of different layers	Solar cell parameters					Reference
		Voc mV	Jsc/Isc mA/cm ^{2}	FF	η %	Cell area(c m^2)	
$CuInS_2$/ CdS	CIS- Dual source evaporation CdS - CBD	–	–	–	5.42	–	Kazmerski et al., 1977 , [75]
n-$CuInS_2$/p-$CuInS_2$	CIS- dual source evaporation CdS- CBD	410	2.34m A	0.43	3.33	0.124	Kazmerski et al., 1977, [76]
$CuInS_2$/Cd(Zn)S	CIS & Cd(Zn)S – Spray pyrolysis	440	8.25	0.27	2.66	–	Raja Ram et al., 1985, [78]
Al/p-$CuInS_2$/a-Si:H/SnO_2:F/glass	-	220	0.20	–	–		Kumar et al., 1986, [79]
(Zn,Cd)S/$CuInS_2$	Three source evaporation	549	19.82	0.56	6.1	–	Walter et al., 1992, [71]
ZnO/CdS/CuIn(Se,S)$_2$	–	492	31.2	0.66	10.1	–	Walter et al., 1992, [71]
Mo/CuInS2/CdS/ZnO	Cis-three source evaporation, CdS-CBD, ZnO-	697	21.5	0.69	10.2	0.4	Scheer et al., 1993,[72]
In_2O_3/CdS/$CuInS_2$	CIS- sulfurization of metallic precursors, CdS-CBD, In_2O_3-	717	22.1	0.61	9.7	–	Ogawa et al., 1994,[73]

Cell structure	Method of fabrication of different layers	Solar cell parameters					Reference
		Voc	Jsc/Isc	FF	η %	Cell area(cm^2)	
ZnO/CdS/$CuInS_2$	CIS-sulfurization of metallic precursors, CdS-CBD, ZnO-Sputtering	570	13.4	0.41	3.1	—	Uenishi et al., 1994,[81]
ZnO/In(OH,S)/$CuInS_2$	CIS-thermal coevaporation, ZnO-	735	23.2	0.67	11.4	.0.38	Braunger et al.,
ITO/CdS/$CuInS_2$	CIS-reactive sputtering with H2S gas, CdS-CBD, ITO-magnetron	547	22.5	0.51	6.32	0.08	Watanabe et al., 1996,[84]
Ga/n-Si/p-$CuInS_2$/ ITO	Cis-epitaxial deposition, Csi-wafers, Ga-metallic alloying,	—	1.2	—	—	—	Metzner et al., 1997,[85]
ITO/ZnO/CdS/$CuInS_2$/Mo/glass	CIS-sulfurization of Cu-In-O, CdS-CBD,	702	16.2	0.65	7.50	—	Negami et al.,
$CuInS_2$/CdS/ZnO	CIS-coevaporation, CdS-CBD, ZnO-sputtering	596	23.4	0.61	8.3	—	Scheer et al., 1997,[88]
$CuInS_2$/CdS/ZnO	CIS-sulfurization of Cu/In stacks, CdS-CBD, ZnO-sputtering	714	22.9	0.64	10.4	—	Klenk et al., 1997,[38]

Cell structure	Method of fabrication of different layers	Solar cell parameters					Reference
		Voc	Jsc/Isc	FF	η %	Cell area(cm^2)	
SLG/Mo/CuInS2/CdS/ZnO:Al	CIS-reactive sputtering, CdS-CBD, ZnO RF	665	18.9	0.52	6.61	.06	Watanabe et al., 1997,[91]
In_2O_3/CdS/$CuInS_2$	CIS-sulfurization of Cu-In precursors, CdS-CBD,	700	24	0.63	10.5	—	Nakabayashi et al., 1997,[89]
Low ρ $CuInS_2$/high ρ $CuInS_2$/ high ρ CdS/low ρ CdS	Electron beam evaporation	580	30.6	0.697	8.25	—	Park et al., 1997,[90]
ZnO/$CuInS_2$	ZnO-CBD	360	19.4	0.55	3.8	—	Ennaoui et al., 1998,[86]
$CuInS_2$/CdS/ZnO/MgF_2	CIS-sulfurization of Cu/In ,	728	21.4	0.71	11.1	—	Klaer et al., 1998,[91
$CuInS_2$/CdS/ZnO:Al	CIS-coevaporation , CdS-	745	21.6	.71	11.4	0.5	Gal et al., 1998,[92]
n-$CuInS_2$/Cu(S,O)	CIS-CISCuT, Cu(S,O)-thermal deposition	653	16.1	0.57	6.1	3	Penndorf et al., 1998, [39]

Cell structure	Method of fabrication of different layers	Solar cell parameters					Reference
		Voc	Jsc/Isc mA/cm^2	FF	η %	Cell area (cm^2)	
SLG/SiO_2/Mo/$CuInS_2$/ CdS/ITO	CIS-sulfirization of In-S/Cu/Na2S/In, CdS-CBD, ITO-RF sputtring	715	20.5	0.59	8.8	–	Watanabe et al., 1998, [68]
ITO/ZnO/CdS/$Cu(In,Ga)S_2$	CIGS-sulfurization of Cu-In-Ga , CdS-CBD, Mo/Ti & ZnO- sputtering	802	20.9	0.66	11.2	–	Watanabe et al., 1999, [93]
Mo/ $CuInS_2$/ CdS/ZnO/ MgF_2	CIS- rapid thermal process, CdS-CBD, ZnO-sputtring	729.4 mV	21.83	0.71	11.4	0.511	Siemer et al., 2001,[96]
Mo/$CuInS_2$/CdS/ZnO (mini module)	CIS- sequential deposition, CdS-CBD, ZnO-sputtering	5.09V(72 7mV/cell)	19.1	0.65	9.2	16.2	Klaer et al., 2001, [97]

2.4 Significance of present study

We developed two new methods for the preparation of $CuInS_2$ thin films. The first one is starting from CBD Cu_xS. In this method, $CuInS_2$ film was prepared by evaporating indium over CBD Cu_xS and subsequently annealing the bilayer in vacuum. In the second method, we prepared $CuInS_2$ using Cu_xS film prepared from CBD CdS (using Clevite process). Attempts were made to fabricate $CuInS_2$/ CdS solar cells using $CuInS_2$ films prepared by these two techniques. However, photoactivity was observed only for the cell fabricated using $CuInS_2$ films prepared starting from CBD CdS. Although open circuit voltage of the junction was quite measurable, current was very feeble.

Also we made attempts to fabricate 'all-sprayed' SnO_2:F/$CuInS_2$/CdS solar cell. For this purpose, we characterized CSP $CuInS_2$ films using XRD, Absorption and transmission studies. In addition, we used XPS analysis to investigate atomic concentration percentage of each element present in the film, from surface up to the substrate. Also photosensitivity was measured by irradiating the sample under illumination (intensity 40 mW/cm^2) and the sample with best photosensitivity was used for fabricating solar cell.

We could fabricate an 'all-sprayed cell' with an efficiency 1.3% (~1.9% when corrected for transmission losses at the SnO_2:F layer). When low resistive CdS film was used as the window layer, there was slight increase in efficiency to 1.7% (~ 2.4% after correction). In most of the efficient solar cells, usually a thin layer of ZnO is deposited over CdS layer. An improvement in efficiency may be obtained using all sprayed $CuInS_2$/CdS/ZnO structure. In our lab, efforts are being made in this direction. Also, since there is a great interest in replacing CdS by a Cd-free buffer layer, $CuInS_2$/In_2S_3 solar cells can be fabricated with chemical spray pyrolysed In_2S_3.

2.5 Conclusion

A review of $CuInS_2$ thin films is made and its preparation, optical properties and electrical properties are arranged separately. Results of etching of $CuInS_2$ using KCN, effect of incorporation of sodium, results of defect studies and different other studies are also discussed. A review on solar cells based on $CuInS_2$ thin films is made and some of the reported devices are tabulated.

References

[1] J.L Shay and J.H.Wernick, Ternary Chalcopyrite Semiconductors: Growth, Electronic properties and Applications, Pergamon Press, Oxford,(1975) p-4

[2] David Cahen, *Solar Energy Materials*, 15 (1987) 225

[3] J Alvarez-Garcia, A Perez-Rodriguez, A Romano-Rodrigues, J R Morante, L Calvo-Barrio, R. Scheer and R Klenk, *J. Vac. Sci. Technol. A*, 19 (2001) 232

[4] J. J M Binsma, and H a Van Der Linden, *Thin Solid Films*, 97 (1982) 237

[5] L I Gurinovich, V S Gurin, V A Ivanov, I V Bodnar, A P Molochko and N P Solovei, *Phys. Stat. sol.(b)*, 208 (1998) 533

[6] R.Scheer, K.Diesner, H.-J.Lewerenz, *Thin Solid Films*, 268 (1994) 130

[7] J.L Shay and J.H.Wernick, Ternary Chalcopyrite Semiconductors: Growth, Electronic properties and Applications, Pergamon Press, Oxford, (1975) p-50

[8] L L Kazmerski, M S Ayyagari, and G A Sanborn, *J. Appl. Phys*, 46 (1975) 4865

[9] Y.L.Wu, H.Y.Lin, C.Y.Sun, M.H.Yang, and H.L.Hwang, *Thin Solid Films*, 168 (1989) 113

[10] A N Y Samaan, S M Wasim, A E Hill, D G Armour and R D Tomlinson, *Phys. Stat. Sol.*(a), 96 (1986) 317

[11] H L Hwang, C Y sun, C Y Leu, C L Cheng and C C Tu, Revue De Physique Appliquee, 13 (1978) 745

[12] K. Djessas, G. Masse, and M. Ibannaim, *J.Electro. Chem. Soc.*, 147 (2000) 1235

[13] G K Padam and S U M Rao, *Solar Energy Materials*, 13 (1986) 297

[14] Siham Mahmoud and Abdel-Hamid Eid, *Fizika A*, 6 (1997)171

[15] R N Bhattacharya, David Cahen and Gary Hodes, Solar Energy materials, 10 (1984) 41

[16] Gary Hodes, Tina Engelhard, David Cahen, L.L.Kazmerski and Charles R Herrington, *Thin Solid Films*, 128 (1985) 93

[17] Sigeyuki Nakamura and Akio Yamamoto, *Sol. Energy Mat. Sol. Cells*, 49 (1997) 415

[18] M K Agarwal, P D Patel, Sunil H Chaki and D Lakshminarayana, Bull. Mater. Sci., 21 (1998) 291

[19] H.Neumann, W Horig, V.Savelev, J.Lagzdonis, B. Schumann, and G.Kuhn, *Thin Solid Films*, 79 (1981) 167

[20] G.Hodes, D.Cahen, J. manassen, and M.David, *J. Electrochem. Soc.*, 127 (1980) 2252

[21] B. Pamplin and R.S.Feigelson, *Thin Solid Films*, 60 (1979) 141

[22] P.Rajaram,R. Thangaraj, A.K.Sharma, A.Raza and O.P. Agnihotri, *Thin Solid Films*, 100 (1983) 111

[23] A.N. Tiwari, D.K. Pandya, and K.L.Chopra, *Thin Solid Films*, 130 (1985) 217

[24] S.K.Kim, W.J.Jeong, G.C.Park, Y.G.Back, Y.G.Jeong, and Y.T.Yoo, *Synthetic Metals*, 71 (1995) 1747

[25] R W Miles, K T Ramakrishna Reddy, I Forbes, *J. Crystal Growth*, 198/199 (1999) 316

[26] C. Dzionk, H.Metzner, S.Hessler, H.-E. Mahnke, *Thin Solid Films*, 299 (1997) 38

[27] Takahiro Wada, Takayuki Negami, and Mikihiko Nishitani, *Appl. Phys. Lett*, 63 (1993) 1943

[28] J J M Binsma, L.J. Giling and J.Bloem, *J. Luminescence*, 27 (1982) 35

[29] G Hodes and D Cahen, *Sol. Cells*, 16 (1986) 245

[30] J Herrero, and J Ortega, *Solar Energy Materials*, 20 (1990) 53

[31] A. N. Tiwari, D.K. Pandya, and K. L. Chopra, *Thin Solid Films*, 129-131 (1985) 217

[32] R.P. Vijaya Lakshmi, R. Venugopal, D. Raja Reddy and B. K. Reddy, *Solid State Communications*, 82 (1992) 997

[33] J. Gonzalez-Hernandez, P.M Gorley, P. P. Horley, O. M. Vartsabyuk, and Yu.V. Vorobiev, *Thin Solid Films*, 403/404 (2002) 471

[34] S. Marsillac, M.C. Zouaghi, J.C. Bernede, T. Ben Nasrallah, and S. Belgacem, *Sol. Energy Mat. Sol. Cells*, [Article in press]

[35] Y D Tembhurkar and J P Hirde, *Bull. Mater. Sci.*, (1992) 143

[36] Takahiro Wada, Takayuki Negami, and Mikihiko Nishitani, J. *Mater.Res.*, 8 (1992) 545

[37] Y. Yamamoto , T. Yamaguchi, T. Tanaka, N. Tanahashi, and A. Yoshida, *Sol. Energy Mater. Sol.Cells*, 49 (1997) 399

[38] R. Klenk, U. Blieske, V. Dieterle, K. Ellmer, S. Fiechter, I. Hengel, A. Jager-Waldau, T. Kampschulte, Ch. Kaufmann, J. Klaer, M.Ch. Lux-Steiner, D. Braunger, D. Hariskos, M. Ruckh, H.W.Schock, *Sol.Energy Mat. Sol. Cells*, 49 (1997) 349

[39] J. Penndorf, M. Winkler, O. Tober, D. Roser, K. Jacobs, *Sol. Energy Mater. Sol. Cells*, 53 (1998) 285

[40] 40[(44) I. Konovalov, O. Tober, M. Winkler, and K. Otte, *Sol. Energy Mater. Sol. Cells*, 67 (2001) 49

[41] J. Moller, Ch.-H. Fischer, H. J. Mufffler, R. Konenkamp, I. Keiser, C. Kelch, and M.Ch. Lux-Steiner, *Thin Solid Films*, 361/362 (2000) 113

[42] N. Kamoun, N. Jebbari, S. Belgacem, R. Bennaceur, J. Bonnet, F. Touhari, and L. Lassabatere, *J. Appl. Phys.*, 91 (2002) 1952

[43] L Y Sun, L L Kazmerski, A.H Clark, P J Ireland and D W Morton, *J. Vac. Sci. Technol.*, 15 (1978) 265

[44] T.M.Hsu, *Physics Letters A*, 133 (1988) 79

[45] W A S Abdul Ghafor, N. A. Awad , and N.S.Othman, *Indian J. Pure & Appl. Phys.*, 31 (1993) 123

[46] P M Bridenbaugh and P Migliorato, *Appl. Phys. Lett.*, 26 (1975) 459

[47] A.W.Verheijen, L.J.Giling, and J. Bloem, *Mater. Res. Bull.*, 14 (1979) 237,

[48] B.Tell, J.L Shay and H M Kasper, J.Appl.Phys.,43(1972) 2469

[49] J.L Shay and J.H.Wernick, Ternary Chalcopyrite Semiconductors: Growth, Electronic properties and Applications, Pergamon Press, Oxford,(1975) p-188

[50] G.Masse, N. Lahou, and C.Butti, *J. Phys. Chem. Solids*, 42 (1981) 449

[51] R.Scheer, I. Luck, H. Sehnert, and H.J. Lewrenz, *Sol. Energy Mater. Sol. Cells*, 41/42 (1996) 261

[52] H. Migge, *J. Mater. Res.*, 6 (1991) 2381

[53] K.Topper, J. Krauser, J. Bruns, R. Scheer, A. Weidinger, and D. Brauning, *Sol. Energy Mater. Sol. Cells*, 49 (1997) 383

[54] J. Grzanna and H. Migge, *J. Mater. Res.*, 12 (1997) 355

[55] A.Weidinger, J.Krauser, TH.Riedle, R.Klenk, M.CH.Lux-Steiner, and M.V.Yakushev, *Mat. Res. Soc. Symp. Proc.*, 513 (1998) 177

[56] Gerd Lippold, Karsten Otte, Hermann Schlemm, and Wolfgang Grill, *Mat. Res. Soc. Symp. Proc.*, 513 (1998) 269

[57] K Otte, G.Lippold, D.grambole, F.Hermann, H.Schlemm, A.Schindler, and F.Bigl, Mat. Res. Soc. Symp. Proc., 513 (1998) 275

[58] D S Su, W Neumann, R Hunger, P Schubert-Bischoff, M Giersig, H J Lewerenz, R.Scheer and E. Zeitler, *Appl. Phys. Lett.*, 73 (1998) 785

[59] Hiroaki Matsushita, Tomohiro Mihira, Takeo Takizawa, J.*Crystal Growth*, 197 (1999)169

[60] M Kanzari, B Rezig, J.Mat.Sci: *Materials in Electronics*, 10 (1999)151

[61] J.M. Gil, P.J.Mendes, L.P.Ferreira, H.V. Alberto, R.C. Vilao, N. Ayres dc Campos, A. weidinger, Y. Tomm, Ch.Niedermayer, M.V. Yakushev, R.D. Tomlinson, S.P. Cottrell, and S.F.J.Cox, *Physical Review B*, 1999; 59(3), 1912

[62] M. Krunks, O. Bijakina, V. Mikli, H. Rebane, T. Varema, M. Altosaar, and E. Mellikov, *Sol. Energy Mater. Sol. Cells*, 69 (2001) 93

[63] M.Aggour, U.Storkel, C.Murrell, S.A.Campbell, H.Jungblut, P.Hoffmann, R.Mikalo, D.Schmeiber, and H,J.Lewrenz, *Thin Solid Films*, 403-404 (2002) 57

[64] N.Tsujii, H.kitazawa, and G.Kido, *Phys. Stat. Sol.(a)*, 189 (2002) 951

[65] Dipl.Ing. Michael Stöger - June 2002 –

[66] H.Neumann, *Cryst. Res. Technol.*, 18 (1983) 483

[67] Takayuki Watanabe, Hidenobu Nakazawa, Masahiro Matsui, Hiroki Ohbo, and Tokio Nakada, *Sol. Energy Mater. Sol. Cells*, 49 (1997) 357

[68] Takayuki Watanabe, Hidenobu Nakazawa, and Masahiro Matsui, *Jpn. J. Appl. Phys.*, 37(11B) (1998) L1370

[69] Koichi Fukuzaki, Shigemi Kohiki, Hideki Yoshikawa, Sei Fukushima, Takayuki Watanabe, and Isao Kojima, *Appl. Phys .Lett.*, 73 (1998) 1385

[70] Tetsuya Yamamoto, *Jpn. J. Appl. Phys.*, 37 (1998) L1478

[71] T. Walter, A. Content, K. O. Velthaus, and H. W. Schock, *Sol. Energy Mater. Sol. Cells*, 26 (1992) 357

[72] R. Scheer, T. Walter, H.W. Schock, M. L. Fearheiley, and H. J. Lewerenz, *Appl.Phys.Lett.*,63 (1993) 3294

[73] Yoshitaka Ogawa, Arnulf Jager-Waldau, Yoshio Hashimoto, and Kentaro Ito, *Jpn .J. Appl. Phys.*, 33(12B) (1994) 1775

[74] Yoshio Hashimoto, Kazuhiro Takeuchi, and Kentaro Ito, *Appl. Phys. Lett.*, 67 (1995) 980

[75] L L Kazmerski, F. R. White, M. S. Ayyagari, Y. J. Juang, and R. P. Patterson, *J. Vac. Sci. Technol.*, 14 (1977) 65

[76] L. L. kazmerski and G. A. Sanborn, J. Appl. Phys., 48 (1977) 3178

[77] M. Gorska, R. Beaulieu, J. J. Loferski, and B. Roessler, *Solar Energy Materials*, (1997) 313

[78] Poolla Raja Ram, R. Thangaraj, A. K. Sharma, and O. P Agnihotri, *Solar Cells*, 14 (1985) 123

[79] Satyendra Kumar, A. N. Tiwari, O. S. Sastry, D. K. Pandya, and K. L. Chopra, *Bull. Mater. Sci.*, 8 (1986) 285

[80] Proc.20th IEEE Photovoltaic Specialist conference, New York, 1988

[81] S. Uenishi, K. Tohyama, and K. Ito, *Sol.Energy Mater.Sol. Cells*, 35 (1994) 231

[82] Harold .J. Hovel, 'Semiconductors and Semimetals', Vol.II-Solar cells, Academic Press, New york, 1975, p-132

[83] D. Braunger, D. Hariskos, T. Walter, H. W. Schock, *Sol. Energy Mater. Sol.Cells*, 40 (1996) 97

[84] Takayuki Watanabe and Masahiro Matsui, *Jpn. J. Appl. Phys.*, 35 (1996) 1681

[85] H. Metzner, Th. Hann, Chr. Schmiga, J. H. Bremer, D. Borchert, W. R. Fahrner, and M. Seibt, *Sol. Energy Mater. Sol. Cells*, 49 (1997) 337

[86] A. Ennaoui, M. Weber, R. Scheer, and H. J. Lewerence, *Sol. Energy Mater. Sol. Cells*, 54 (1998) 277

[87] Takayuki Negami, Yasuhiro Hashimoto, Mikihiko Nishitani, and Takahiro Wada, *Sol. Energy Mater. Sol. Cells*, 49 (1997) 343

[88] R. Scheer, M. Alt, I. Luck, and H. J. Lewerenz, *Sol. Energy Mat. Sol. Cells*, 49 (1997) 423

[89] T. Nakabayashi, T. Miyazawa, Y. Hashimoto, and K. Ito, *Sol. Energy Mater. Sol. Cells*, 49 (1997) 375

[90] Gye-Choon Park, Hae-Duck Chung, Chang-Dae Kim, Hyuk-Ryeol Park, Woon-Jo Jeong, Jong-Uk Kim, Hal-Bon Gu, and Ki-Sik Lee, *Sol. Energy Mater. Sol. Cells*, 49 (1997) 365

[91] J. Klaer, J. Bruns, R. Henninger, K. Seimer, R. Klenk, K. Ellmer, and D. Braunig, *Semicond. Sci. Technol.*, 13 (1998) 1456

[92] Dori Gal, Gary Hodes, Dimitri Hariskos, Deiter Braunger, and Hans-Werner Shock, *Appl. Phys. Lett.*, 73 (1998) 3135

[93] Takayuki Watanabe, and Masahiro Matsui, *Jpn. J. Appl. Phys.*, 38 (12A), (1999) L1379

[94] Joachim Kneisel, Kai Seimer, Ilka Luck, and Dieter Braunig, *J. Appl. Phys.*, 88 (2000) 5474

[95] Kentaro Ito, Naoki Matsumoto, Tsuyoshi Horiuchi, Katsuhiko Ichino, Hiroshi Shimoyama, Tsuyoshi Ohashi, Yoshio Hashimoto, Imke Hengel, Jutta Beier, Reiner Klenk, Arnulf Jager-Waldau and Martha Ch. Lux-Steiner, *Jpn. J. Appl. Phys.*, 39 (2000) 126

[96] Kai Siemer, jo Klaer, Ilka Luck, Jurgen Bruns, Reiner Klenk and Dieter Braunig, *Sol. Energy Mater. Sol. Cells*, 67 (2001) 159

[97] Jo Klaer, Kai Siemer, Ilka Luck, and Dieter Braunig, *Thin Solid Films*, 387 (2001) 169

[98] Yoshio Onuma, kenji Takeuchi, Sumihiro Ichikawa, Mina Harada, Hiroko Tanaka, Ayumi Koizumi, and Yumi Miyajima, *Sol. Energy Mater. Sol. Cells*, 69 (2001) 261

[99] J. Wienke, V. Groen-Smit, M. Burgelman, S. degrave, and J. Penndorf, *Thin Solid Films*, 387 (2001)165]

[100] I. Luck, J. Kneisel, K. Siemer, J. Bruns, R. Scheer, R. Klenk, N. Janke, D. Braunig, *Sol. Energy Mater. Sol. Cells*, 67 (2001) 151

[101] I. Keiser, K. Ernst, Ch.-H. Fischer, R. Konenkamp, C. Rost, I. Sieber, M.Ch. Lux-Steiner, *Sol. Energy Mater. Sol. Cells*, 67 (2001) 89

Chapter 3

PREPARATION OF $CuInS_2$ THIN FILMS STARTING FROM CBD Cu_XS AND CBD CdS

3.1 Introduction 92
3.2 Deposition techniques 93
3.2.1 Chemical bath deposition (CBD) 93
3.2.1.1 Chemical aspects of CBD 94
3.2.2 Vacuum Evaporation 95
3.3 Experimental Details 96
3.3.1 Brief review of Cu_xS films 96
3.3.2 Preparation of Cu_xS films using CBD 97
3.3.3 Evaporation of indium 98
3.3.4 Annealing of the bilayer film 98
3.4 Results and Discussion 99
3.4.1 XRD Analysis 99
3.4.2 Optical Absorption Studies 103
3.4.3 Electrical properties 105
3.4.3.1 Sheet resistance 105
3.4.3.2 Hall measurement 106
3.3.4 Energy Dispersive X-ray analysis (EDAX) 107
3.3.5 Scanning Electron Micrograph (SEM) 107
3.3.6 Electron Spectroscopy for Chemical analysis (ESCA) 109
3.5 Sulfurization of $CuInS_2$ films 117
3.6 Experimental Details 117

3.7 Results and Discussions 118
3.7.1 XRD 118
3.7.2 Electrical properties 119
3.7.3 Optical Properties 121
3.7.4 Photosensitivity measurements 124
3.7.5 XPS analysis 124
3.8 Conclusion 127
3.9 Experimental Details 128
3.11 Results and Discussions 131
3.11.1 XRD Analysis 131
3.11.2 XPS Analysis 134
3.12 Trial for the fabrication of $CuInS_2$/ CdS solar cell 136
References 138

Chapter 3

PREPARATION OF $CuInS_2$ THIN FILMS STARTING FROM CBD Cu_XS AND CBD CdS

3.1 Introduction

It is well known that a major reason that limits popular usage of PV devices today is high cost. Apart from material cost, cost of production is very decisive factor determining the cost of solar cells. As far as thin film solar cells are concerned, material consumption is very low. Hence for lowering the cost, adoption of low cost thin film deposition techniques is inevitable. Also the technique adopted should be simple, reproducible, suitable for large area deposition and should not create any environmental or health problems.

Recently, there has been considerable interest in developing $CuInS_2$ thin films using various techniques. This chapter describes preparation and characterization of $CuInS_2$ thin films prepared using two new techniques developed in our lab.

Although CBD is one of the prominent techniques for the preparation of binary compounds, when we prepare ternary films using this method, it is very difficult to control various parameters and produce films with good stoichiometry. In our lab, we tried to prepare $CuInS_2$ films using CBD technique. We were able to prepare uniform, adherent films. However, XPS and ICP analysis indicated that In content in the film is very low, and hence we concluded that the film was most probably the binary compound Cu_xS, with traces of indium.

Hence we selected another route to prepare $CuInS_2$ thin films and reported the preliminary results of our attempt [1]. For this, Cu_xS films were prepared using CBD technique and In was introduced into this film by thermal diffusion. For this, 99.999% pure In was evaporated onto the Cu_xS film and was subsequently annealed in vacuum. This is quite new technique and is simple and low cost as the binary film Cu_xS is prepared using the low-cost CBD technique at room temperature itself. Moreover, there is no requirement of vacuum for Cu_xS deposition. Earlier, Yukawa et al have reported electrodeposited Cu_2S thin films as the first step for the preparation of $CuInS_2$ films by two-stage elctrodeposition and to the best of our knowledge, this is the only technique similar to ours' and reported earlier [2].

Brief description of CBD and vacuum evaporation techniques used in the present work is given below.

3.2 Dcposition tcchniqucs

3.2.1Chemical bath deposition (CBD)

Although CBD has been used as a technique for preparing films since 1910, utilization of this technique to deposit thin films of semiconductors in photovoltaic devices started very recently. Later CBD became a useful method for the deposition of thin films of compound semiconductor materials, which are sulfides and selenides of some metals. Many of these compound semiconductors were identified as good candidates for PV device fabrication. Many groups started working in this area as this technique involves only low-tech process and is suitable for deposition of large area films.

3.2.1.1 Chemical aspects of CBD

Like any other thin film deposition process, CBD involves three main steps: 1) production of appropriate atomic, molecular or ionic species, 2) their transport to substrate through a medium and, 3) condensation on substrate, either directly or via a chemical reaction, to form a solid deposit. Formation of a thin film takes place via nucleation and growth process [3].

According to solubility product principle, in a saturated solution of a weakly soluble compound, ionic product is a constant at a given temperature. If the ionic product exceeds the solubility product, precipitation occurs. It is necessary to eliminate spontaneous precipitation in order to form a thin film by a controlled ion-by-ion reaction. Concentration of the ions in the solution can be controlled by adding appropriate complexing agents and by adjusting the temperature and pH of the solution. When precipitation is controlled, the compound gets deposited on the substrates, kept immersed in the reaction bath. Growth kinetics depend on concentration of ions, their velocities, as well as nucleation and growth processes on the immersed surfaces. Effect of these parameters on film deposition process is discussed in detail in references [4] & [5].

CBD process has several advantages over other methods of thin film deposition, which can be listed as follows. 1) the technique is simple and requires very low capital investment, 2) the process may be easily adapted to large area processing at low fabrication cost, 3) in many cases, films may be deposited at room temperature itself upon a variety of substrates, 4) thickness of the deposited layers may be readily controlled by variation of deposition time 5) does not require vacuum, 6) does not require high purity materials for film deposition, 7) can be operated by a technition for large scale production 8) no reaction involving gas or vapor.

3.2.2 Vacuum Evaporation

This is probably the most popular technique used for thin film deposition. There are several review articles / books giving detailed descriptions of this technique [6-9].

In this process, material is heated to a high temperature in a vacuum chamber so that large number of atoms or molecules leaves the surface of the material and gets deposited on the substrate. Because of low pressure in the chamber, most evaporated molecules suffer no collisions with residual gas molecules and travel in straight lines to the substrate. Small amounts of active residual gases can cause contamination and can change significantly the properties of the evaporated film.
Rate of free evaporation of vapor molecules from clean surface of unit area in vacuum is given by

$$N_e = 3.513\times10^{22}\, p_e \sqrt{\frac{1}{MT}} \text{ molecules/(cm}^2\text{)(sec)} \quad \text{.....(3.1)}$$

where p_e is the equilibrium vapor pressure (in Torr) of the evaporant under saturated-vapor conditions at a temperature T, and M is the molecular weight of the vapor species. Rate of deposition of vapor on substrate also depends on source geometry, its position relative to substrate and condensation coefficient.

Thermal evaporation can be achieved directly or indirectly (via a support) by a variety of physical methods such as resistive heating, flash evaporation, arc evaporation, exploding-wire technique, laser evaporation, RF heating, and electron bombardment heating. In the present work, we used resistive heating method for the evaporation of indium.

This method consists of heating the material using resistively heated filament or boat, generally made of refractory metals such as W, Mo, Ta and Nb, with or without ceramic coatings. Choice of supporting material is primarily determined by

evaporation temperature and resistance to alloying and/or chemical reaction with evaporant. Vapor sources of various types, geometries and size can easily be constructed or obtained commercially. Details of dependence of growth, structure and adhesion of evaporated films etc with different deposition parameters are described in many references [7-9].

Part-1 $CuInS_2$ thin films from CBD Cu_xS

3.3 Experimental Details

3.3.1 Brief review of Cu_xS films

Cu_xS (x = 1-2) thin films have recently received considerable attention due to numerous technological applications in the area of PV devices. At room temperature, Cu_xS in bulk form, is known to exist in five stable phases: chalcocite (Cu_2S), djurleite($Cu_{1.95}S$), digenite($Cu_{1.8}S$), anilite($Cu_{1.75}S$), and covellite(CuS). Mixed phases are also known in the intermediate compositions [10] This material (especially Cu_2S) possesses extremely favorable properties which make it suitable for large-scale photovoltaic applications, particularly in combination with CdS. Low production cost and material availability make this cell suitable for large scale PV applications. Cu_xS/CdS thin film solar cell has been the most extensively investigated thin film photovoltaic system. Main problem regarding this cell is degradation in presence of moisture. Interestingly, Partain et al., observed that degraded Cu_xS/CdS solar cells could be recovered by annealing in presence of H_2 and air [11].

Kimihiko et al. studied electrical conductivity and phase transition of copper sulfide [12]. Various techniques such as vacuum evaporation [13], spray pyrolysis [10], sputtering [14], and chemical bath deposition [15,16], were

employed to prepare Cu_xS thin films. Fatas et al. prepared Cu_xS from a bath containing 1M $CuSO_4$, 1M sodium acetate, 1M thiourea and 7.4 M TEA. A. J. Varkey reported deposition from bath containing CuCl, NaCl and hydroxylamine hydrochloride solutions, using EDTA as a complexing agent. Rezig et al. prepared Cu_xS films by conversion of spray deposited CdS by ion exchange [17].

3.3.2 Preparation of Cu_xS films using CBD

In the present work, Cu_xS films were prepared using CBD technique. Bath used for this contained 1M Cupric Chloride (10 ml), 2M Thiourea (10 ml) and 5ml Ammonia solution (25%). Here triethanolamine (TEA) was used as complexing agent. pH of final solution was maintained at 9.8. Microscope glass slides (75mm × 25mm × 1.25mm) were used as the substrate. These slides were washed thoroughly first using soap solution and then using chromic acid. Microscopic impurities were removed using ultrasonic cleaning. These cleaned glass slides were dipped vertically in the bath. Four slides were dipped at a time and time of deposition was 15 minutes at room temperature. No stirring was given during deposition. Films obtained were uniform and golden in colour. Multiple dip films were prepared for the present work. Thickness of the double-dip sample, measured using Stylus method, was found to be 0.1 micron.

It is reported that annealing in hydrogen and other reducing atmospheres causes an increase in stoichiometry of Cu_xS layers where as exposure to or annealing in air always causes oxidation, with a deterioration in the stoichiometry and a decrease in the resistivity [13]. Hence, prepared Cu_xS samples were dried and were immediately transferred to vacuum chamber of the coating unit to deposit thin films of indium.

3.3.3 Evaporation of indium

The Cu_xS samples were masked 5mm from the four edges using teflon-tape (were having an area ~ 25mmx15mm) and were loaded in the vacuum chamber. Required amount of 99.999% pure indium was weighed accurately using a microbalance and was placed in the Mo boat which was at a distance of 14cm from the substrates. Chamber was evacuated to a pressure of $<10^{-5}$ torr. The boat was resistively heated until whole In was evaporated and deposited on surface of Cu_xS film. In this case, thickness of the In layer was varied as 200Å, 400Å, and 600Å and for this, 20 mg, 40 mg and 60 mg of indium were used respectively.

3.3.4 Annealing of the bilayer film

The In/Cu_xS bilayer film was then annealed in vacuum at 300 ^{0}C for 2 hours. Annealing chamber was made of a glass tube over which nichrome wire was wound uniformly along the entire length. This tube was heated by passing a current through the nichrome wire. Temperature was controlled by adjusting current using a variac. Two samples were placed well inside the tube, at a time to ensure uniform heating. The tube was then placed in the vacuum chamber and was evacuated to a pressure of $<10^{-5}$ torr. Temperature on the sample surface was measured using chromel-alumel thermocouple, kept in contact with the samples. In all the cases, heating and cooling rate was 3^0C/minute.

After annealing, it was found that entire indium diffused into Cu_xS film, forming a uniform film with a dark brown appearance. No indium layer was left behind at the surface after annealing. New preparation method developed for $CuInS_2$ thin films can be summarized as follows

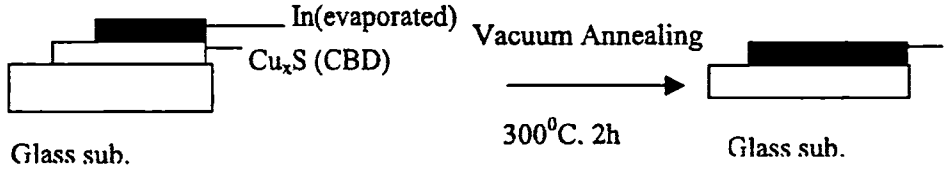

I Step: Preperation of Cu_xS

1M $CuCl_2$ (10 ml) + 2M $CS(NH_2)_2$ (10 ml) + 5drops TEA + 5ml NH_3 solution (25%) at pH 9.8, time of deposition- 15mts at room temp

II step : deposition of indium over Cu_xS film by vacuum evaporation

III Step: annealing bilayer Cu_xS/In for 120mts., in vacuum

3.4 Results and Discussion

3.4.1 XRD Analysis

XRD is one of the most powerful methods for exploring structure of materials. It can be used to determine phase content in many minerals and materials. It requires no elaborate sample preparation and is essentially non-destructive. Generally, it gives a whole range of information about crystal structure, orientation, crystallite size, composition (with the help of standards), defects and stresses in thin films. Experimentally obtained diffraction pattern of sample is compared with Joint Council Powder Diffraction (JCPDS) data for standards. This gives information of different crystallographic phases, relative abundance and preferred orientations. From width of the diffraction peak, average grain size in the film can also be estimated.

Interplanar spacing d was calculated from X-ray diffraction profiles using the formula,

$$2d \sin\theta = n\lambda \quad \text{.....(3.2)}$$

where θ is the Bragg angle and n is order of the spectrum, λ is the wavelength of X-rays. Using d- values the set of lattice planes (h k l) were identified from standard data and lattice parameters are calculated using following relations.

For the tetragonal systems,

$$\frac{1}{d^2} = \frac{(h^2 + k^2)}{a^2} + \frac{l^2}{c^2} \quad \ldots\ldots\ldots\ldots\ldots\ldots\ldots\ldots\ldots\ldots \quad (3.3)$$

and for hexagonal systems,

$$\frac{1}{d^2} = \frac{4(h^2 + hk + k^2)}{3a^2} + \frac{l^2}{c^2} \quad \ldots\ldots\ldots\ldots\ldots\ldots\ldots\ldots\ldots\ldots \quad (3.4)$$

where a and c are lattice parameters. Grain size (L) can be evaluated using Scherrer's formula,

$$L = \frac{k\lambda}{\beta \cos\theta} \quad \ldots\ldots\ldots\ldots\ldots\ldots\ldots\ldots\ldots\ldots \quad (3.5)$$

where k is a constant, which is nearly equal to one and β is "full width at half maximum (FWHM)", usually measured in radians.

In the present study, XRD analysis was done using Rigaku (D.Max.C) X-Ray Diffractometer, with Cu Kα (λ = 1.5405 Å) radiation and a Ni filter operated at 30kV and 20mA. XRD studies of as-prepared Cu_xS sample revealed that films were not crystalline. So these samples were annealed at different temperatures 200°C and 300°C for two hours in rotary vacuum. Even after annealing, there was no improvement in the crystallinity as revealed by the XRD analysis (Fig.3.1a, b & c)

$CuInS_2$ films obtained after diffusing indium layer thickness of 200Å, 400 Å and 600 Å are named CIII(2), CIII(4) and CIII(6) respectively. All these films were annealed at 300 °C for 120 minutes in order to diffuse indium.Fig.3.2 shows XRD pattern obtained for films after diffusing indium into Cu_xS film. When indium film

of thickness 200Å was diffused into Cu_xS layer [sample CIII(2)], 100% intensity peak (112) of $CuInS_2$ appeared in the spectrum (Fig.3.2a). Second peak corresponding to (220) of $CuInS_2$ at $2\theta = 46^\circ$ has also become visible. But when thickness of the indium layer was increased to 400Å [Sample CIII(4)], peaks became more prominent as evident from Fig.2b. This clearly indicated that annealing Cu_xS samples after giving a thin layer of indium over the surface improved the crystallinity and lead to formation of $CuInS_2$ phase in the film. On further increasing the indium layer thickness to 600 Å [sample CIII(6)], there is no appreciable change in the XRD pattern (Fig.3.2c). Hence for latter studies, thickness of the indium layer was fixed at 400 Å, annealing temperature at 300°C and annealing time at 120 minutes. Calculated 'd' values are listed in Table-1. One can see that predominant plane of the $CuInS_2$ is (112)

Table-3.1

X-ray data of $CuInS_2$ thin film

2θ	D Å	hkl	Standard 'd' Value(Å)	Variation (Δd)
27.8	3.2	112	3.19	+0.01
32.66	2.74	200	2.74	0
46.00	1.97	220	1.95	+0.02

Grain size of the film was calculated from peak at $2\theta = 27.8^\circ$ using Scherrer's formula $D = 0.9\lambda / \beta\cos\theta$ where D is diameter of the crystallites forming the film, λ is the wavelength of the CuK_α line, β is FWHM and θ is the Bragg angle. Grain size value obtained is 32 nm.

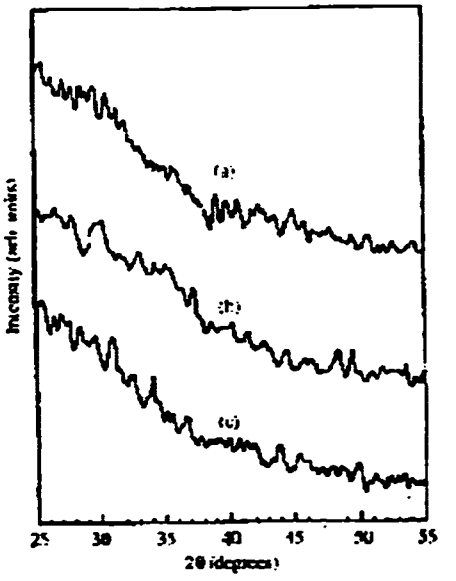

Fig. 3.1 XRD pattern of CuxS films: a) as-prepared Cu_xS; b) annealed at 200^{0}C;c) annealed at 300^{0}C

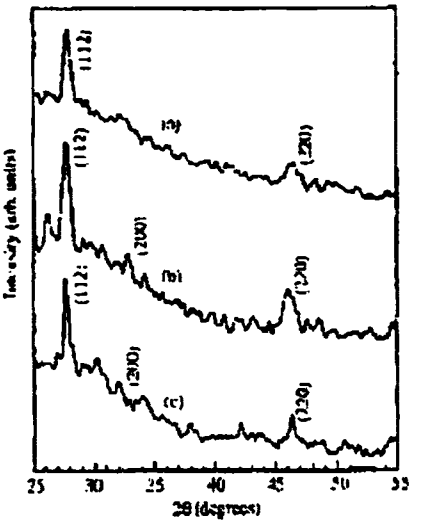

Fig.3.2 XRD pattern obtained after diffusing indium into the Cu_xS film: a) CIII(2); b) CIII(4); c) CIII(6)

3.4.2 Optical Absorption Studies

The most direct and the simplest method for probing the band structure of semiconductors is to get optical absorption spectrum. Absorption is expressed in terms of a coefficient $\alpha(h\nu)$ which is defined as relative rate of decrease in light energy $L(h\nu)$ along its propagation path: [18]

$$\alpha = \frac{1}{L(h\nu)} \frac{d[L(h\nu)]}{dx} \quad \text{.....(3.6)}$$

absorption coefficient α is related to the energy gap E_g according to the equation

$$\alpha h\nu = A(h\nu - E_g)^n \quad \text{.....(3.7)}$$

where A is a constant, h is Plank's constant, ν the frequency of incident beam and n is equal to ½ for a direct gap and 2 for an indirect gap.

Absorption spectra of samples were recorded using UV-VIS-NIR spectrophotometer (Hitachi 3410) model. Fig.3.3a and 3.3b show variation of the absorption coefficient with photon energy (hν) of incident light for samples Cu_xS and CIII(4) . From the plot of $(\alpha h\nu)^2$ against photon energy (hν) (Fig.3.4a) , a direct band gap of 1.86 eV was obtained for the Cu_xS film which compares well with published data [19]. But due to the sensitivity of optical properties to the exact structure and composition of layers, there is a wide variation in the reported results regarding the bandgap in Cu_xS films.

$(\alpha h\nu)^2$ Vs hν plot of the sample CIII(4) (Fig3.4b) shows a direct band gap of 1.41 eV which can be attributed to p-type $CuInS_2$ films [20]. This is lower than band gap value reported for crystals of $CuInS_2$ [21]. Such lower band gap has been reported earlier for $CuInS_2$ thin films [22-23]

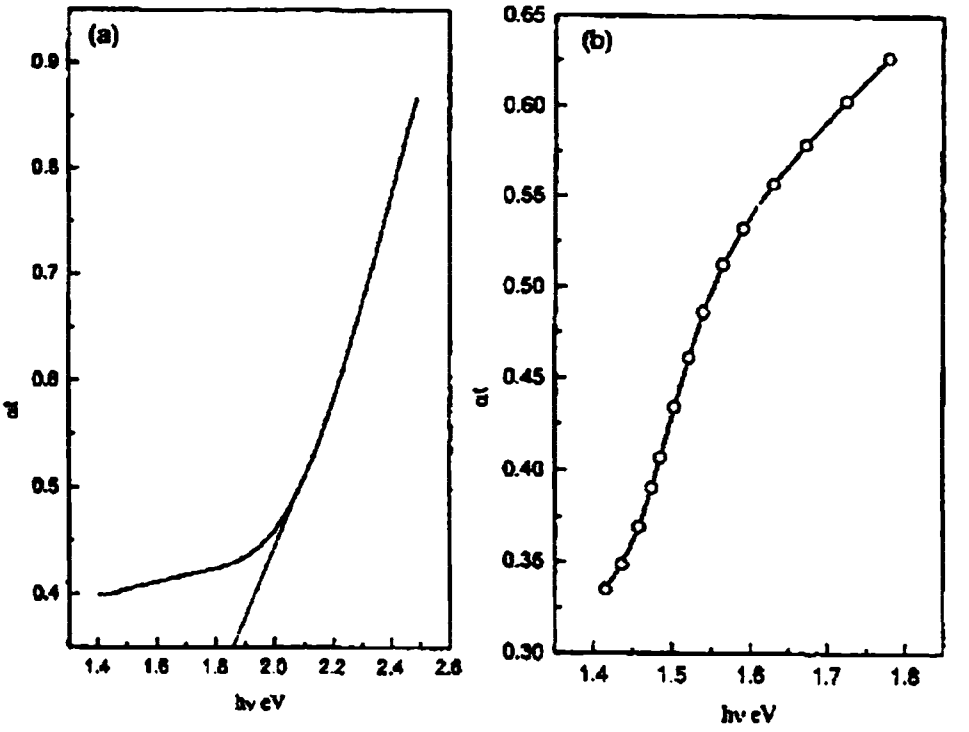

Fig.3.3. Variation of α with photon energy (hν): a) Cu_xS; b) CIII(4)

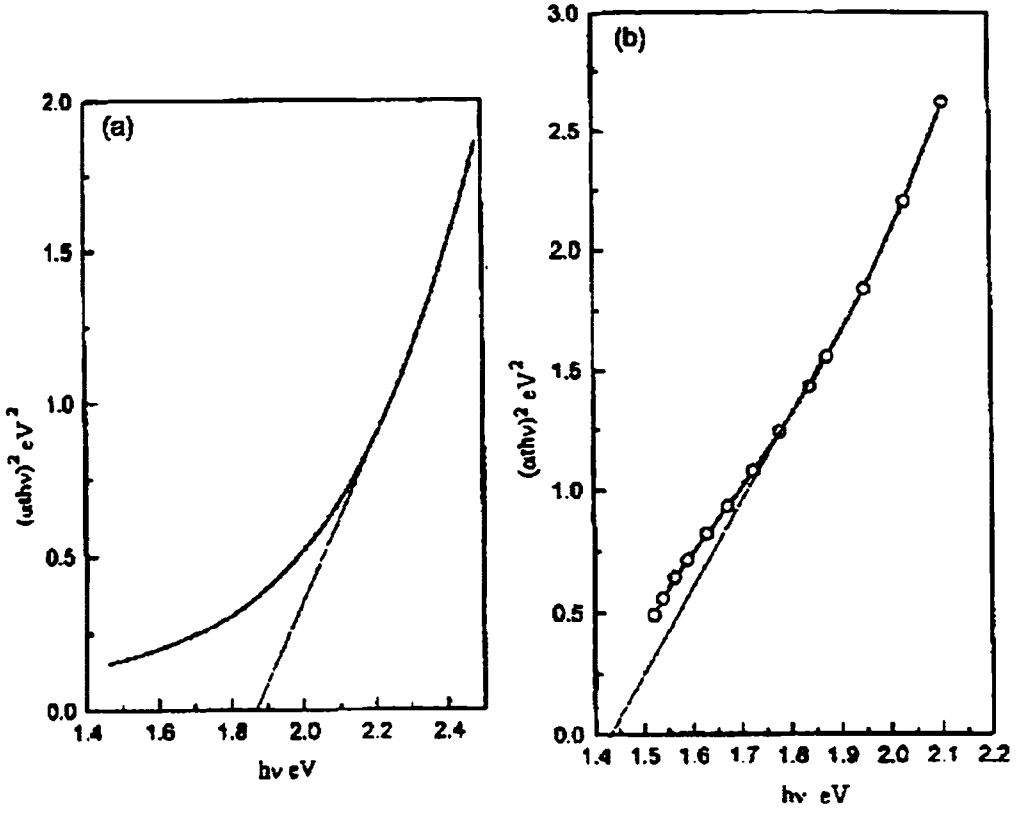

Fig.3.4. $(athν)^2$ vs. (hν) plot for samples : a) Cu_xS; b) CIII(4)

3.4.3 Electrical properties

3.4.3.1 Sheet resistance

Sheet resistance of Cu_xS and CIII(4) was measured at room temperature using Keithley I-V measurement system. Silver electrodes were painted on top surface of the film keeping a distance of 5mm between the electrodes. Sheet resistance of as-prepared Cu_xS (sample A) was1.267 kΩ/□. After indium diffusion,

sheet resistance decreased to 119.5 Ω/□. Using hot probe technique, it was observed that both Cu_xS and $CuInS_2$ samples were p-type.

3.4.3.2 Hall measurement

Conductivity type, mobility and density of charge carriers of samples were investigated at room temperature using Hall measurement set up made by MMR Technologies Inc. having MP350 power supply to vary magnetic field and K50 temperature controller. These parameters were evaluated using Vander Pauw method by four-probe measurement technique [24].

Resistivity, mobility, and carrier concentration of Cu_xS and $CuInS_2$ films are given in table-3.2. Resistivity of Cu_xS is 19.5 Ω- cm and this decreases as amount of In in the film increases. When 400Å of indium was introduced by thermal diffusion, mobility and carrier concentration became 5.10 cm^2/V-s and 4.77×10^{20} cm^{-3} respectively. On increasing the In layer thickness to 600 Å, slightly increased carrier mobility, with no significant change in carrier concentration, was observed (6.84×10^{20} cm^{-3} and 7.47 cm^2/V-s respectively). Mobility values obtained are greater than the values reported earlier for p-type $CuInS_2$ films, prepared using two source evaporation, ($0.2cm^2/V$-s and $3.2cm^2/V$-s) [25], but is less than the mobility value reported for p-type crystals ($15cm^2/V$-s) [26]. Type of carriers in all these films was found to be holes.

Table-3.2

Hall measurement results of different samples

Sample	Resistivity (ρ) Ω- cm	Mobility (μ) cm^2/Vs	Carrier density (cm^{-3})	Hall coeff. cm^3/C	Type of carriers
Cu_xS	19.5	0.152	2.11×10^{18}	2.96	holes
CIII(4)	2.56×10^{-3}	5.10	4.77×10^{20}	0.0137	holes
CIII(6)	1.22×10^{-3}	7.47	6.85×10^{20}	9.11×10^{-3}	holes

3.3.4 Energy Dispersive X-ray analysis (EDAX)

Here the sample is irradiated by electron beam and emitted x-rays is directly measured using energy dispersive X-ray spectrometer, producing a spectrum of counts versus energy. As each x-ray photon enters the detector, it produces photoelectrons, whose total number is linearly proportional to the energy of the entering X-rays. Charge collected from detector is very small since only a few hundreds or thousands of electrons are produced by each X-ray photon. Hence it is amplified by a pre-amplifier whose output voltage is proportional to the X-ray energy [27].

In the present work, we used this technique to confirm presence of indium in the $CuInS_2$ samples. EDAX spectrum of CIII(2) and CIII(4) samples showed presence of Cu, In and S in the samples and is shown in Fig.3.5 and Fig.3.6 respectively. For CIII(4) sample, indium peak intensity is high, showing a higher concentration of indium in the film. Concentration of sulfur is also higher in this film than that for CIII(2) sample. There is one peak corresponding to Si, which is from the glass substrate used for the preparation of the films.

3.3.5 Scanning Electron Micrograph (SEM)

SEM is the most widely used instrument for obtaining microstructural and surface features of thin films. A finely focused electron beam is scattered over the surface of the specimen and secondary electrons emanating from the specimen are used for imaging the surface. Since secondary electrons come from the surface layer, picture obtained is a faithful reproduction of surface features. Secondary electron imaging can provide high-resolution imaging of fine surface morphology. Quantitative and qualitative chemical analysis information can also be obtained using Energy Dispersive X-ray spectrometer (EDS) with the SEM [28].

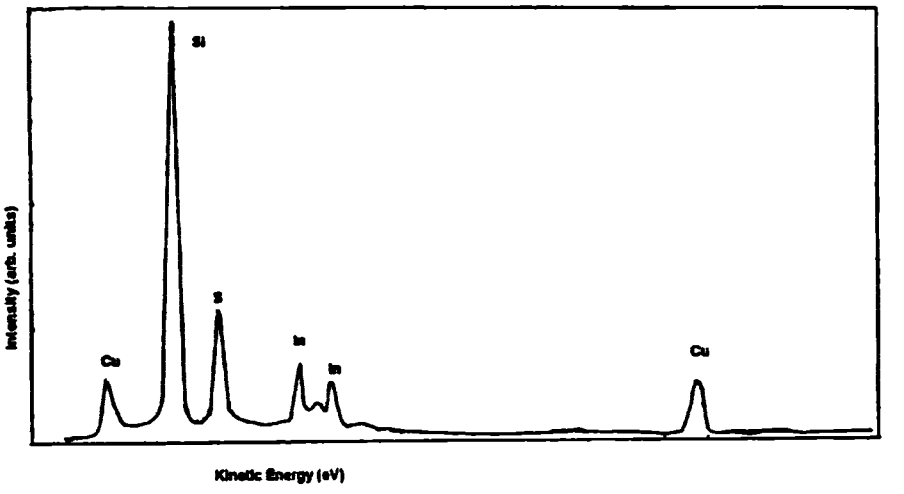

Fig.3.5 EDAX spectrum of CIII(2)

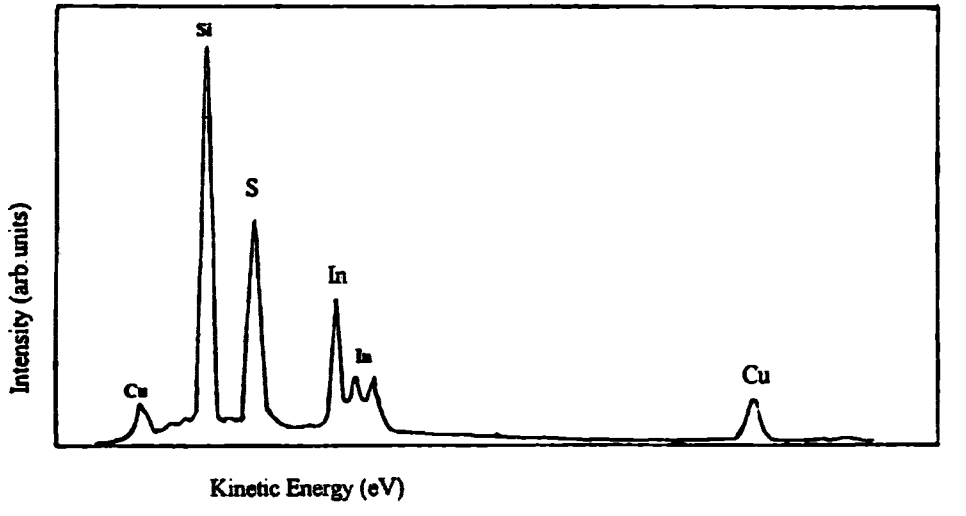

Fig.3.6 EDAX spectrum of CIII(4)

SEM was used to find out uniformity of $CuInS_2$ films prepared. Fig.3.7 gives the SEM micrograph of the same area of CIII(4) sample with two different magnifications. Films are uniform over a large area with defined grains and no pinholes or cracks are found. There are some agglomerated areas in this film, which may be due to segregated Cu_xS impurity phase. A similar feature was obtained for Cu-rich sprayed samples [29].

3.3.6 Electron Spectroscopy for Chemical analysis (ESCA)

ESCA is one of the major techniques for studying thin films. It provides information on the elemental composition of a sample as well as on the chemical state of the observed atoms.

In this technique, sample is irradiated using electromagnetic radiation of energy hv. Due to photoelectric effect, electrons are emitted with kinetic energy

$$E_{kin} = h\nu - E_B - \phi \quad \text{.....(3.8)}$$

where E_B is binding energy of a particular electron shell and Φ is the sample work function. Photoelectrons are energy-analyzed in the spectrometer and , since photon energy is known, one can determine characteristic binding energies of valence electrons coming from different elements present in the sample. Depending on the energy of incident radiation, this technique is called either "Ultra Violet Photoelectron Spectroscopy (UPS)" for lower photon energies ($\leq$ 50eV) or "X-ray Photoelectron Spectroscopy (XPS)" for higher photon energies ($\geq$1k eV) [30].

Chemical composition of film was evaluated using XPS technique in the present work. XPS spectra of samples were recorded using an ULVAC-PHI unit (model: ESCA 5600 CIM) employing argon ion sputtering (Voltage = 3 kV, Raster size = 3×3 mm^2, pressure 10^{-8} mbar) Al Kα X-ray (1486.6eV) with a beam diameter of 0.8mm and power of 400W was used as the incident beam.

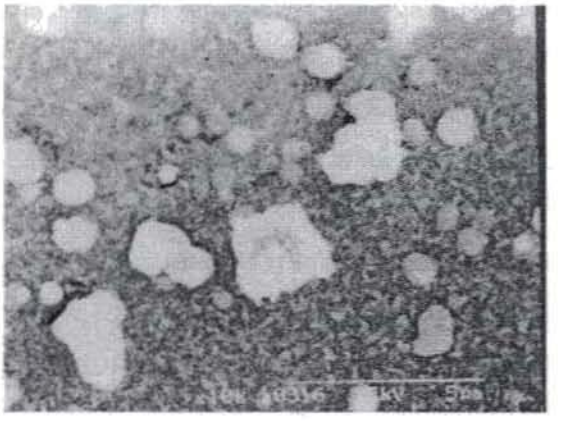

(a)

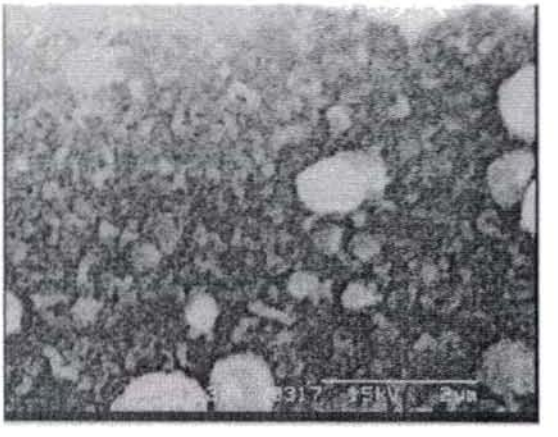

(b)

Fig.3.7 SEM of CIII(4) sample at magnifications: (a) 10K ; (b)20K

XPS technique gives information about chemical state of elements present in surface layer only (of thickness few hundred angstroms). In order to know variation in stoichiometry as well as chemical state all along the thickness of the samples, we performed XPS depth profile of all these samples. Here the presence of the elements Cu, In, S, O, & Si was checked along the sample thickness. For this, measurements on sample surface was taken first and then the sample was etched slowly using Ar ion sputtering for 3 minutes to remove approximately 100Å thickness of the film. Again the sample was checked for these elements (this is called one cycle). This process was repeated till substrate surface was reached.

In this fashion, sample was etched for about 100 cycles and the depth wise presence of the elements plotted together for sample CIII(4) is shown in Fig.3.8. Binding energies of the elements are represented along the X-axis. The spectra were calibrated against shifts due to machine errors, using the C 1s line (of the hydrocarbon contamination in the films) as the standard. (Binding energy of C 1s is 284.5 eV). After 40 cycles, peaks corresponding to O, and Si could be seen, which indicates the beginning of the glass substrate (SiO_2). So the film is present up to this, after which the glass substrate starts. Hence from this cycle, only peaks corresponding to O and Si were obtained.

From (Fig.3.8), it is obvious that indium diffused uniformly throughout the depth of the sample and is present up to the glass substrate. At the surface, there is one peak at binding energy value 531.7 eV corresponding to O, which is due to surface contamination. Its atomic concentration decreases along depth of the sample as evident from Fig.3.9b. It can also be seen that all these elements have diffused slightly into the glass substrate, probably during the annealing of the films at 300^0C for 2 hours. Binding energy values obtained are 952.5 eV & 932.5 eV for Cu $2p_{3/2}$

& Cu $2p_{1/2}$; 452.5 eV & 444.6 eV for In $3d_{5/2}$ & In $3d_{3/2}$; and 162 eV for S 2p, which are in agreement with reported values of $CuInS_2$ [23,31,32]. Similar binding energy values were obtained for Cu levels in $CuInS_2$ [33] and they also noticed no significant shift in binding energy for Cu levels from metallic state.

Fig.3.9 shows depth profile of atomic concentrations of Cu, In & S for samples CIII (2), CIII(4) & CIII(6). For sample CIII(2), Cu and In are not uniformly present throughout the depth of the sample (Fig.3.9a). Concentration of In is maximum at surface and gradually decreases to very small value (7.5%) near the substrate. After applying Ar ion sputtering for 10 minutes, it was found that Cu/In ratio in the film is equal to 1(28.4% each). At the same time in the depth, the ratio increases to 5.58. Although S was uniformly present throughout the depth of the sample, its atomic percentage was only around 10%. So it becomes clear that indium layer of thickness 200Å is not sufficient to produce films of uniform composition.

Fig.3.9b shows depth profile of atomic concentration of sample CIII(4). From the figure, it is clear that Cu, In and S are present almost uniformly from the surface to the substrate. Cu/In ratio in the film is 1.29 Here also sample exhibits a deficiency of sulfur. Atomic concentration of sulfur is almost half the value expected for stoichiometric $CuInS_2$. This may be probably due to the preferred sputtering of group VI elements such as sulfur and selenium. Also sensitivity factors of Cu and S are very different. Similar problem was observed in the case of $Cu_{2-x}Se$ films prepared in our lab. In that case, for applying correction, Cu/Se ratio was measured with a standard sample of CuSe powder and the correction factor was found to be 2 [4,5].

Percentage atomic concentration of sample CIII(6) is shown in Fig.3.9c. Here again the concentration of Cu & In is not uniform throughout depth of the

sample. Cu/In in that film is 1.5 after etching for 20 minutes. Percentage of sulfur is lower than that of CIII(4).

In the case of sample CIII(4), there is slight decrease in atomic concentration of S at the surface and in the bulk. This is may be due to the fact that S has a high vapor pressure and hence during deposition process, mainly at the stage of indium diffusion, some S may escape from the surface of the film.

From Fig.3.9a,b&c, it is evident that all above samples contain a good percentage of oxygen. This is due to the fact that after coating indium, all samples were annealed at 300°C for 2 hours in rotary vacuum. To reduce the oxygen content in the films, for later preparations, all the samples were annealed in high vacuum (~ 10^{-5} torr). XPS spectra of such samples showed nearly zero percentage concentration of oxygen throughout the depth of the sample (Fig3.16b).

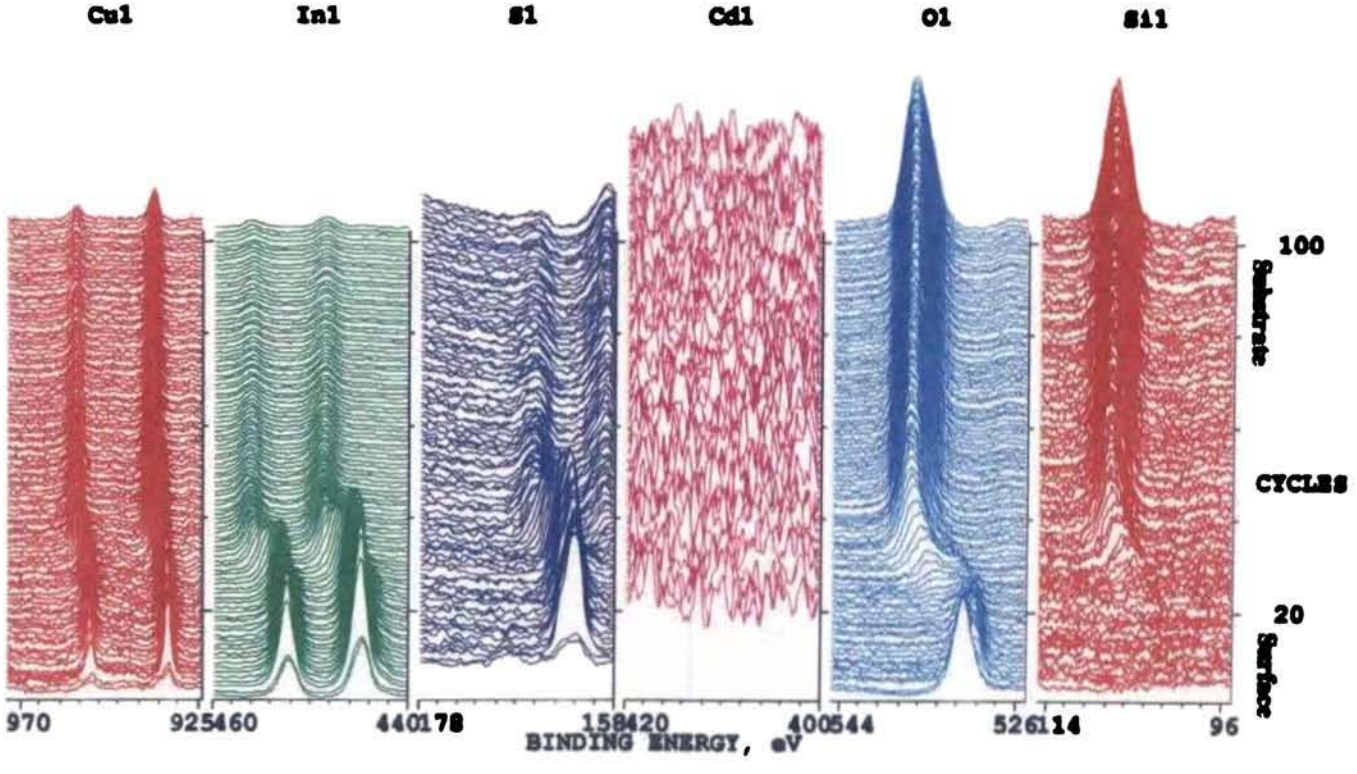

Fig.3.8. XPS depth profile of sample CIII(4)

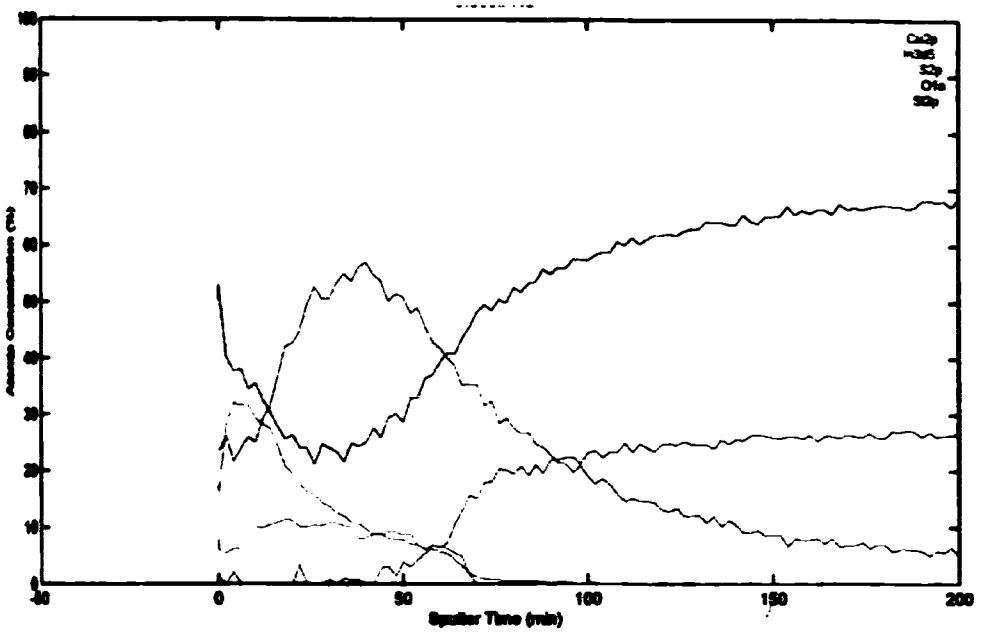

Fig.3.9a, At.conc.% vs sputter time graph of sample CIII(2)

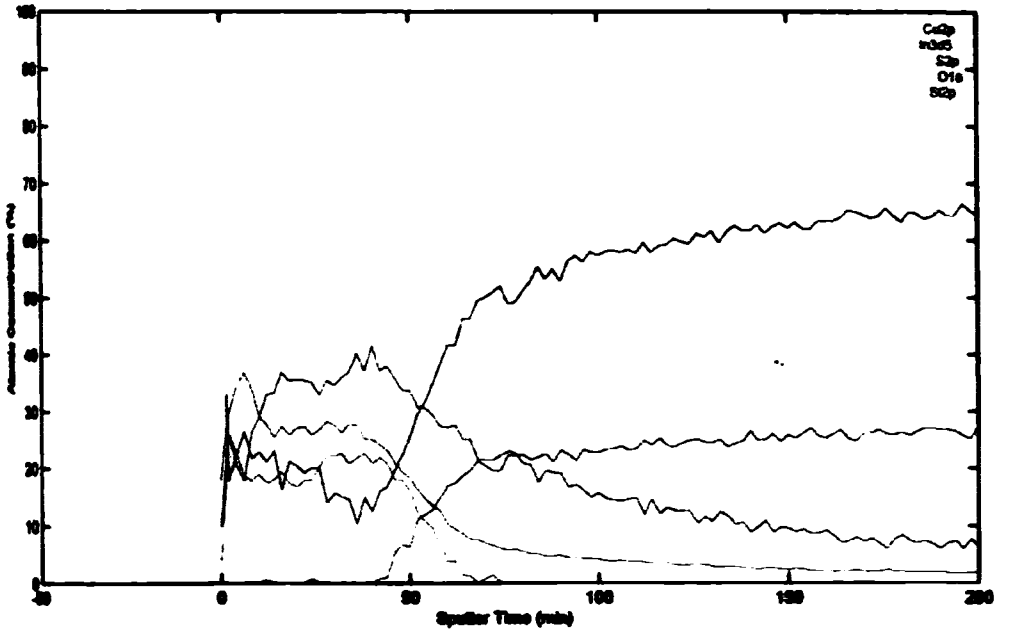

Fig.3.9b, At.conc.% vs sputter time graph of sample CIII(4)

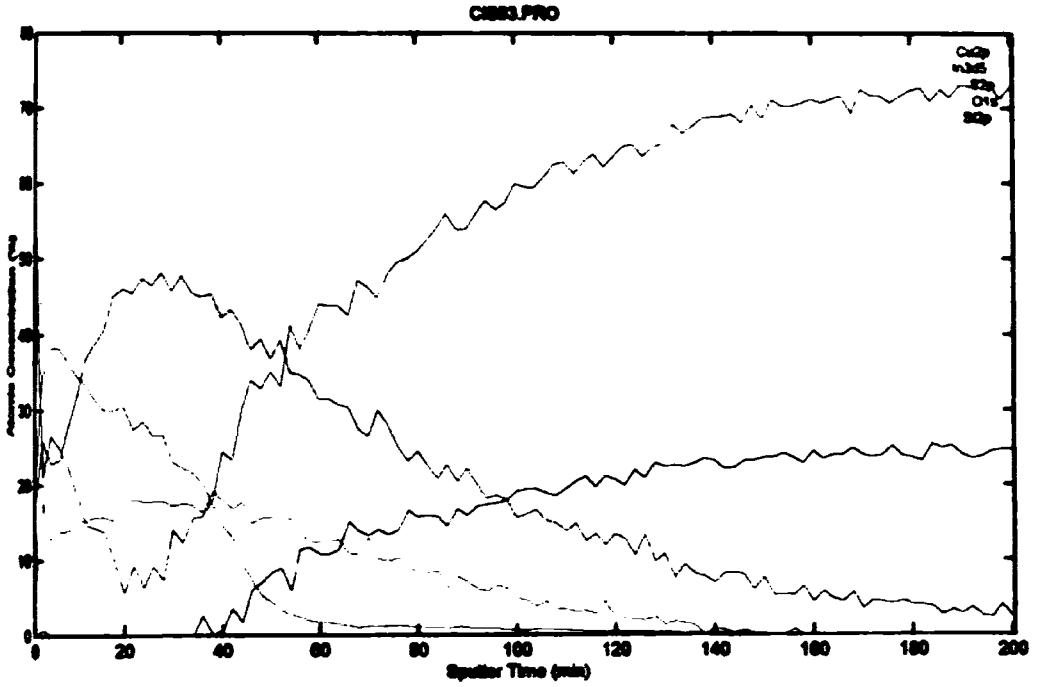

Fig.3.9c, At.conc.% vs sputter time graph of sample CIII(6)

3.5 Sulfurization of $CuInS_2$ films

From the results of above analyses, one can understand that it is possible to prepare $CuInS_2$ thin films by evaporating indium over chemical bath deposited Cu_xS films and subsequently annealing the films. The best result was obtained for sample prepared by diffusing 400Å indium [sample CIII(4)]. The XRD spectrum matched well with standard data. XPS depth profile of the sample showed presence of Cu, In and S throughout the depth. However, atomic concentration of S was less than that of stoichiometric $CuInS_2$. In order to increase the S content in the films, samples were annealed in sulfur vapor in an open tube at different temperatures for different durations. Again these films were characterized using the above techniques. Following section deals with the annealing of CIII(4) sample and the characterization.

3.6 Experimental Details

Sulfur-annealing chamber had two horizontal tubular sections; the upper one was "sample chamber" and the lower one was "sulfur-powder-chamber". Resistive heating could be given to both sections separately. Sample chamber could be heated to 300^0C and sulfur chamber to 200^0C. Two thermocouples were used to measure temperature of these two chambers separately.

Sulfur chamber was maintained at a temperature of about 150 ^{0}C to obtain a sulfur flux during the process. Temperature of samples was varied as 100 ^{0}C, 130 ^{0}C, 160 ^{0}C, 200 ^{0}C, 250 ^{0}C & 300 ^{0}C keeping the annealing time constant at 1 hour. Deposition of sulfur in cold regions at the end of the chamber indicated existence of sulfur flux. When sample was annealed at temperatures below 200^0C, a thin layer of S gets deposited on film surface.

When annealed at temperatures greater than 200 ^{0}C, there is a clear reduction in thickness of the film. Hence after several trials, temperature of the sample source was fixed at 200 ^{0}C and the films were annealed for different time periods. These films were again characterized.

3.7 Results and Discussions

3.7.1 XRD

XRD spectrum of samples annealed at 200 ^{0}C in sulfur atmosphere for ½ hour, 1 hour, 1½ hours and 2 hours (named as S½, S1, S1½ and S2 respectively) are illustrated in Fig.3.10. After annealing for ½ hour, peak corresponding to (112) plane became sharper, showing an improvement in the crystallinity of the films. However, on increasing the annealing time, intensity of the peak decreased.

Grain size of these films was found to increase with sulfur annealing time. For the S1 & S2 samples, grain size values were 65 nm & 118 nm respectively.

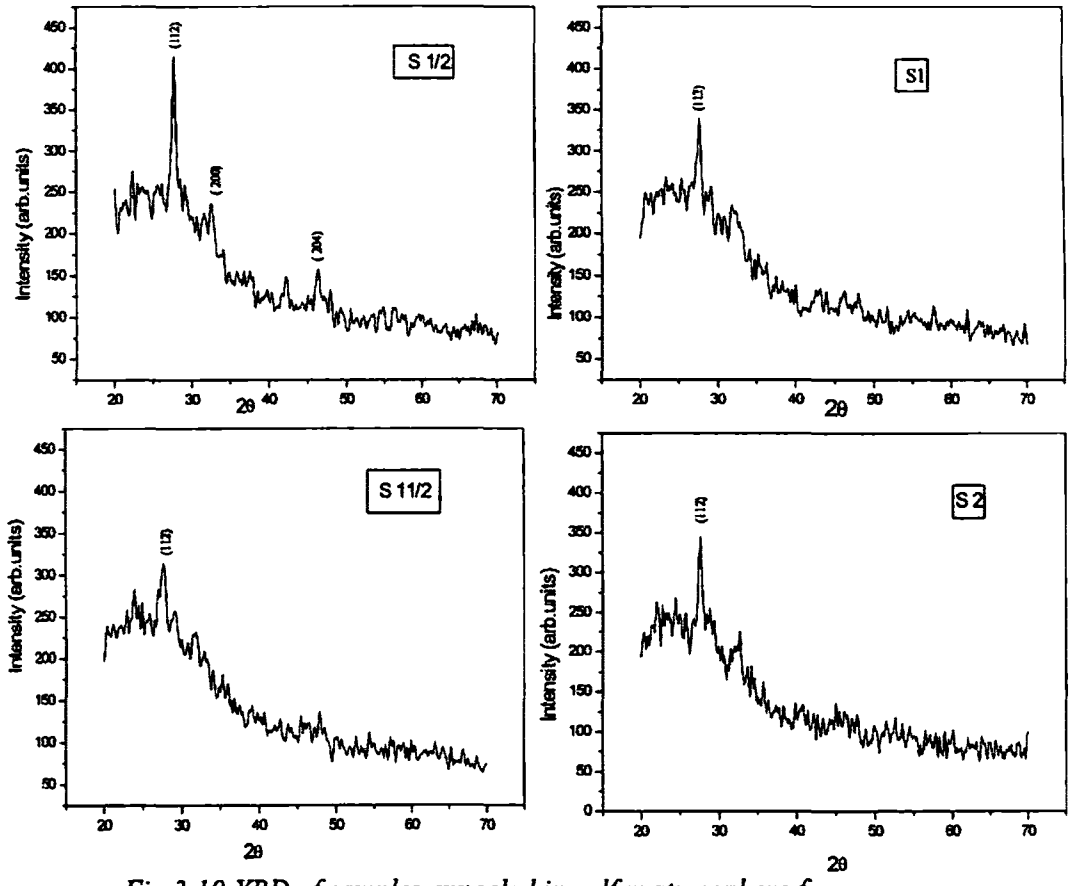

Fig.3.10 XRD of samples annealed in sulfur atmosphere for different durations

3.7.2 Electrical properties

In order to clarify effect of S annealing on resistivity and mobility of $CuInS_2$ films, Hall effect measurement was carried out. Table-3.3 shows results of samples annealed for different time. Resistivity increased for samples annealed for a time up to 1 hour. After that, resistivity again decreased. Variation of mobility and carrier

concentration with annealing time is represented in Fig.3.11. It is evident that annealing in sulfur vapor decreases mobility and carrier density.

Table-3.3
Hall measurement

Sample	Resistivity (ρ) Ω cm	Mobility (μ) cm^2/Vs	Carrier density (cm^{-3})	Hall coeff. cm^3/C	Type of carriers
CIII(4)	2.56×10^{-3}	5.10	4.77×10^{20}	0.0137	holes
S1/2	6.52×10^{-3}	2.95	3.25×10^{20}	1.92×10^{-2}	holes
S1	0.2067	3.22	9.37×10^{18}	0.6659	holes
S11/2	6.52×10^{-3}	2.59	3.25×10^{20}	0.0192	holes
S2	1.12×10^{-2}	1.93	2.89×10^{20}	2.16×10^{-2}	holes

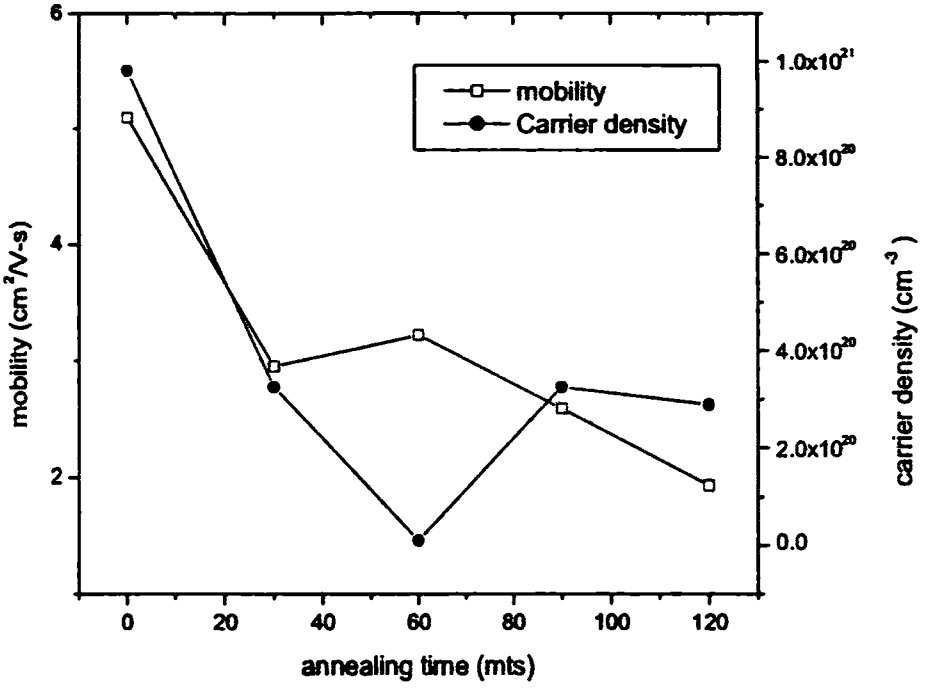

Fig.3.11 Variation of mobility and carrier density with ann. time

3.7.3 Optical Properties

Fig.3.12.shows transmission graph of Cu_xS film, As prepared $CuInS_2$ [CIII(4)] and films annealed in sulfur atmosphere. As prepared $CuInS_2$ sample (CIII(4)) has transmission around 12%. On annealing, transmission increases slightly for all samples except the one annealed for 1½ hours. For the sample annealed for 2 hours, transmission corresponds closely to the transmission of Cu_xS films. This may be due to formation of Cu_xS impurity phases in the sample. There is also a decrease in atomic concentration of indium in the sample as indicated by XPS analysis (section 3.7.5).

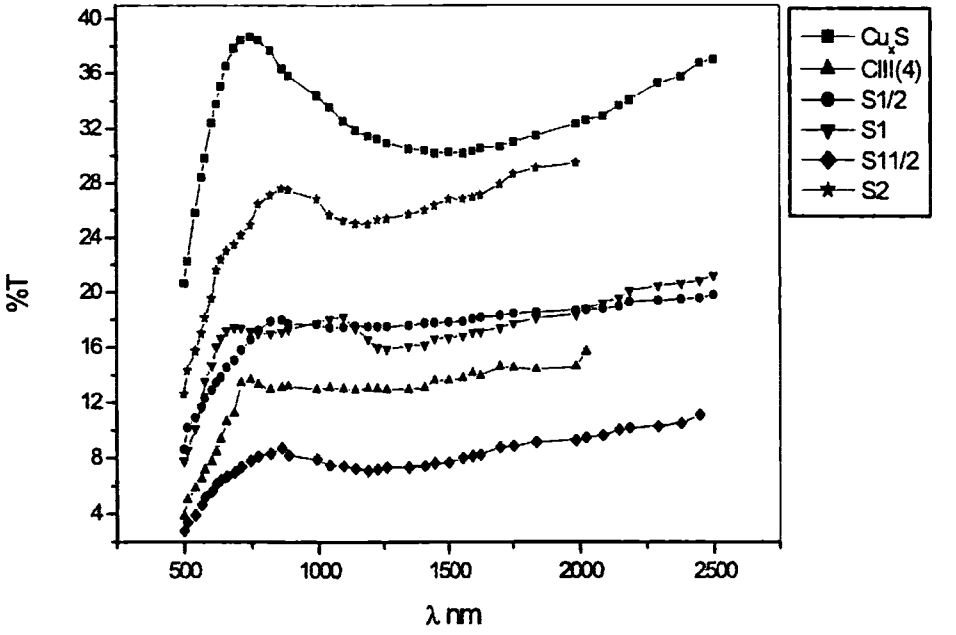

Fig.3.12 Transmission spectrum of annealed samples

Absorption spectra of these samples are illustrated in Fig.3.13 and variation in optical band gap with annealing time is represented in Fig.3.14. There is an increase in band gap with increase in annealing time. This may be due to the increase in grain size of the films with annealing time, as revealed by XRD analysis.

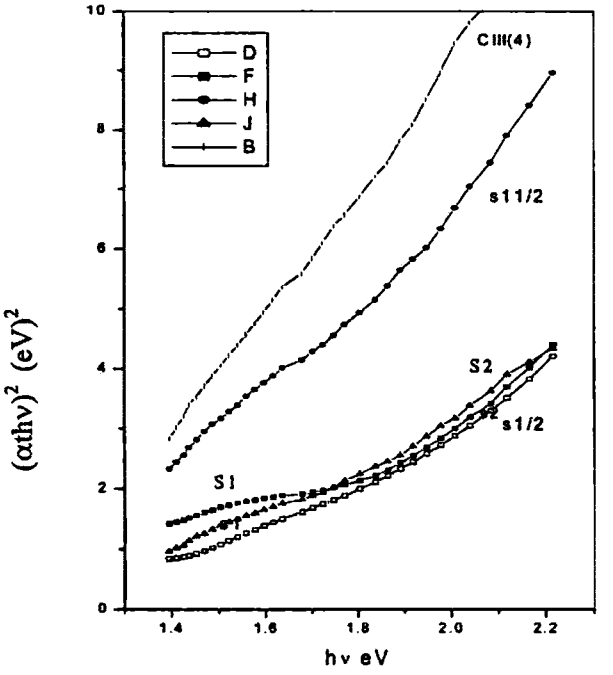

Fig.3.13 Absorption spectrum of annealed samples

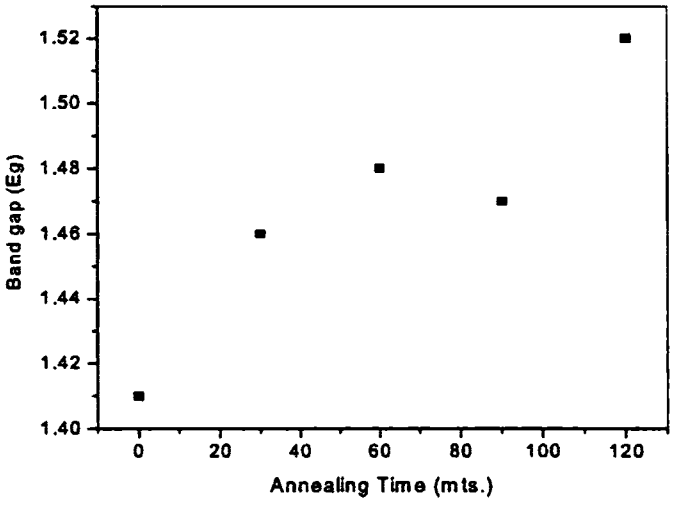

Fig.3.14 Variation in the optical band gap with annealing time.

3.7.4 Photosensitivity measurements

Photoelectrical properties of these samples were investigated by measuring photosensitivity (S) defined as,

$$S = \frac{(R_D - R_L)}{R_D} \times 100 \quad \text{.....(3.9)}$$

where R_D is dark resistance of the film, R_L is the resistance of the film under illumination. Photosensitivity is measured for different samples annealed in sulfur atmosphere for different periods. These samples were irradiated with white light of intensity 40mW/cm^2. An I-R filter was used to remove heat content in the radiation. Variation of S with annealing time is represented in Fig.3.15. Photosensitivity is high for the samples annealed in sulfur atmosphere for 30 to 60 minutes.

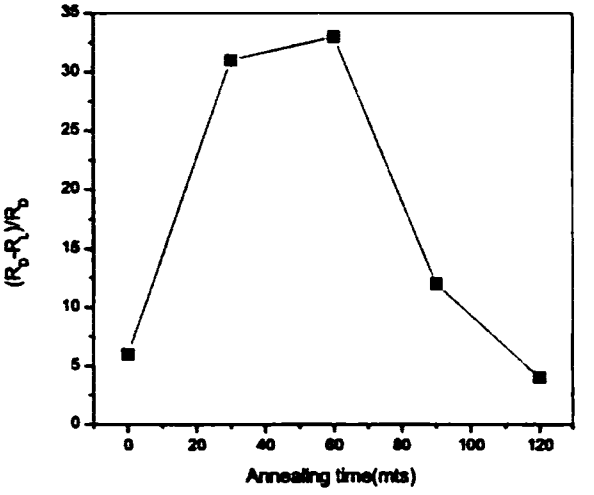

Fig.3.15. Photo response of films annealed for different time

3.7.5 XPS analysis

Accurate and quantitative analysis of atomic percentage in this compound is difficult to obtain using XPS because binding energies and sensitivity factors of

Cu2p and S2p are very different. (S2p = 162 eV, s = 0.44 and $Cu2p_{3/2}$ =932.6 eV , s = 5.3) [23]. However, a qualitative analysis of $CuInS_2$ samples annealed in sulfur atmosphere for 1 hour and 2 hours was analysed using XPS. Atomic percentage (at %) vs. sputter time graph of these samples is depicted in Fig. 3.16. Table 3.4 gives approximate at % of Cu, In and S in these films. Also ratio of atomic concentration of Cu to In and the ratio of the total (Cu+In) in the film to the S content in the film is shown in the table. From this, it follows that when samples are annealed for 1 hour, there is an improvement in sulfur content in the film. (increases from 21% to 33%) (Fig.3.16a). On increasing annealing time to 2 hours, there is no significant increase in S content compared to the one annealed for 1 hour (Fig.3.16b). On the other hand, there is decrease in atomic concentration of In. Regarding oxygen, from Fig3.16 it is very clear that at % in the film is nearly 0% for 1 hour annealed sample. But, at % of oxygen is 3% for the sample annealed for 2 hours.

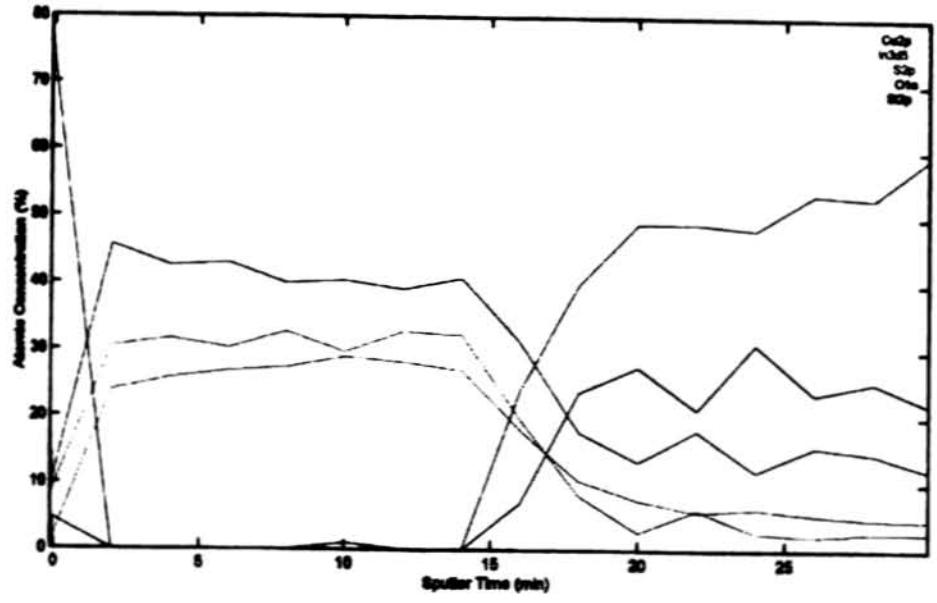

Fig.3.16a, At.conc.% vs sputter time graph of sample CIII(4), annealed for 1 hour

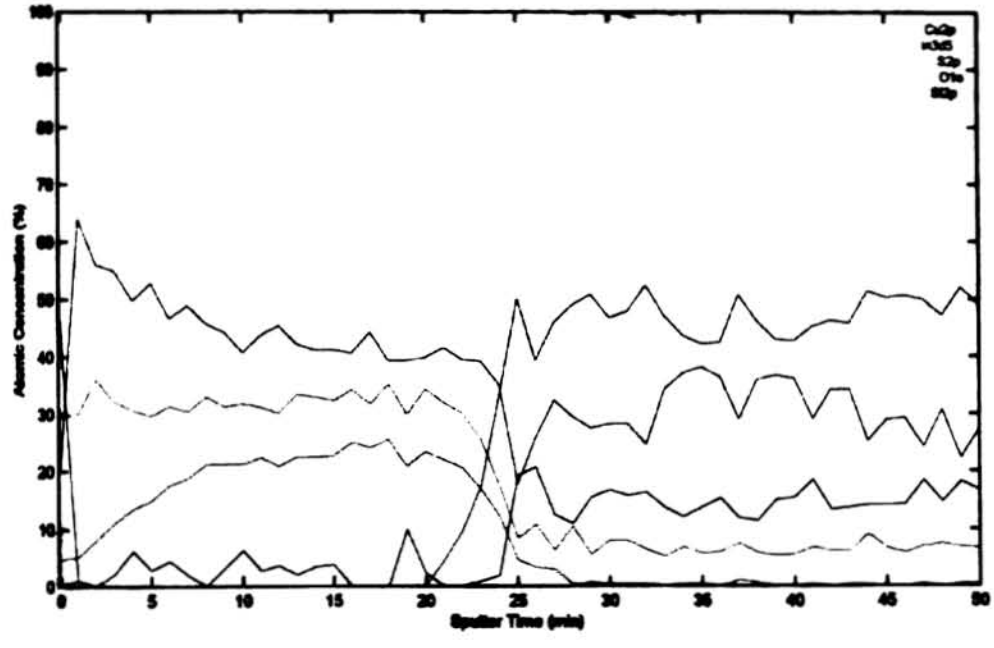

Fig.3.16b, At.conc.% vs sputter time graph of sample CIII(4), annealed for 2 hours

Table-3.4
Atomic percentage from XPS analysis

Sample Name	Cu%	In%	S%	Cu/In in the film	(Cu+In)/S
CIII(4)	37	27	21	1.37	3.04
CIII(4)S1	40	27	33	1.48	2.03
CIII(4)S2	41	23	33	1.78	1.93
Standard $CuInS_2$ powder[23]	12	36	52	0.33	0.923

The BE values of these samples are given in Table-3.5. There are no appreciable change in the BE values due to S annealing.

Table-3.5
Binding Energy values of samples (in eV) annealed in sulfur atmosphere.

Sample	Cu $2p_{3/2}$	Cu $2p_{1/2}$	In $3d_{5/2}$	In $3d_{3/2}$	S 2p
CIII(4) as prepared	952.5	932.6	452.5	445	162
S1	951.8	932.5	452.5	445	162
S2	952.5	932.5	452.5	445	162

3.8 Conclusion

We prepared $CuInS_2$ thin films using a new and low cost technique. The films obtained were characterized using different techniques. Even though XRD

peaks were clearly indicating the formation of $CuInS_2$ compound, XPS analysis indicated that the films are deficient in sulfur. In order to increase sulfur content, films were annealed in sulfur atmosphere for different times. There is an increase in atomic concentration of sulfur due to annealing up to one hour. But this could not be increased above 33%. There is reduction in the at % of In with increase in the annealing time and about 3% of Oxygen is present in samples annealed for two hours.

Part-II $CuInS_2$ thin films from CBD CdS films

With an aim of fabrication of $CuInS_2$/ CdS solar cells, we tried another new procedure for the preparation of $CuInS_2$ thin films. In the earlier part of this chapter, we saw that it is possible to prepare $CuInS_2$ thin films by thermally diffusing indium into the Cu_xS layer. If we can convert top layer of a sufficiently thick CdS into Cu_xS, and then convert it into $CuInS_2$, $CuInS_2$/ CdS solar cells can be fabricated in an easy way. Metallurgical junction will be formed within the CdS film thereby avoiding atmospheric contamination of the interface. With this intention, we tried to prepare $CuInS_2$ films using CBD CdS films.

3.9 Experimental Details

Preparation of $CuInS_2$ is a three-stage process, the first stage is preparation of CdS using chemical bath deposition; second is preparation of Cu_xS from CdS and the third stage is preparation of $CuInS_2$ by evaporating indium on Cu_xS and subsequently annealing the samples.

i) Preparation of CdS thin films

Among various deposition techniques used for preparation of CdS films, chemical deposition is rather simple and inexpensive.

It yields stable, uniform, adherent and hard films with good reproducibility. These films are found to be near-stoichiometric [34].

For the present case, CdS thin films are prepared on glass substrate as well as on SnO_2 coated glass plates using CBD. Details of this technique are mentioned in section 3.2.1. Basic principle involved is the chemical reaction between cadmium chloride and thiourea in aqueous solution. Chemical deposition of CdS films requires slow release of Cd^{2+} ions in aqueous medium. This is achieved by forming a complex with triethanolamine (TEA). Cd^{2+} ions released from the $Cd(TEA)_2$ complex and S^{2-} ions from thiourea condense on the substrate. Thus film formation is an ion-by-ion condensation process. pH of the solution is controlled by adding ammonia solution.

Chemical equation representing the above reaction is,

$$CdCl_2 + 2TEA \longrightarrow 2Cl^- + Cd(TEA)_2$$

$$Cd(TEA)_2 + CS(NH_2)_2 + H_2O \longrightarrow CdS + TEA + O{=}C(NH_2)_2$$

For preparing the bath, 10ml cadmium chloride (1M) was mixed with 4ml of TEA. A thick white precipitate was formed. To this, 25% ammonia solution was added slowly, till the precipitate just dissolved completely. Then 10 ml of thiourea was added. pH of the solution is around 10.5. Well-cleaned substrates were dipped in this solution and beaker containing the solution was kept in hot air oven with temperature stabilized at 80^0C. No stirring was given. The arrangement was kept undisturbed for 75 minutes for deposition. Single-dipped and double-dipped films were prepared for the present study.

ii) Preparation of Cu_xS thin films

Cu_xS thin films were prepared by converting CBD CdS films using the well-known Clevite process, which is widely used for Cu_xS formation in high efficiency Cu_xS /CdS solar cells [13]. Clevite process for polycrystalline cell fabrication was developed during 1970's and the most notable feature of this process is fabrication of the Cu_xS layer in CdS substrates by ion exchange. In addition, ion exchange process affects only the cations so that sulfur content of CdS remains intact [35].

In the present case, CdS samples were dipped in 0.5M $CuCl_2$ solution (50 ml) for different periods, (<1 minute) until yellow colour of CdS film turns black. When CdS is dipped in the $CuCl_2$ solution, Cd ions are replaced by Cu ions and thus Cu_xS is formed. Reaction can be represented by the following equation

$$CdS + xCuCl_2 \longrightarrow Cu_xS + CdCl_2$$

To terminate the reaction, and to remove unreacted $CuCl_2$, sample was rinsed in distilled water kept at room temperature. Excess water was removed and the sample was dried in hot air.

As the time of dipping was increased in order to convert the CdS film completely to Cu_xS, cracks are developed in the film. Also, the Cu_xS film gets detached from the substrate. To reduce time of dipping, temperature of the $CuCl_2$ solution was increased to 95^0C. Then the time of dipping was optimized as 3 seconds for the complete conversion of the double dipped CdS film to Cu_xS.

iii) Evaporation of In on Cu_xS

Pure indium (99.999%) was deposited on Cu_xS samples prepared as mentioned above. Thickness of the indium layer was varied as 100Å, 400Å, and 600Å. Then these films were annealed at 300^0C in vacuum (10^{-5} torr) for two hours. Evaporated indium completely diffused into Cu_xS film to form $CuInS_2$.

3.11 Results and Discussions

3.11.1 XRD Analysis

Before conversion into a Cu_xS layer, CdS samples were investigated using X-ray diffraction studies. Fig3.17 represents the XRD pattern of CdS and the Cu_xS film formed by converting the CdS film. Table-3.6 Shows the angular position θ, corresponding inter planar distances and (h k l) values of these films. Diffraction pattern of the as-prepared CdS film exhibits peaks corresponding to cubic CdS phase. When CdS is converted to Cu_xS, comparison of observed X-ray diffraction spectra with standard JCPDS data revealed that the Cu_xS film consists of many phases. Most of the lines were identified as those of chalcocite. Hence it was quiet impossible to give an estimation of composition (ie, value of x) of these films. Similar problem was faced by Rezig et al. who reported structural and optical properties of topotaxially-grown Cu_2S [17]. They also observed that Cu-rich chalcocite phase transforms into minor phases, when let under air-ambient atmosphere. This transformation is enhanced in the case of thin layers and it is argued that copper migration to the surface is the origin of this formation.

When 100Å indium is evaporated onto the Cu_xS film, there is slight variation in XRD pattern and it shows presence of $CuInS_2$ phase in the sample. When In layer thickness is increased to 400 Å, $CuInS_2$ peak appears in the XRD pattern, which shows formation of chalcopyrite $CuInS_2$ phase with preferred orientation along the (112) plane. In addition to peaks corresponding to $CuInS_2$, some Cu_xS peaks are also present. But on increasing In layer thickness to 600 Å, all Cu_xS peaks disappear and $CuInS_2$ peaks become prominent as shown in Fig3.18. The d values are listed in Table3.7.

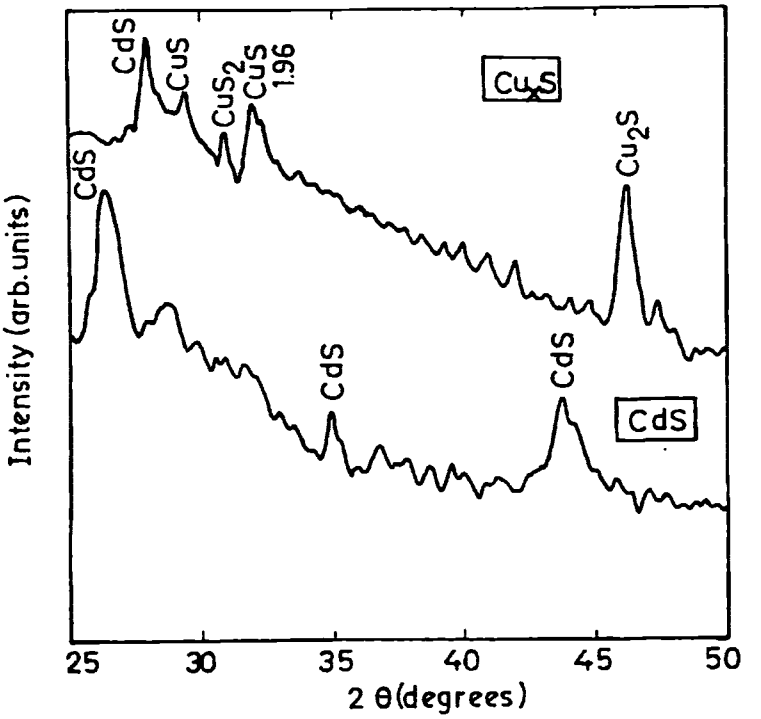

Fig.3.17. XRD pattern of CdS and Cu_xS films

Table-3.6 – XRD analysis of CdS and Cu_xS

Sample	2θ	d Å		(h k l)	Phase identified
		Observed	Standard		
CdS	26.65	3.342	3.360	(111)	CdS (c)
	43.75	2.067	2.058	(220)	CdS (c)
Cu_xS	27.95	3.189	3.16	(101)	CdS (H)
	29.35	3.040	3.04	(102)	CuS
	31.0	2.882	2.89	(200)	CuS_2
	32.5	2.752	2.74	(103)	$Cu_{1.96}S$
	46.25	1.961	1.98	(060)	Cu_2S

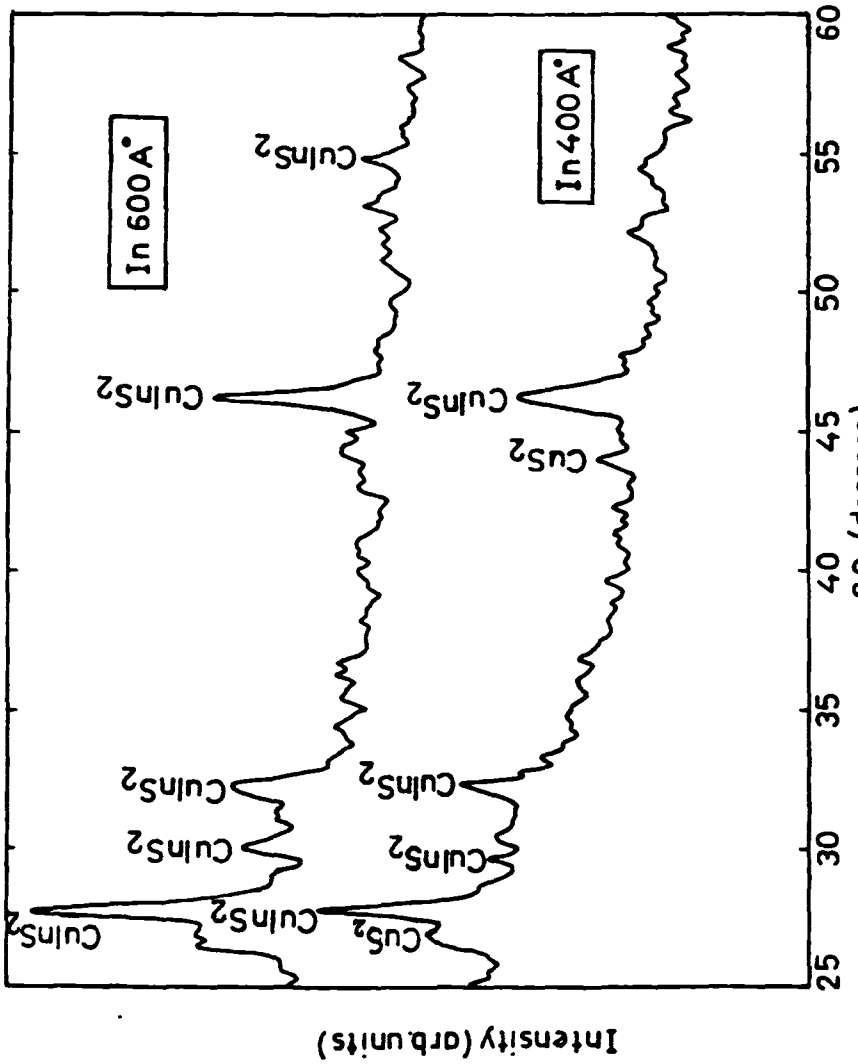

Fig.3.18 XRD of $CuInS_2$ sample

Table 3.7

X- ray analysis data of $CuInS_2$

In 400Å			In 600Å		
d(Å)	(h kl)	Phase	d(Å)	(hkl)	Phase
3.32	(111)	CuS_2	3.21	(112)	$CuInS_2$
3.21	(112)	$CuInS_2$	2.97	(103)	$CuInS_2$
3.03	(103)	$CuInS_2$	2.77	(200),(004)	$CuInS_2$
2.78	(200),(004)	$CuInS_2$	1.97	(220),(204)	$CuInS_2$
2.06	(220)	CuS_2	1.67	(312),(116)	$CuInS_2$
1.97	(220)	$CuInS_2$			

3.11.2 XPS Analysis

XPS analysis of the $CuInS_2$ films was carried out by investigating Cu, In, S and C spectra, using MgK_α line (1253.6 eV) for excitation. (Fig.3.19). Analysis was repeated by removing layers of the film by Ar ion sputtering for 1minute, 2 minutes and 3 minutes. Binding energy values were corrected with reference to C 1s peak at 284.5 eV. Peaks corresponding to Cu, In& S are clearly visible at binding energies 933.01 eV & 953.4 eV for Cu $2p_{3/2}$ & Cu $2p_{1/2}$, 444.75 eV & 452.42 eV for In 3d5/2 & In 2d3/2, and 161.12 eV for S 2p respectively. These values are in agreement with the binding energy values of different elements in $CuInS_2$; which confirms formation of $CuInS_2$ phase.

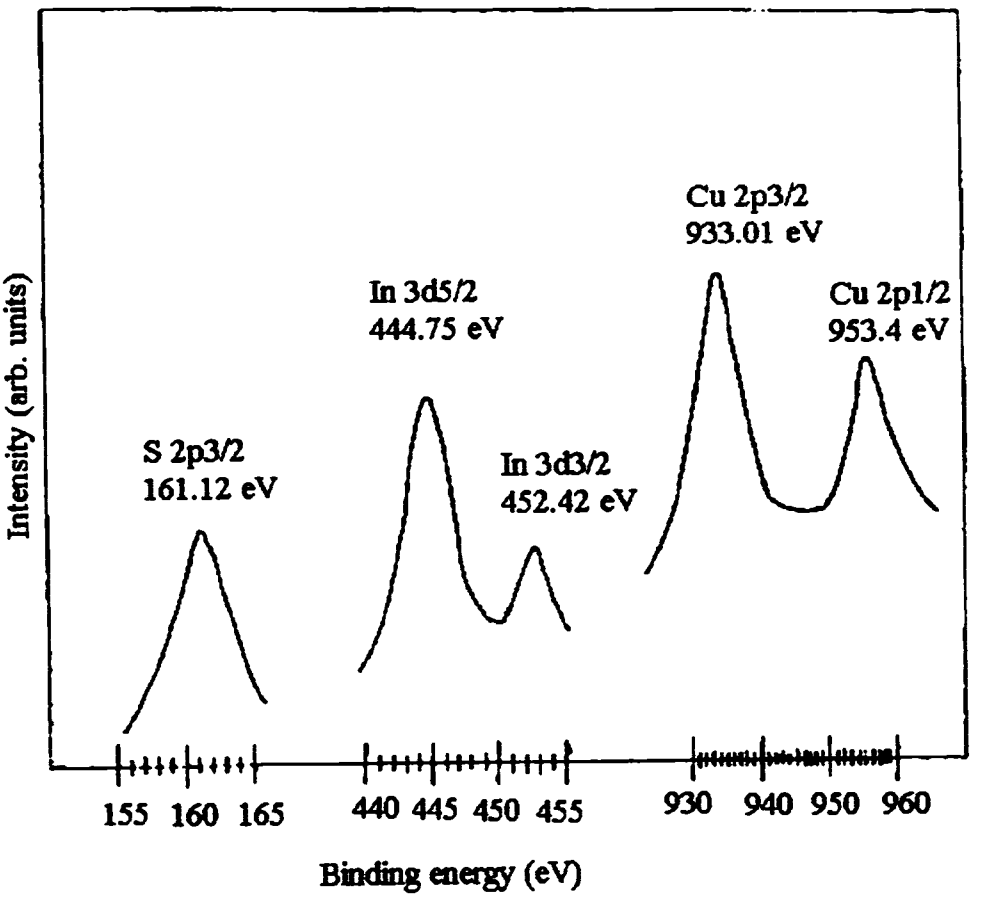

Fig.3.19 XPS of $CuInS_2$ sample

3.12 Trial for the fabrication of $CuInS_2$/ CdS solar cell

In the above section, we saw that it is possible to prepare $CuInS_2$ thin films by the thermal diffusion of indium into Cu_xS films, prepared from CBD CdS films. As mentioned earlier, $CuInS_2$/ CdS heterojunction can be fabricated in a quite simple way if the top layer of a sufficiently thick CdS film can be converted into $CuInS_2$. This process has the advantage that it will avoid atmospheric contamination at the interface.

We tried to fabricate $CuInS_2$/ CdS cell using the above-mentioned method. SnO_2 coated glass plates were used as the substrate and it will serve as the back electrode of the cell. Over this, CdS films of thickness 1.5μm (triple-dipped) were deposited using CBD. These films were then dipped in $CuCl_2$ solution kept at a temperature of about 90^0C for 3 seconds so that top layer is converted to Cu_xS. Then 600Å indium is evaporated over this film and is annealed at 300^0C for 2 hours. Indium uniformly diffused into the film to form $CuInS_2$ layer at the top and hence $CuInS_2$/ CdS structure was fabricated. Silver was used as the top electrode. The I-V characteristic of the cell was measured at an intensity of $40mW/cm^2$ (Fig.3.20). This junction gave a voltage of 480mV; but there was no significant current.

Low value of the photocurrent points toward the limitations of the preparation process. In this method, there is a chance of shorting during the dipping process for the preparation of Cu_xS film due to rapid diffusion of highly mobile copper ions through the imperfections in the CdS layer. Also, there may be an inhomogeneous pattern of growth of Cu_xS layer due to the sudden interruption of reaction as soon as the desired thickness is reached. In addition, this process lacks control of stoichiometry.

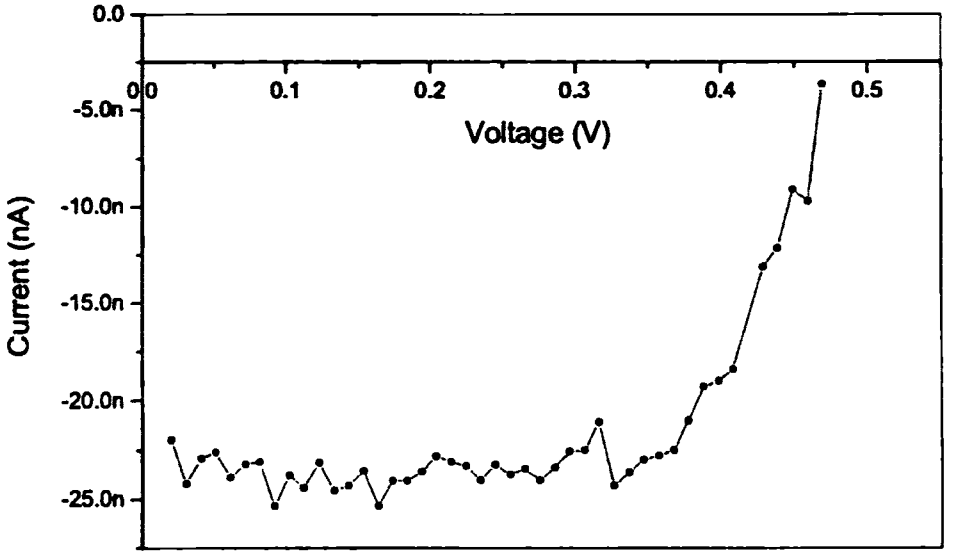

Fig.3.20 J-V Characteristics of the cell

3.13 CONCLUSION

$CuInS_2$ thin films were prepared using CBD CdS film and were characterized. Junction was fabricated by converting the top layer of CdS to $CuInS_2$. Although open circuit voltage of this junction was quite measurable, current was very feeble.

References

[1] S.Bini, K.Bindu, M.lakshmi, C Sudha Kartha, K P Vijayakumar, Y.Kashiwaba, and T.Abe, *Renewable Energy*, 20 (2000) 405

[2] Sigeyuki Nakamura and Akio Yamamoto, *Sol. Energy Mat. Sol. Cells*, 49 (1997) 415

[3] Thin film Device Applications, K. L. Chopra and Inderjeet Kaur, Plenum Press, New York, 1983, p-2

[4] Lakshmi M, Ph.D Thesis, Cochin University of Science and Technology, Kochi, 2001,

[5] Bindu K, Ph.D Thesis, Cochin University of Science and Technology, Kochi, 2002

[6] P.Hedenqvist and A.Roos, Surface and coating Technology, 48 (1991), L149,

[7] Robert W. Berry, Peter M. Hall, and Murray T. Harris, 'Thin Film Technology', D.Van Nostrand company, Princeton, (1968), p-113,

[8] K. L. Chopra and Suhit Ranjan Das, Thin Film Solar Cells, Plenum Press, New York, 1983,

[9] K. L. Chopra, Thin Film Phenomena, Kreiger, New York, (1979)

[10] Cristina Nascu, Ileana Pop, Violeta Ionescu, E. Indrea, and I. Bratu, *Materials Lettres*, 32 (1997); p-73]

[11] L.D. Partain, P.S. McLeod, J.A. Duisman, T.M. Peterson, D.E.Sawyer, and C.S.Dean, J.Appl.Phys., 54 (1983) 6708

[12] Kimihiko Okamoto and Shichio Kawai, *Jpn. J. Appl. Phys.*, 12 (1973) 1130

[13] Aperathitis, F.J. Bryant, and C.G. Scott, *Sol. Energy Mater.*, 20 (1990) 15

[14] G. A. Armantrout, D.E.Miller, K.E. Vindelov, and T.G.Brown, J. Vac. Sci. Technol., 16 (1979) 212

[15] E. Fatas, T. Garcia, C. Ontemoyer, A. Media, E. G. Camerevo, and F. Arjona, *Mater. Chem. Phys.*, 12 (1985) 121

[16] A. J. Varkey, *Solar Energy Mater.*, 19 (1989) 415

[17] B. Rezig, J. Bougnot, M. El Hammouti, M. Perotin, Vu Bay , and M. Savelli, *Solar Energy Materials*, 9 (1983) 189

[18] J.I. Pankov, 'Optical processes in semiconductors', Dover publications, New York., (1971); p-34

[19] Paul S McLeod, Larry D Partain, Dave E Sawyer and Terry M Peterson, Appl.Phys.Lett., 45 (1984) 472

[20] L Y Sun, L L Kazmerski, A H Clark, *J. Vac. Sci. Technol.*, 15 (1978) 265

[21] Takahiro Wada, Takayuki Negami and Mikihiko Nishitani, *Appl. Phys. Lett.*, 62 (1993) 1943

[22] A N Tiwari, D K Pandya and K L Chopra, *Thin Solid Films*, 130 (1985) 217

[23] M. C. Zouaghi, T. Ben Nasrallah, S. Marsillac, J. C. Bernede, and S. Belgacem, Thin Solid Films, 382 (2001)39

[24] Dieter.K.Schroder, Semiconductor Material and Device Characterization, John Wiley & Sons, INC, New York, (1998)]

[25] L L Kazmerski, M S Ayyagari, and G A Sanborn, *J. Appl. Phys*, 46 (1975) 4865

[26] J.L Shay and J.H.Wernick, Ternary Chalcopyrite Semiconductors: Growth, Electronic properties and Applications, Pergamon Press, Oxford, (1975) p-188

[27] J.H.Richardson and R.V.Peterson(Ed), Systematic materials analysis, Vol-II, Academic press, New York, (1974)

[28] Hand Book of Analytical Methods for materials, (2000), Materials Evaluation and Engineering, INC

[29] Malle Krunks, Valdek Mikli, Ogla Bijakina, and Enn Mellikov, *Applied Surface Science*, 142 (1999) 356

[30] Rosenberg and Tu, 'Treatise on Materials Science and Technology', Vol-27, Academic Press, 1988, p-65

[31] Koichi Fukuzaki and Shigemi Kohiki, *Appl. Phys.Lett.*,73 (1998) 1385

[32] Poolla Raja Ram, R. Thangaraj, A. K. Sharma, and O. P. Agnihotri, *Solar Cells*, 14 (1985) 123

[33] W Gaarenstroom and N Weinograd, *J.Chem.Phys.*, 67 (1997) 3500

[34] M. T. S. Nair, P. K. Nair, R. A. Zingaro, and E. A. Meyers, *J. Appl. Phys.*, 75 (1994) 1557

[35] T. Sands, J. Washburn, and R. Gronsky, *Solar Energy Materials*, 10 (1984) 349

Chapter- 4

STUDIES ON $CuInS_2$ THIN FILMS PREPARED USING CHEMICAL SPRAY PYROLYSIS TECHNIQUE

4.1 Introduction 143

4.2 Experimental Details 144

4.3 Variation of Cu/In at 400°C, keeping S/Cu = 4 147

4.3.1 X- ray diffraction 148

4.3.2 Optical properties 149

4.3.3 Scanning Electron Micrograph 151

4.3.4 Electrical properties 153

4.3.5 Photosensitivity 153

4.3.6 XPS Analysis 153

4.4 Variation of deposition temperature 155

4.4.1 XRD 155

4.4.2 Optical properties 158

4.4.2 Electrical properties 160

4.4.3 Photosensitivity 162

4.5 Variation of (Cu+In)/S ratio, keeping Cu/In = 1 163

4.5.1 XRD 163

4.5.2 Optical properties 163

4.5.2 Electrical properties 165

4.5.4 Photosensitivity measurement 168

4.6 Variation in Cu/In at 300°C, keeping S/Cu = 4 168

4.6.1 XRD 169

4.6.2 Optical properties 170

4.6.3 Thickness 172
4.6.4 Electrical properties 172
4.6.5 Photosensitivity 174
4.6.6 XPS 174
4.7 Variation in S/Cu ratio, keeping Cu/In = 0.5 178
4.7.1 XRD 178
4.7.2 Optical properties 179
4.7.3 Electrical properties 181
4.7.4 XPS 182
4.7.4 Photosensitivity 186
4.8 Conclusion 186
References 191

Chapter- 4

STUDIES ON $CuInS_2$ THIN FILMS PREPARED USING CHEMICAL SPRAY PYROLYSIS TECHNIQUE

4.1 Introduction

Two of the principal requirements for a thin film solar cell material for terrestrial applications are high optical absorption as well as quantum efficiency and low fabrication costs. Several promising materials are currently being investigated in various research laboratories to improve optical/ electrical properties and to reduce process cost. $CuInS_2$ is one such material. Even though cell efficiency may not be as high as with competitive materials like Silicon, CdTe and $CuInSe_2$, a very low processing cost and eco friendly nature would allow it to be a good candidate.

Chemical Spray pyrolysis (CSP) deposition, one of the chemical techniques suitable for preparation of thin films, has been applied to deposit a wide variety of thin films. It involves spraying a solution, usually aqueous, containing soluble salts of constituents of the desired compound onto a heated substrate. It is quite suitable for depositing large area thin films using simple apparatus with good reproducibility. Major shortcoming of this technique is that some times it may make films with voids.

CSP was developed in the early 1960s by Hill and Chamberlin and preparation of thin films of certain inorganic sulfides and selenides using this technique was first reported by Chamberlin and Skarman in 1966 [1]. At present, this method is used for preparation of ternary compounds and their quartenary and quinary alloys. Spray pyrolysis of $CuInS_2$ and other I-III-VI_2 compounds has been reported by Pamplin *et al.* in 1979 [2]. Electrical and structural properties of $CuInS_2$ thin films prepared using spray pyrolysis has been reported by Gorska et al. [3]. Hernandez et al. reported structural, kinetic and optical properties of spray pyrolysed $CuInS_2$ films [4]. Again in a

very recent paper, Marsillac et al. reported the post-annealing treatment of spray-deposited $CuInS_2$ films [5]. An attempt to evaluate the content of chlorine, oxygen, carbon and nitrogen impurities in sprayed films was made by Krunks et al.[6].

One of the major problems with preparation of ternary chalcopyrites like $CuInS_2$ is the control of stoichiometry, i.e., control of the excess copper content and of the copper-to-indium and metal to chalcogen ratios. Interestingly in CSP technique, ratios of the constituent elements can be easily varied by controlling their concentration in the spray solution. In the present investigation, we varied the copper-to- indium and metal to chalcogen ratio in a wide range, at different growth temperatures. By means of detailed analysis of these films, we obtained further information about film resistivity and photosensitivity as a function of the composition in the solution. This information is helpful when designing solar cells made using this material. This chapter describes preparation and characterization of $CuInS_2$ films prepared using CSP.

4.2 Experimental Details

Experimental set-up for the deposition is schematically shown in Fig.4.1. Cleaned glass slides were placed on a thick iron block ($15x9x1cm^3$), which can be heated to the required temperature with a controlled heater. Temperature of substrate holder was measured using a digital thermometer (Thermins, series 4000) and temperature control was achieved using a variable transformer. Spray head and heater with substrate are kept inside a chamber provided with an exhaust fan for removing gaseous by-products and vapor of the solvent (here water). During spray, temperature of substrate was kept constant with an accuracy of $\pm 5^0$C. Pressure of carrier gas was noted using a manometer and was kept at 90±0.5 cm. of Hg. Spray rate was 15ml/min., and distance between spray head and the substrates was ~15cm. In order to get uniform

composition and thickness, spray head was moved to either side manually with uniform speed.

$CuInS_2$ thin films were deposited over glass substrates from aqueous solutions of cupric chloride ($CuCl_2.2½H_2O$),indium tri chloride ($InCl_3$), and thiourea ($CS(NH_2)_2$) using compressed air as the carrier gas. Thiourea was chosen as the source of sulfur ions in spray solution because it avoids precipitation of metallic sulfides and hydroxides since it forms complexes with copper and indium ions easily [7]. Aqueous solutions of these salts were prepared in distilled water, and Cu/In ratio and S/Cu ratio in spray solutions were varied. Substrates were kept at different temperatures in order to study its effects on the deposited films.

We varied deposition temperature from 200°C to 400°C, Cu/In ratio from 0.5 to 1.5 and S/Cu ratio from 4 to 8. Even though deposition and characterization of $CuInS_2$ thin films using spray pyrolysis was reported previously by several groups [8-10], such wide variation in composition of spray solution has not been reported yet. Structural, electrical, optical and composition analysis of all these films were done. Photosensitivity of these films were measured and obtained conditions for depositing films with good photoresponse (87%). To the best of our knowledge, such study has not been conducted for $CuInS_2$ thin films prepared from solutions with wide compositional variations. Each of these cases will be discussed in the following sections.

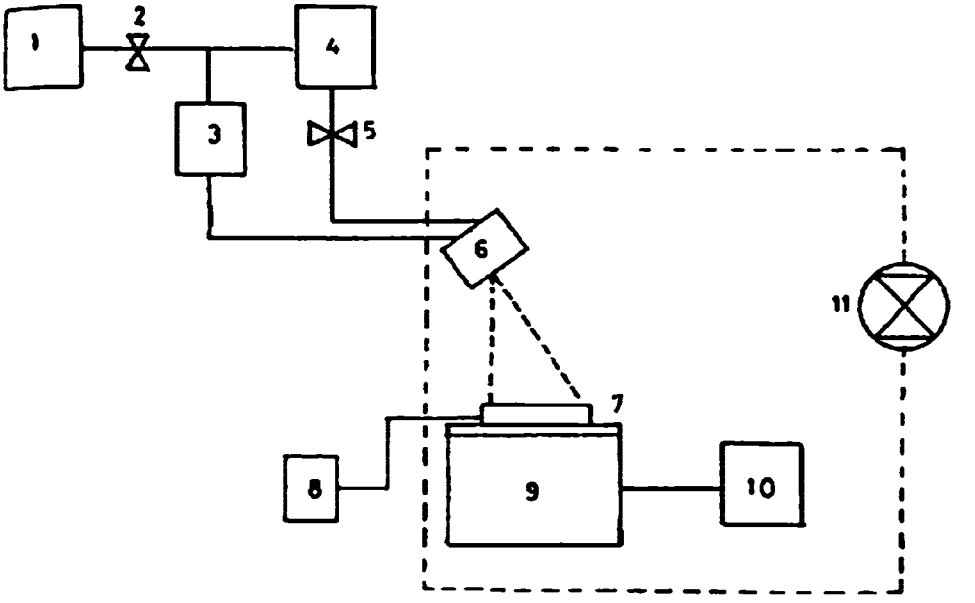

1. Air compressor
2. Gas flow control valve
3. Manometer
4. Solution reservoir
5. Solution flow control valve
6. Spray head
7. Substrate
8. Thermometer
9. Substrate heater
10. Heater control
11. Exhaust fan

Fig.4.1 Experimental set up for spray pyrolysis system

4.3 Variation of Cu/In at 400°C, keeping S/Cu = 4

Cu/In ratio in the solution was varied by adding appropriate amounts of indium chloride with respect to a fixed concentration of copper in the form of $CuCl_2.2\ ½\ H_2O$. At first, Cu/In molar ratio in spray solution was varied as 0.9, 1 & 1.1. It was already reported that because of loss of chalcogen during pyrolysis process, the amount of sulfur relative to copper in the spray solution should be at least double that required theoretically for stoichiometry [11]. Hence to compensate the loss of sulfur during spraying, S/Cu molar ratio was fixed at 4. The samples are named A, B, & C respectively. Composition of the spray solution was:

$CuCl_2.2½H_2O$ – 0.025M ; 100ml

$CS(NH_2)_2$ -0.1M ;100ml

$InCl_3$ – 0.0277M (for sample A) , 0.025M (sample B) , & 0.022M(sample C) ;100ml

In all cases, pH of solution was kept at 3. The deposition temperature was 400^0C. Glass slides (37.5mm×12.5mm×1.25mm) cleaned as described in section 5.2.1 were placed on the substrate holder and were heated to the required temperature. These were kept in that stabilized temperature for one hour and then solution was sprayed at a rate of 15ml/min. After completion of spray, the samples were kept at the same temperature for ½ hour and were then allowed to cool at a rate of 3^0C/min.

$CuInS_2$ is formed by pyrolytic decomposition of sprayed droplets on the surface of the heated substrates. Films obtained were extremely adherent to the substrates and were homogeneous in appearance. In order to characterize these films, structural, optical and electrical studies were carried out.

4.3.1 X- ray diffraction

X-ray diffraction patterns of the films are shown in Fig.4.2. They show good crystallinity with preferred orientation along (112) direction. Peak intensity is maximum for sample A, but the peak is sharper for sample B. For sample C (Cu/In = 1.1), peak height is very much less than that obtained for sample A.

Grain size was calculated from the (112) peak using Scherrer's formula and is tabulated in Table 4.1. Among the three samples, sample B has the largest grain size.

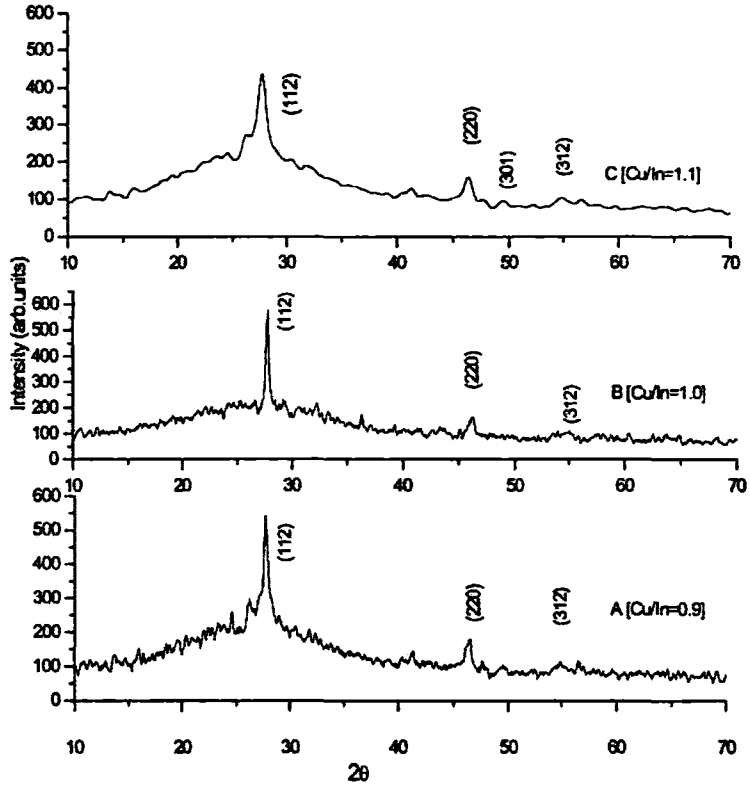

Fig.4.2 X-ray diffraction pattern of samples A, B & C

Table-4.1. Grain size of samples A,B & C

Sample	A	B	C
Grain size (nm)	23	30	16

4.3.2 Optical properties

Figure 4.3 shows the transmission (T) as a function of wavelength for samples A, B & C. Transmission decreases sharply after a particular wavelength and onset of the decrease represents the fundamental absorption edge [12]. It was observed that this onset shifted slightly towards lower wavelength side as Cu/In ratio in the spray solution increased.

To calculate value of the bandgap, a graph with $(\alpha h\nu)^2$ against hν was plotted for region near and above the fundamental absorption edge (Figure 4.4). Extrapolated intercept on hν axis gave value of the bandgap. From the graph, band gaps obtained for samples A & C are 1.42eV. For sample B, band gap is 1.4 eV. Band gap of sprayed films is expected to be lower than that of single crystal as a result of appearance of an exponential or nearly exponential absorption tail, due to the formation of density of states tail at band edge [8].

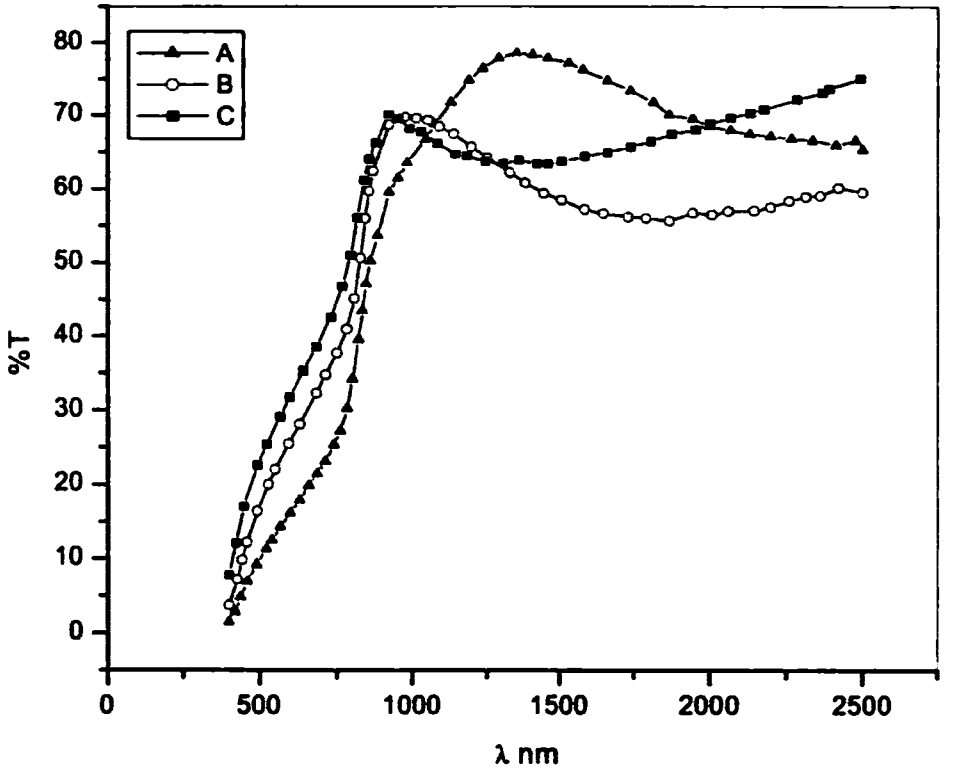

Fig.4.3 Transmission spectra of samples A, B, & C

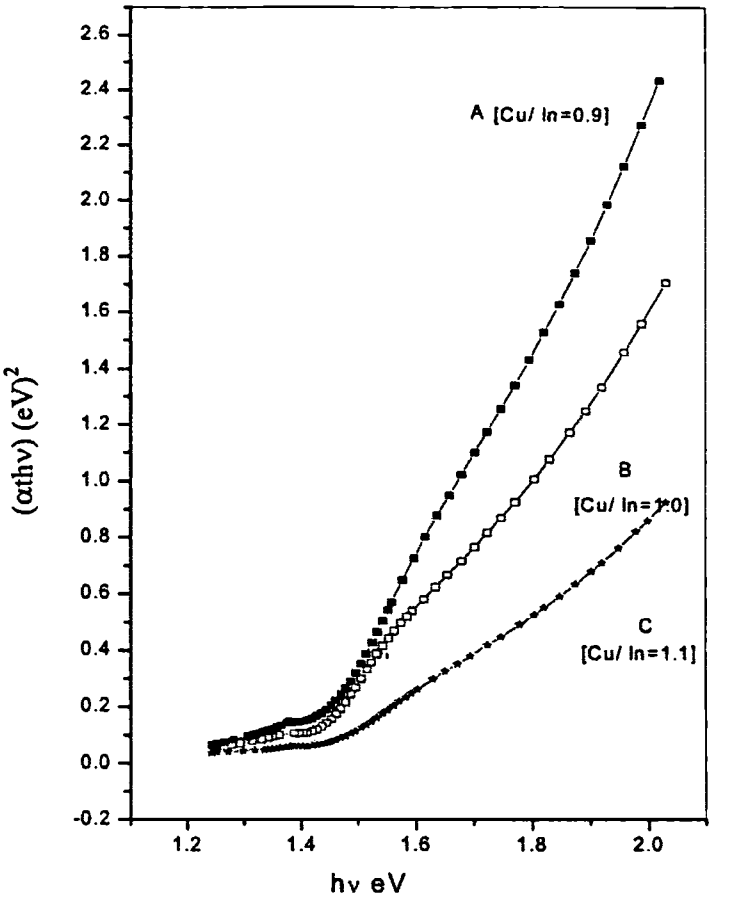

Fig.4.4 $(\alpha h\nu)^2$ vs. hν plot of A, B, &C

4.3.3 Scanning Electron Micrograph

SEM micrographs of the films indicated polycrystalline nature with well-defined circular grains and are shown in Fig.4.5. Among these samples, sample B has better crystalline nature as is evident from XRD as well.

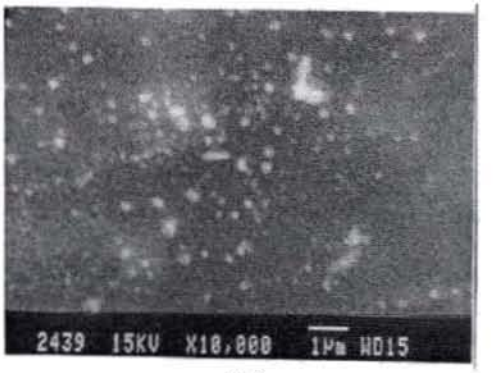

(A)

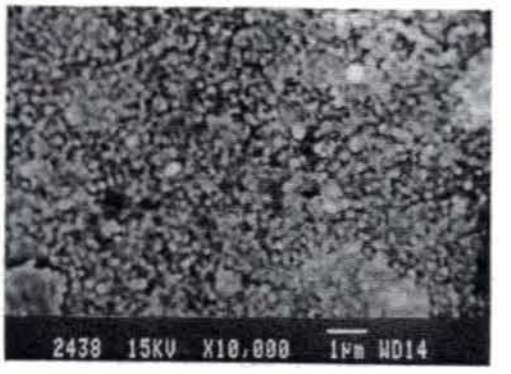

(B)

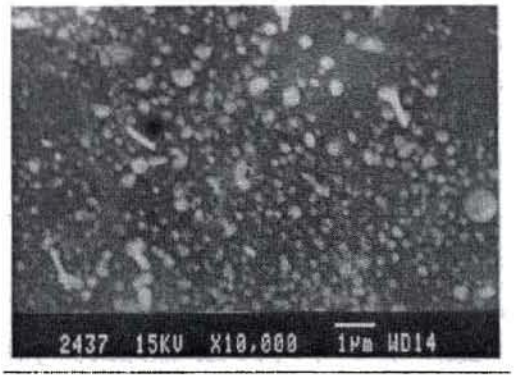

(C)

Fig.4.5 SEM of samples A, B, & C

4.3.4 Electrical properties

Resistivity, carrier concentrations and mobility of the films were determined using Hall measurement and results are tabulated in Table-4.2. All these films were found to be p-type. Resistivity of these films varies with variation in Cu/In ratio. Sample B (Cu/In =1) had the lowest resistivity (1.21Ω cm). Sample A and C had almost equal resistivity (70 & 60Ω cm. respectively).

Table-4.2 Hall measurement results

Sample	Resistivity (ρ) Ω cm	Mobility (μ) cm^2/Vs	Carrier density (cm^{-3})	Type of carriers
A	70	4.73	1.88×10^{16}	holes
B	1.21	2.24	2.29×10^{18}	holes
C	60	103	1×10^{15}	holes

4.3.5 Photosensitivity

Photosensitivity (S) was determined from measured values of resistance of the film in darkness and under an illumination of $40mW/cm^2$, as described in section 3.7.4. Values obtained for samples A,B,& C are 13.8%, 14.2%, and 27.8% respectively. Here sample C was found to be better in photosensitivity.

4.3.6 XPS Analysis

Atomic concentration percentage (at.%) of different elements present in these samples was compared using XPS depth profile. In all the cases, Cu/In ratio in film was found to be greater than that in spray solution. Also, these samples are found to be deficient in sulfur. Table-4.3 gives approximate atomic concentration % of different elements present in the sample. Results of XPS analysis of sample B prepared at a lower temperature of 250^0C are also included in the table.

Table-4.3 Atomic percentage from XPS analysis

Sample	Cu %	In %	S %	O %	Cu/In	(Cu+In)/S
A	44	24	27	5	1.83	2.51
B	44	24	28	4	1.83	2.42
C	40	25	31	4	1.6	2.09
B(L.T)	35	28	35	2	1.25	1.8

From Table 4.3, it is evident that for the sample prepared at low temperature, at.% of S and Cu/In ratio is better. Depth profile of atomic concentration of sample B is shown in Fig.4.6. All the elements are almost uniformly present throughout the thickness of the sample.

Even though air was used as the carrier gas for spraying, only 2-5% of oxygen is present in these films, and for the sample prepared at low temperature, at. % of oxygen is only 2%.

Binding energy values obtained for different elements are in conformity with earlier reported values. XPS depth profile showing binding energy of one of these samples (sample B) is shown in Fig. 4.7. There is one peak corresponding to oxygen at the surface. This peak situated at binding energy of 531.75eV can be attributed to elemental oxygen due to surface contamination [10]. After etching, this contribution decreases strongly, which confirms that this is due to surface contamination itself.

Peaks corresponding to all elements are very slightly shifted as the analysis proceeds from the surface to the substrate. This is due to the influence of the substrate

as it is possible that all these elements may slightly diffuse into the glass substrate during deposition.

From above analysis, it is found that high substrate temperature does not favor better stoichiometry of $CuInS_2$ films. In order to optimize growth temperature, sample B was prepared at different temperatures.

4.4 Variation of deposition temperature

$CuInS_2$ films were prepared using CSP over glass substrates heated to different temperatures ranging from 200 ^{0}C to 400 ^{0}C, keeping composition of the spray solution same as that used for the preparation of sample B. i.e., using the solution in which Cu/In = 1, and S/Cu = 4. At 200 ^{0}C, the films formed were not uniform and had several pinholes and adhesion was very poor. Films prepared at higher temperatures (like 380^{0}C and 400 ^{0}C) appeared thinner than those prepared at lower temperatures. Characterization of all these films was done using different techniques and these are described below

4.4.1 XRD

As growth temperature increases, crystallinity of the films improves as indicated in Fig. 4.8. Good crystallinity was achieved between 350 °C and 400 °C. Preferred orientation of the crystallites is along the (112) plane. Peak corresponding to (220) plane is visible only for samples prepared above 300 °C. Grain size of these samples is listed in Table-4.4. From which, it is clear that grain size increases with deposition temperature.

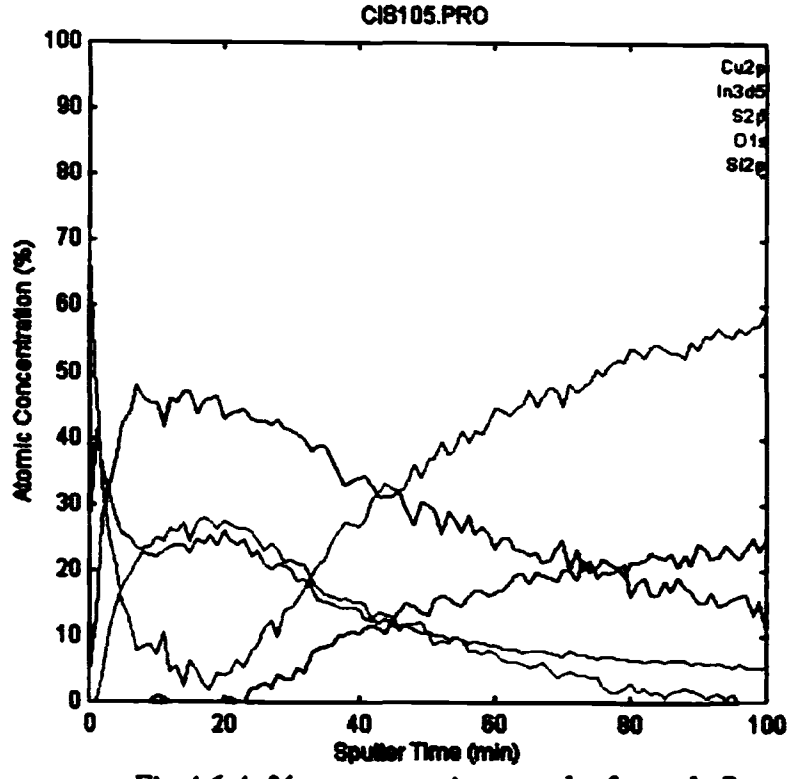

Fig.4.6 At.% vs. sputter time graph of sample B

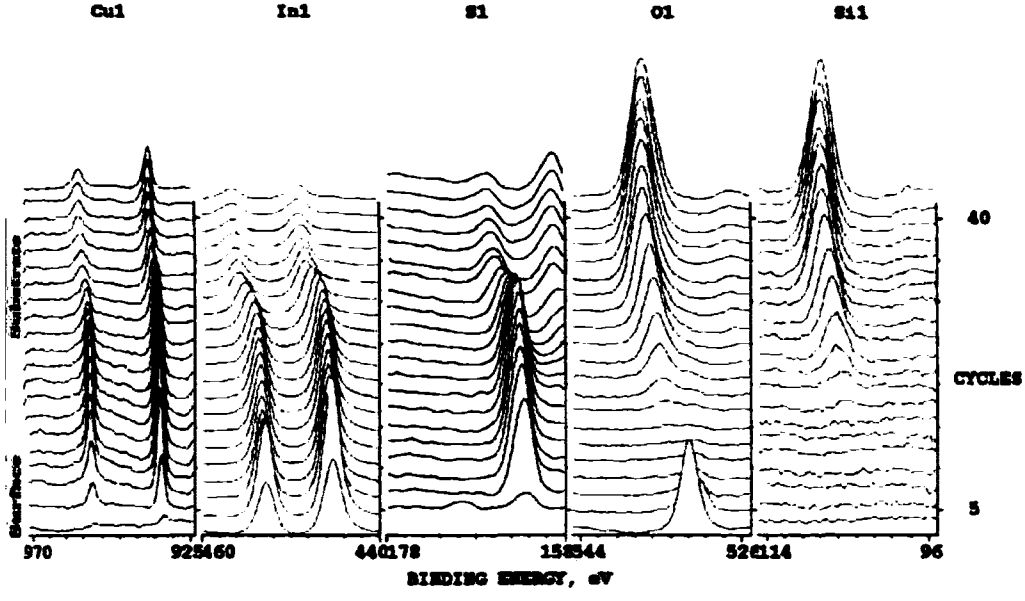

Fig.4.7 XPS depth profile of sample B

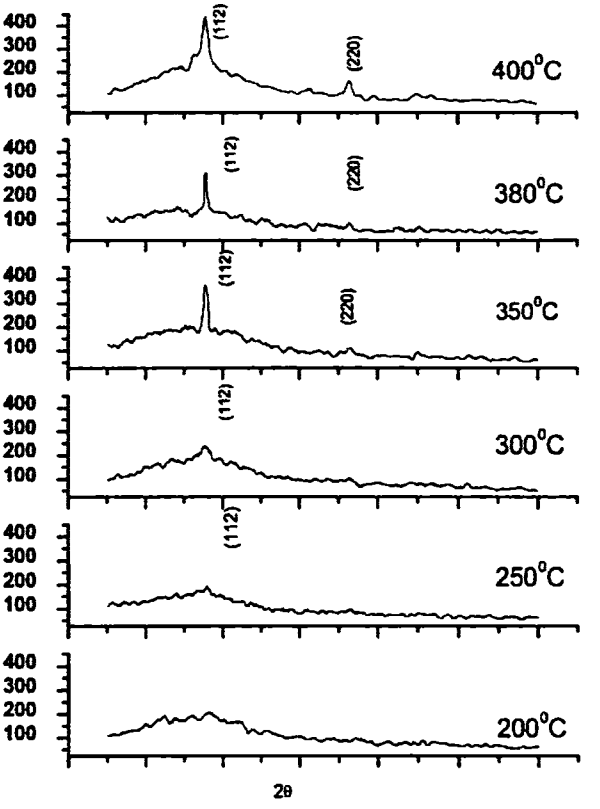

Fig.4.8 XRD of samples prepared at different deposition temperatures

Table-4.4

Grain size of samples prepared at different deposition temperatures

Deposition temperature	300°C	350°C	380°C	400°C
Grain size (nm)	22	48	38	30

4.4.2 Optical properties

Fig.4.9 presents typical transmittance spectra obtained for $CuInS_2$ films deposited at different substrate temperatures. The spectra show that the transmission is around 55%-65% for these films in the 1000-2500 nm wavelength range. For samples prepared at 200^{0}C and 250^{0}C, there is only a single slope in the region 250nm - 1000nm, whereas, curves for samples prepared at temperatures above 350^{0}C have two distinct slopes. For the sample prepared at 300^{0}C, second slope is just beginning to appear while this is more prominent for the sample prepared at 380^{0}C. Occurrence of two distinct slopes in the absorption edge suggests the presence of impurity phases in the sample [11]. However no such impurity phase could be detected using XRD.

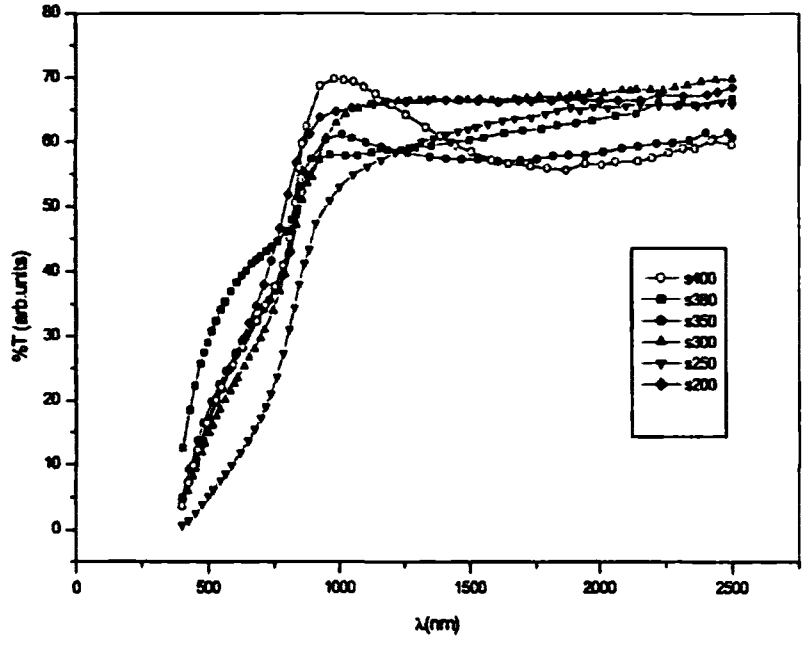

Fig.4.9 Transmission spectrum of samples prepared at different growth Temperatures

To determine the energy gap, $(\alpha h\nu)^2$ vs. hν graph was drawn for all these films and is represented in Fig.4.10 . Variation of the band gap with growth temperature is shown in Fig.4.11. Except for the sample prepared at 200°C, band gap value lies in between 1.39eV and 1.43 eV. In addition to the direct transition at 1.43 eV, films prepared at 380°C show a second transition at about 1.27 eV, which matches with optical gap of Cu_xS. In the case of samples prepared at 400°C, second transition is at 1.17eV. However, these Cu_xS impurity phases could not be detected from XRD spectra. This indicates that these phases may be present in traces, which could not be detected using XRD.

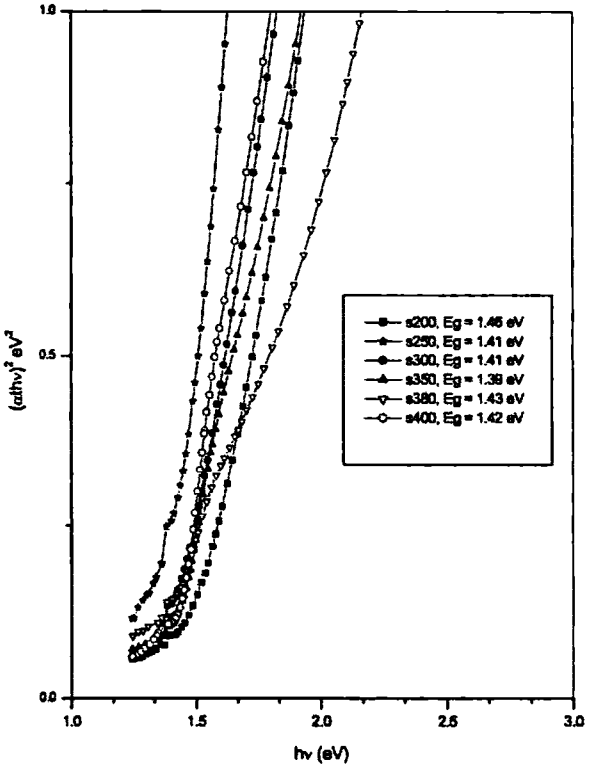

Fig.4.10 $(\alpha h\nu)^2$ vs. hν plot for the samples

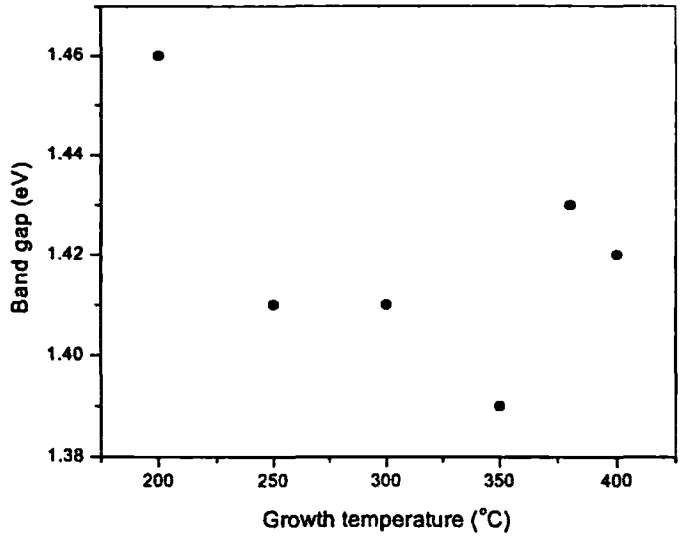

Fig.4.11 Variation of bandgap with growth temperature

4.4.2 Electrical properties

Electrical properties of these films were studied using Hall effect measurements and the results are represented in Table- 4.5. Variation of electrical resistivity and mobility with deposition temperature is indicated in Fig. 4.12. Type of carriers was "holes" in all these cases. When deposition temperature is increased from 300°C to 380°C, electrical resistivity of films decreases. This is obviously caused by increase in grain size due to recrystallization processes. For sample prepared at 300°C, grain size was 22nm, and it increased to 48nm & 38nm respectively for samples prepared at 350°C & 380°C. For the sample prepared at 400°C, grain size was 30nm.

Table- 4.5

Electrical properties of samples prepared at different deposition temperatures

Substrate temperature (^{0}C)	Resistivity Ω-cm	Mobility cm^2/Vs	Carrier density (cm^{-3})	Type
250	1.21	0.285	$1.81x10^{19}$	holes
300	34.9	7.19	$2.49x10^{16}$	holes
350	3.04	4.06	$5.05x10^{17}$	holes
380	0.219	6.5	$4.38x10^{18}$	holes
400	1.21	2.24	$2.29x10^{18}$	holes

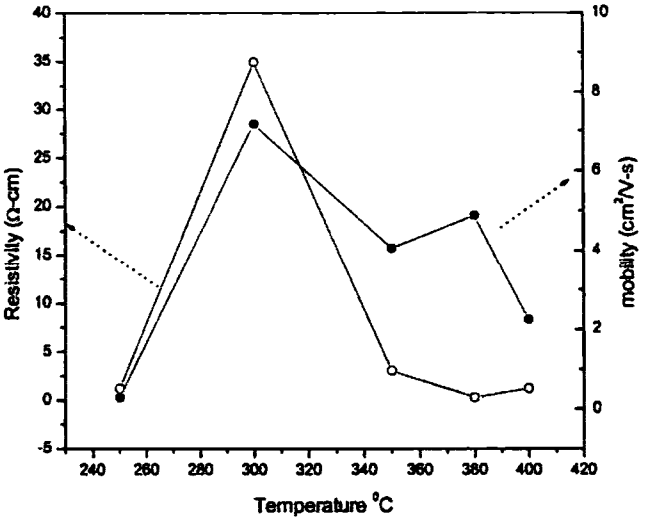

Fig.4.12 Variation in resistivity and mobility with growth temperature

4.4.3 Photosensitivity

Change in photosensitivity of these films with deposition temperature is illustrated in Fig.4.13. It follows that photosensitivity is maximum for the samples prepared at 300^{0}C, and for samples prepared at temperatures above 350^{0}C, photosensitivity is very low. Photosensitivity is an important criterion that should be given due importance while fabricating cells using these films. Hence although crystallinity was better for the samples prepared at higher temperatures, growth temperature for further preparations was fixed at 300^{0}C.

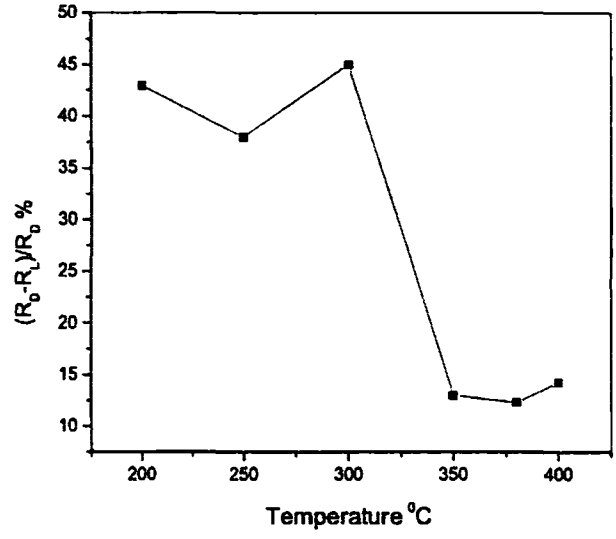

Fig.4.13. Photosensity of samples prepared at different deposition temperatures

4.5 Variation of (Cu+In)/S ratio, keeping Cu/In = 1

$CuInS_2$ films were prepared by maintaining Cu/In ratio in the spray solution as 1 and by increasing S/Cu ratio from 2 to 8 in steps of one {i.e., (Cu+In)/S ratio from 1 to 0.25}. Molarity of copper chloride and indium chloride solutions was fixed at 0.025M, and the molarity of thiourea alone was varied. An equal volume (100ml) of these three solutions was mixed together and was sprayed onto heated glass substrates kept at 300^0C.

4.5.1 XRD

Fig.4.14 shows the XRD spectra of these samples. As S/Cu ratio is increased, X-ray diffraction pattern indicated deterioration of crystallinity of the films. Grain size decreases from 33nm to 20nm as S/Cu ratio increases from 2 to 4. Grain size is still smaller and could not be evaluated for samples with S/ Cu ratio 5 & 6.

4.5.2 Optical properties

Transmission spectra of samples with different S/Cu ratio are represented in Fig.4.15. Here also, all these samples have transmission around 55%-65% in 1000 to 2500nm wavelength region, except the sample for which S/Cu =2. In this case, transmission is only around 10%.

Figure 4.16 shows the plots of $(\alpha h\nu)^2$ vs. hv and band gap values obtained are in the range 1.40-1.47 eV. For the samples prepared from solution containing S/Cu = 2, band gap is 1.51 eV. In addition to this, there is another absorption edge at 0.87 eV for this sample, which may be due to the presence of Cu_xS impurity phases in the sample.

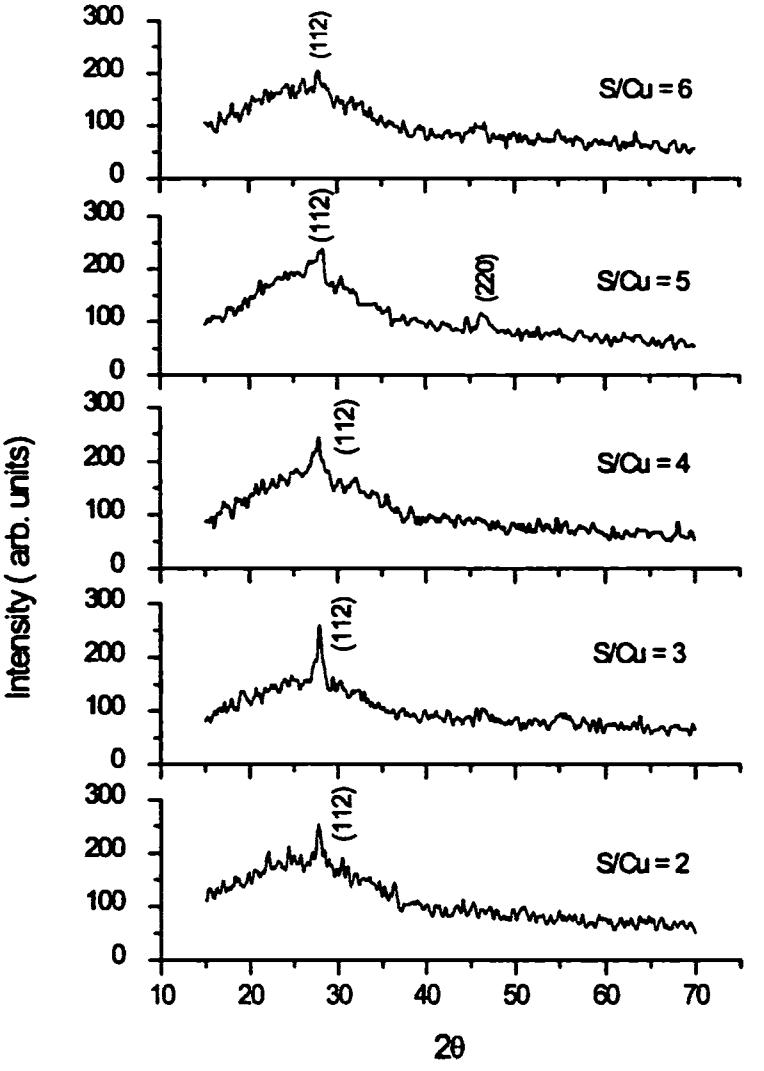

Fig.4.14 XRD of samples prepared with different S/Cu ratio

4.5.2 Electrical properties

Sheet resistance of the samples was measured at room temperature using Keithley I-V measurement system and the values obtained are depicted in Table-4.6. Silver electrodes were painted on the surface of the film keeping a distance of 5mm between the electrodes.

Table-4.6

Sheet resistance of samples with different S/Cu ratio

S/Cu ratio in the spray solution	2	3	4	5	6
Sheet resistance KΩ/□	13.6	2.2	143.5	39.8	80

Conductivity type of samples was determined using hot probe method. Samples prepared from solutions with S/Cu ratio 2 and 3 showed n-type conductivity and other samples showed p-type conductivity. This clearly indicates that excess of sulfur is not present in these two samples. But as sulfur concentration increases in solution, samples are converted into p-type.

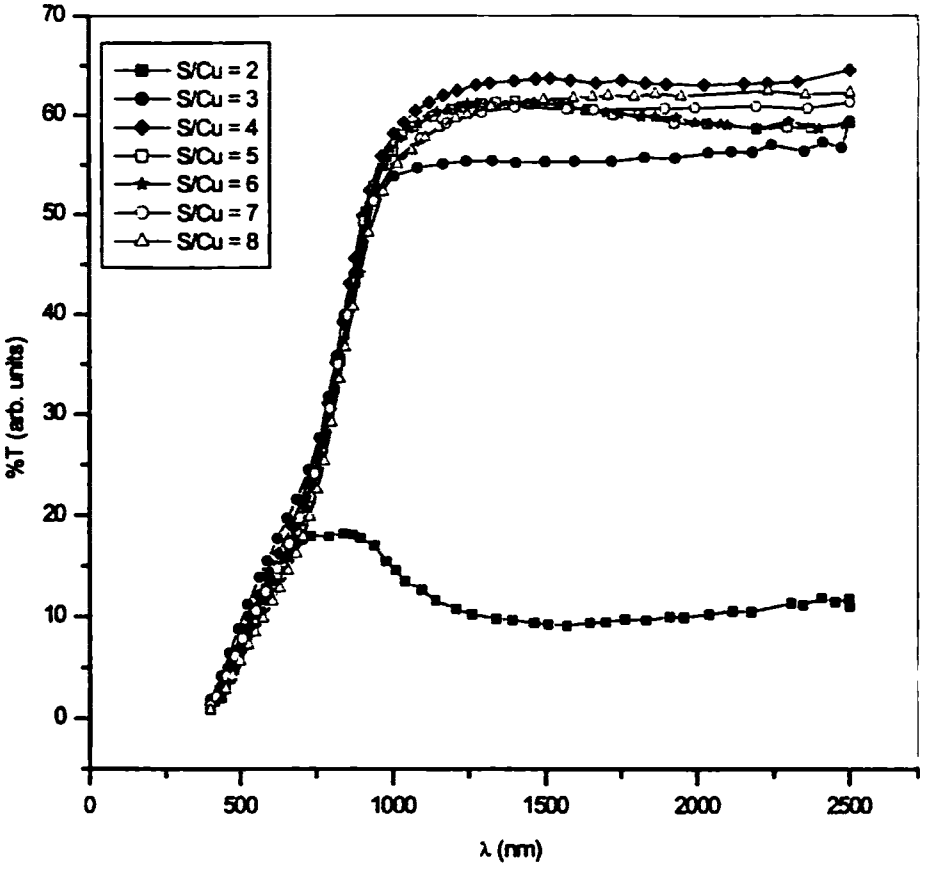

Fig.4.15 Transmission spectrum of samples prepared with different S/Cu ratio

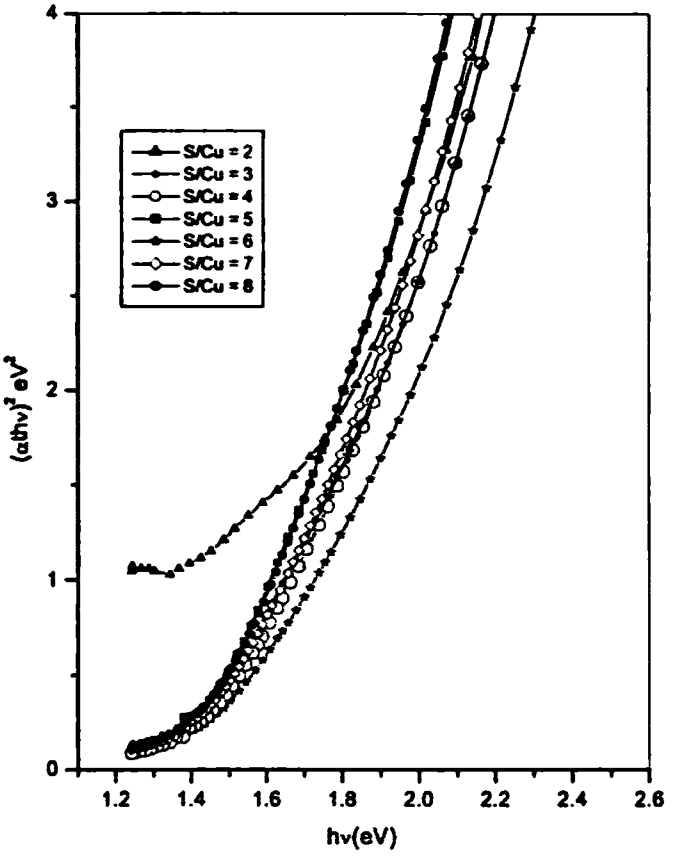

Fig.4.16 $(\alpha h\nu)^2$ vs. hν plot for samples with different S/Cu ratio

4.5.4 Photosensitivity measurement

Photosensitivity of these samples is shown in Fig.4.17. It decreases with increase in the S/Cu ratio and is maximum for samples prepared using the sulfur deficient solution containing S/Cu ratio = 2. Among the other samples the one prepared from a solution containing S/Cu ratio 4 is the best.

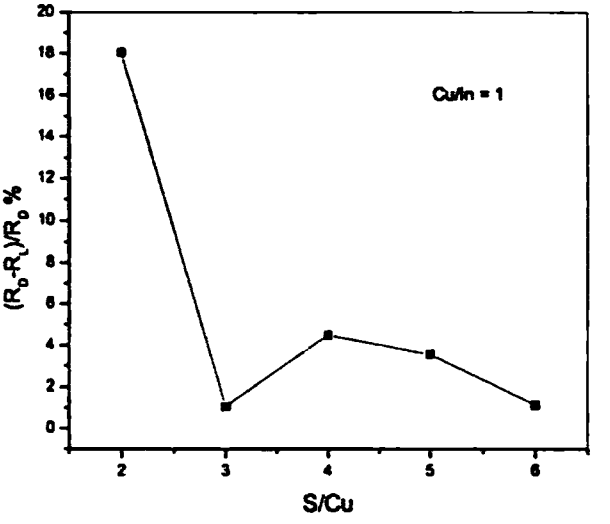

Fig.4.17 Variation in photosensitivity with S/Cu variation in the spray Solution

4.6 Variation in Cu/In at 300°C, keeping S/Cu = 4

Another set of $CuInS_2$ films were prepared by varying Cu/In ratio in the spray solution, in a wide range. This time, the deposition temperature is 300°C, S/Cu ratio was 4 and the Cu/In ratio was varied from 0.5 to 1.5. Again these samples were characterized as in the earlier cases.

4.6.1 XRD

XRD pattern of samples prepared from different Cu/In ratios in solutions were compared and XRD spectra of some of these samples are represented in Fig.4.18. As Cu/In ratio increases in the spray solution, samples improve in crystallinity as indicated by the sharpness and intensity of the peaks. Also, an increase in grain size was observed with increase in Cu/In ratio and this is given in Table-4.7.

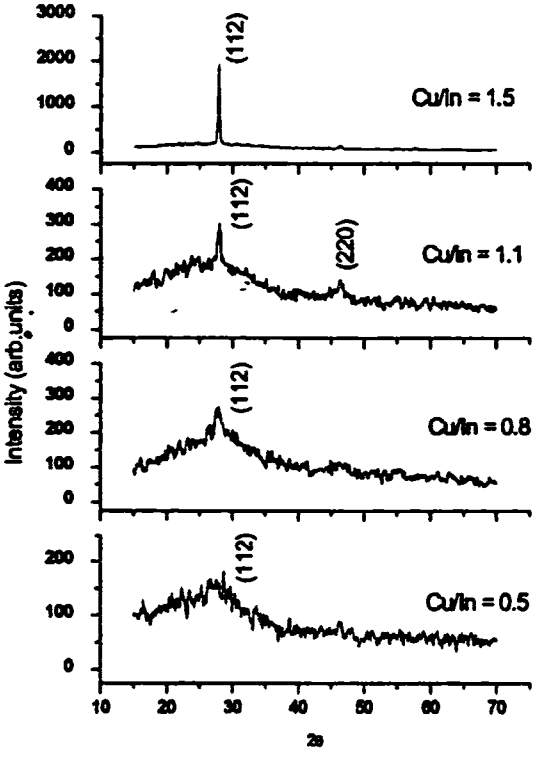

Fig.4.18 XRD pattern of samples with different Cu/In ratio

Table-4.7

Grain size of samples prepared from solution with different Cu/In ratio

Cu/In ratio in solution	0.8	1.0	1.1	1.2	1.3	1.4	1.5
Grain size (nm)	4.2	15	22	43	58	51	51

4.6.2 Optical properties

Optical band gap of these films was determined from the plot of $(\alpha h\nu)^2$ versus photon energy, and is represented in Fig.4.19. Extrapolation of the linear portion to the hv-axis gives value of energy gap, which falls in the range between 1.3 to 1.52 eV. For the sample prepared from Cu/In =1.2 solution, there are two slopes in the absorption edge region of which the first one corresponding to an energy transition at 1.47eV. The second one corresponding to a transition at 1.22eV, matches with the optical band gap of Cu_xS. Similar effect was observed by Tiwari et al. also for $CuInS_2$ films prepared with 50% excess copper [11].

For the sample prepared from a solution containing Cu/In =1.3, the band gap value is 1.3 eV, which is less than that of the other samples. However, an energy band gap of 1.3 has been reported earlier for sprayed films [2]. They attributed this to poor crystallinity. Variation in band gap with different Cu/In ratio in the solution is depicted in Fig.4.20. As Cu/In ratio in the solution increases, band gap gradually decreases. A possible cause for this effect may be carrier degeneracy in $CuInS_2$ due to the defects in the crystalline lattice [7]. It has been reported that copper and indium vacancies (V_{Cu} and V_{In}), interstitial sulfur(S_i) and substitutional copper in indium sites (Cu_{In}) can introduce shallow accepter levels [13]. In the case of samples with high value for Cu/In ratio, probable defect may be Cu_{In}. Bandgap of the film prepared from a solution with

Cu/In ratio 0.5 (1.52eV) is close to 1.55eV, which is the reported value for bulk crystalline $CuInS_2$. For films prepared from solution with Cu/In ratio 0.5 (In-rich solution), probable defects are V_{Cu} and V_S [14]. It is reasonable to assume that the Cu_{In} and V_{In} defect densities may increase when Cu/ In increases, so that the material may become p-type degenerate. From thickness measurement, it was found that as Cu/In ratio increases, thickness decreases.

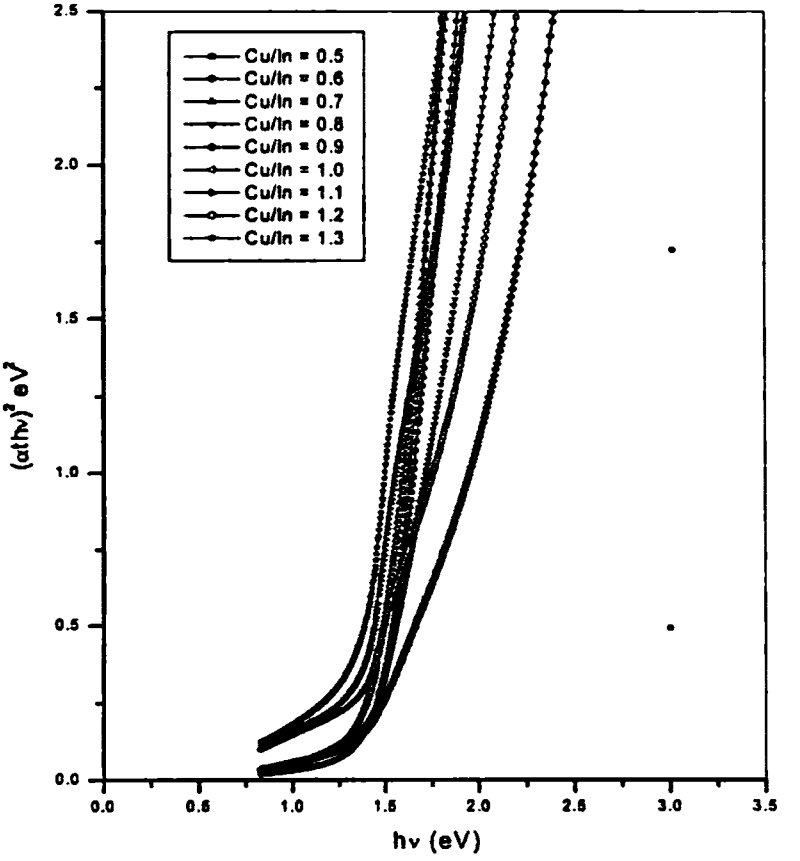

Fig.4.19 Optical absorption of films deposited from solutions with different Cu/In ratio.

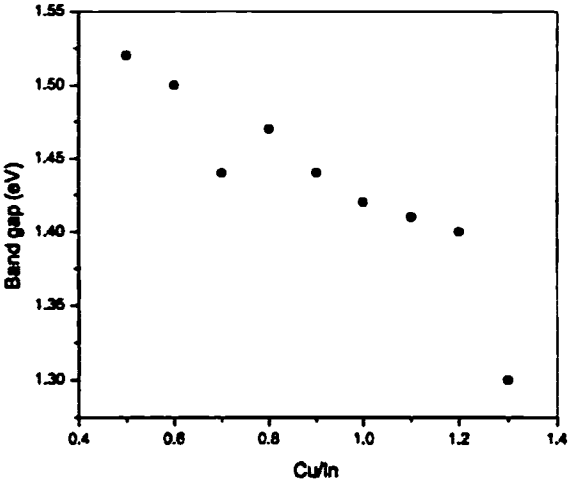

4.20 Variation in band gap with different Cu/In ratio in the spray solution

4.6.3 Thickness

Thickness of some of these films was measured using stylus profilometer. Thickness measurement was carried at three different regions in the film and the average of the consistent values were taken as the approximate thickness of the sample. Fig.4.21 shows typical profile of the measurement done on a sample prepared using the solution with Cu/In ratio 0.5. Here the thickness is 0.77μm. For both the samples prepared using solutions with Cu/In ratio 1.0 and 1.7, thickness was found to be 0.46μm.

4.6.4 Electrical properties

Sheet resistance of all samples was measured using Keithley I-V measurement system. There is drastic decrease in the resistance value from 3009MΩ to 486 Ω, on

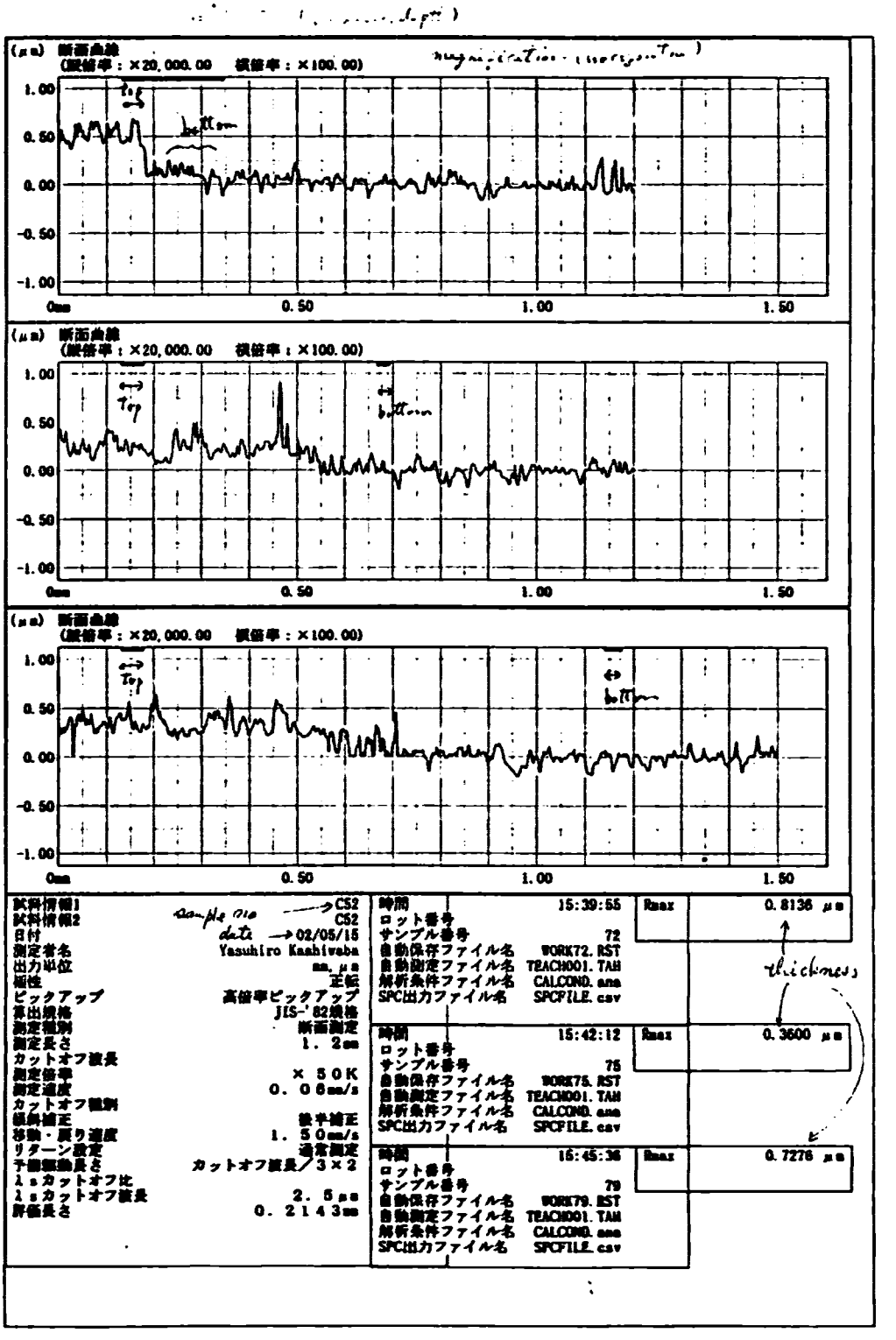

Fig.4.21. Profile of thickness measurement

increasing the Cu/In ratio in the spray solution from 0.5 to 1.7. On increasing the copper concentration, copper impurity levels may increase and the extent of compensation provided by the indium donor levels decrease, leading to the lower dark resistance. Variation in sheet resistance of the samples with different Cu/In ratio (0.5 to 1.7) in the spray solution is shown in Fig.4.22. Raja Ram et al. observed an improvement in conductivity of films with increase in Cu/In ratio in the starting solution from 0.96 to 1.2 [8].

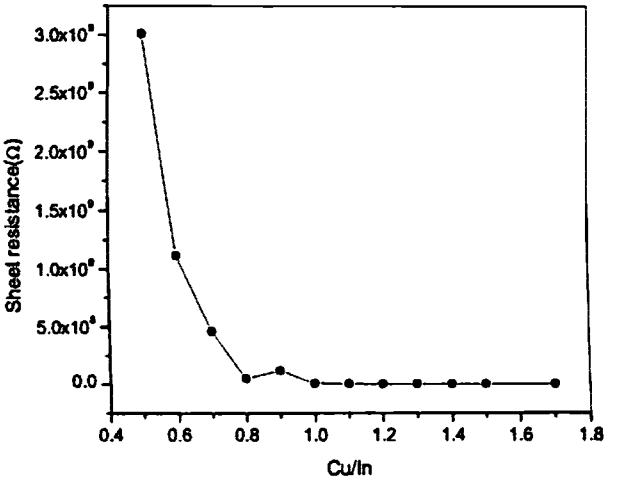

Fig.4.22. Variation in sheet resistance of the samples with Cu/In ratio in the spray solution

The type of conductivity of these samples was determined using hot-probe method. All the samples showed p-type conductivity irrespective of the Cu/In ratio in the spray solution. This indicated that carrier type is very much sensitive to S/Cu ratio (or sulfur to metal ratio).

4.6.5 Photosensitivity

Photosensitivity measurements of these samples (Fig.4.23) revealed that it is maximum for the sample prepared from the solution in which the Cu/In ratio is 0.5. Photosensitivity decreases gradually with increase in the Cu/In ratio up to 0.9, and thereafter it decreases rapidly to very low values as Cu/In value increased upto 1.2. Samples having still higher Cu/In ratio turn to be very poor in photosensitivity.

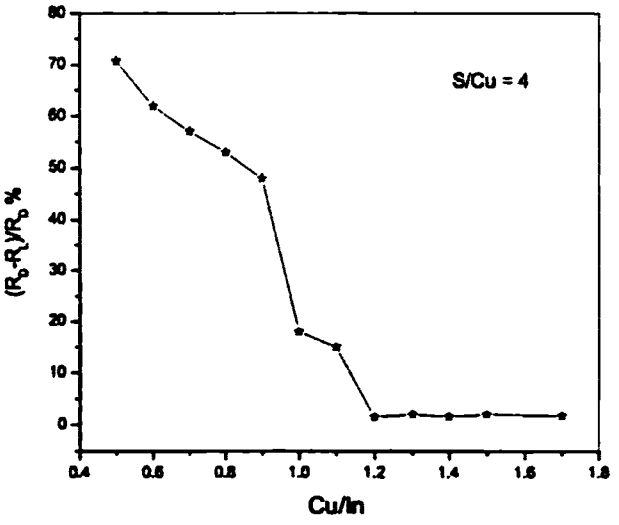

Fig.4.23 Photosensitivity of samples with different Cu/In ratio in the solution

4.6.6 XPS

XPS spectra of these films prepared from solutions with four different Cu/In ratios (i.e., Cu/In = 0.5,1.0,1.5 & 1.7) were taken. At. conc.% of Cu, In, S and O in these films are tabulated in Table- 4.8. Fig.4.24 illustrates the Cu/In ratio in the film as a function of Cu/In ratio in the solution.

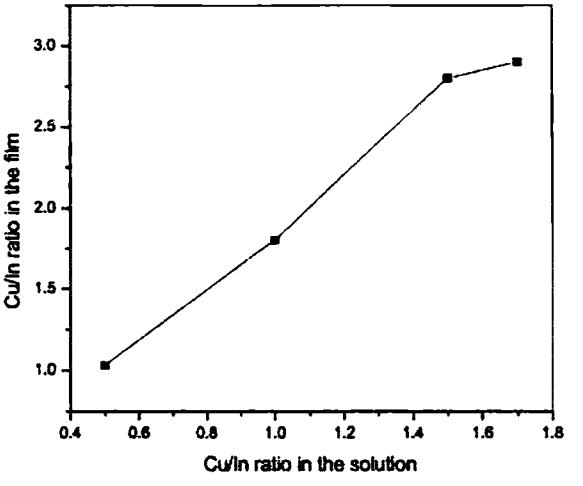

Fig.4.24 Cu/In ratio in the film as a function of Cu/In ratio in the solution

Table-4.8
At. % from XPS analysis

Cu/In ratio in the spray solution	Cu%	In%	S	O	Cu/In in the film
0.5	34	33	26	7	1.03
1.0*	42	24	29	3	1.8
1.5	52	18	27	3	2.8
1.7**	50	17	27	3	2.9

* 2% Cl was detected in this sample

** 3% Na was detected

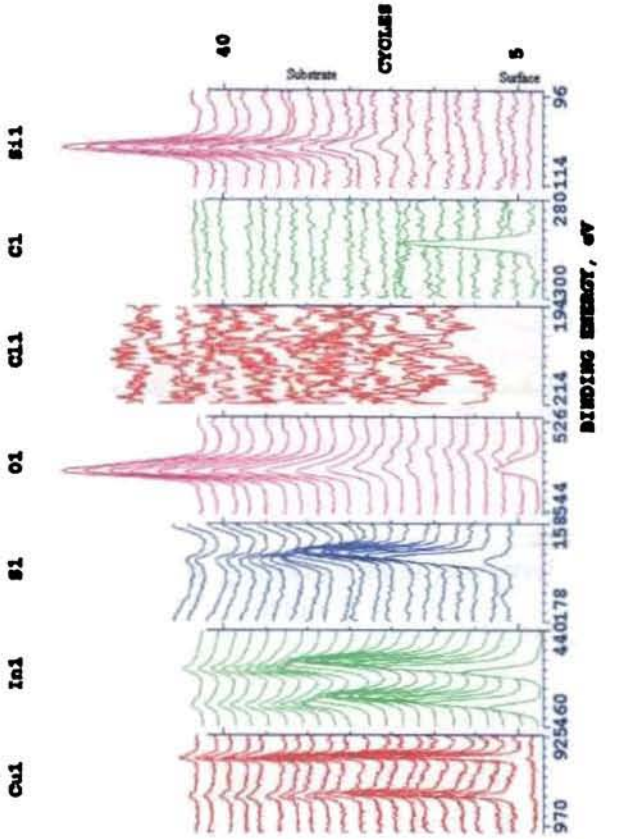

Fig.4.25 XPS depth profile of sample prepared from the solution with Cu/In ratio 0.5

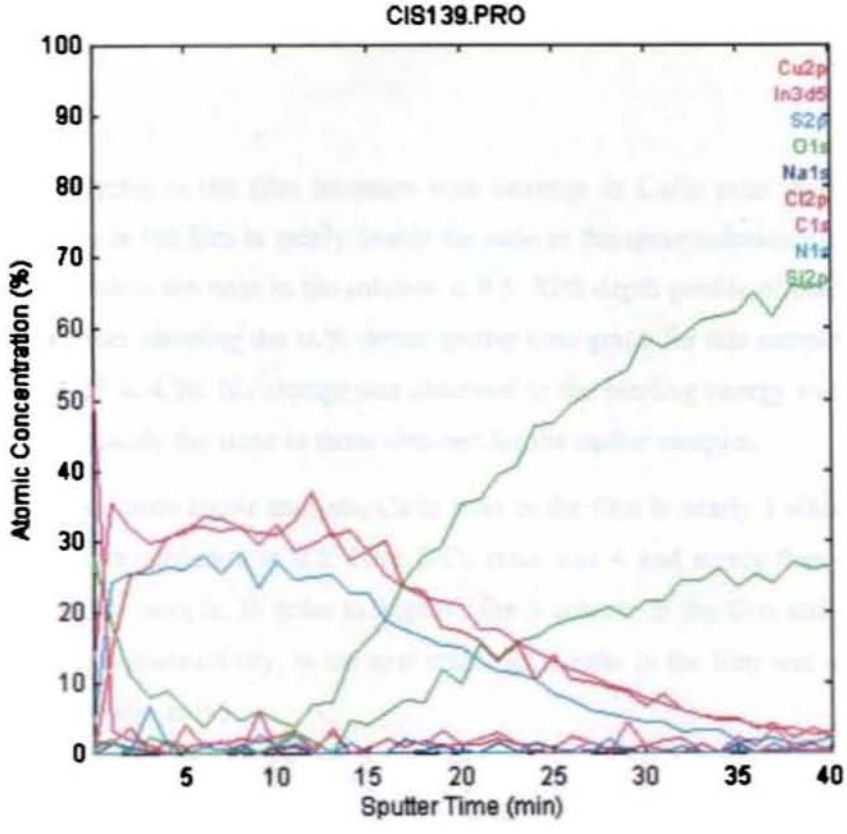

Fig.4.26 At.conc.% vs. sputter time graph of sample prepared from solution with Cu/In ratio 0.5

Cu/In ratio in the film increases with increase in Cu/In ratio in the solution. Also, the ratio in the film is nearly double the ratio in the spray solution. Cu/In ratio in the film is 1 when the ratio in the solution is 0.5. XPS depth profile of binding energy and the spectrum showing the at.% versus sputter time graph for this sample are shown in figures 4.25 & 4.26. No change was observed in the binding energy and the values obtained are exactly the same as those obtained for the earlier samples.

As seen from above analysis, Cu/In ratio in the film is nearly 1 when the Cu/In ratio in the spray solution is 0.5. Here S/Cu ratio was 4 and surely there is some S deficiency in the sample. In order to improve the S content in the film and to study its effect on the photosensitivity, in the next stage, S/Cu ratio in the film was again varied keeping Cu/In ratio as 0.5.

4.7 Variation in S/Cu ratio, keeping Cu/In = 0.5

Molarity of copper chloride and indium chloride was fixed at 0.0125M & 0.025M respectively and the molarity of thiourea solution was varied to get different S/Cu ratios (from 4-8) in the initial spray solution. 300ml solution was sprayed at a time onto heated glass substrates kept at a temperature of 300^0C at a spray rate of 15ml/min. These samples were also analyzed as in the previous cases.

4.7.1 XRD

XRD analysis of these samples revealed that they lack crystallinity. Fig.4.27 represents XRD spectrum of some of these samples. As S/Cu ratio increases, amorphous nature of films also increases.

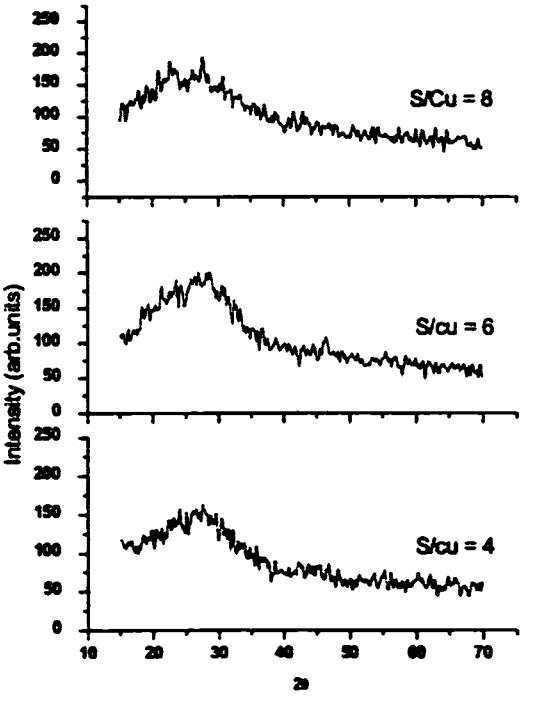

Fig.4.27 XRD of samples with Cu/In ratio 0.5 and different S/Cu ratio

4.7.2 Optical properties

Optical transmission of these films was recorded at room temperature and the curves for wavelength range of 450 nm to 2500 nm are shown in Fig.4.28. As in earlier cases, transmittance is constant for wavelengths higher than 1000 nm and then it decreases sharply in lower wavelength regions.

Bandgap values were calculated from the $(\alpha h\nu)^2$ vs. hν graph (Fig.4.29). The values obtained were 1.55eV, 1.50eV, 1.51eV, 1.51eV & 1.54eV for S/Cu ratio 4,5,6,7 & 8 respectively. An additional absorption edge at 1.76 eV was observed for the sample prepared from the solution containing S/Cu ratio 8, which closely matches with the direct band gap of Cu_xS with x =2.

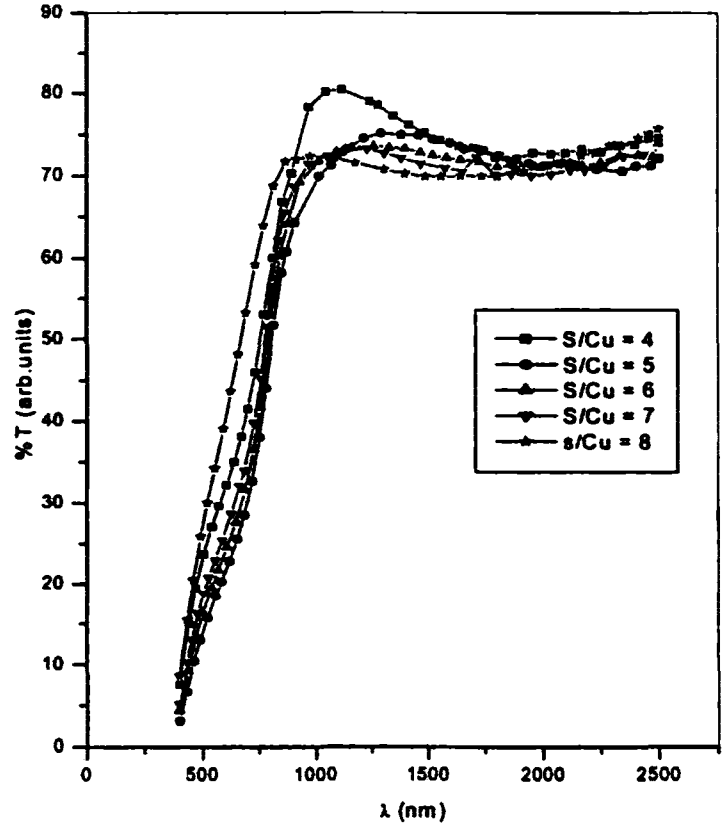

Fig.4.28 Transmission spectra of samples with different S/Cu ratio, keeping Cu/In = 0.5

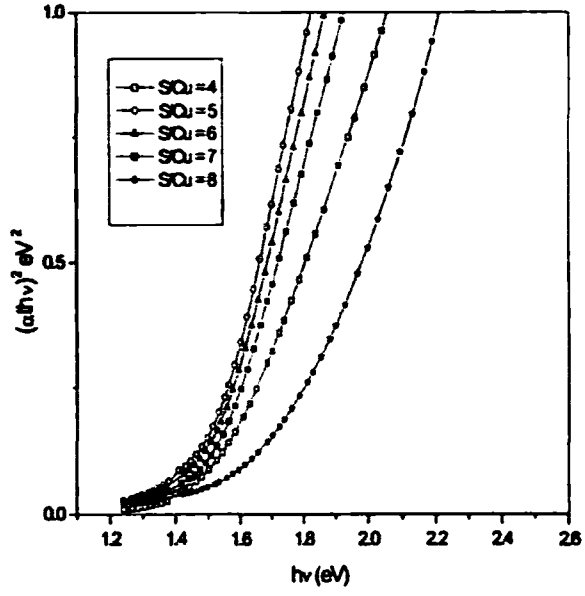

Fig.4.29 Absorption spectrum of samples with Cu/In ratio 0.5 and different S/Cu ratio

4.7.3 Electrical properties

Sheet resistance of samples with different S/Cu ratio is represented in Fig.4.30. It is found that as the S/Cu ratio increases, there is gradual increase in the sheet resistance of these samples. Conductivity type of these samples was tested using hot probe method and was found to be p-type for S/Cu ratios from 4 to 8

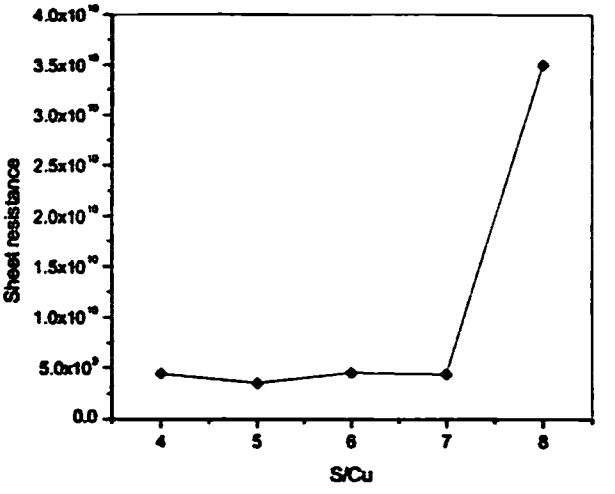

Fig.4.30 Variation in sheet resistance of samples with Cu/In ratio 0.5 and different S/Cu ratio

We could not conduct Hall measurement with most of these high resistive samples. It is to be noted that efforts of Hwang et al. to measure the mobility of rf sputtered $CuInS_2$ films were also unsuccessful [15]. However, we could measure the carrier concentration and mobility values for the sample prepared from the solution with S/Cu = 5. The resistivity, carrier concentration and mobility values for this film are, 254Ω-cm, 1.21×10^{15} and 20.3 respectively.

4.7.4 XPS

XPS depth profile of four samples prepared from solutions containing S/Cu ratio 4,5,6 & 8 were recorded and chemical composition of the films was analyzed. Approximate at.% of different elements in these samples are listed in Table-4.9.

Table-4.9

At.conc.% from XPS Analysis

S/Cu ratio in solution	Cu%	In%	S%	O%	Cu/In ratio in the film
4	34	33	26	7	1.03
5	35	31	31	3	1.12
6	38	29	29	4	1.31
8	24	37	39	0	0.65

As the S/Cu ratio is increased from 4 to 5, there is slight increase in the atomic concentration of S from 26% to 31%. When the S/Cu ratio is 8, at.% of S has increased to 39%, however, for this sample, Cu/In ratio in the film is only 0.65. Atomic conc.% versus sputter time graph for the samples prepared from solutions with S/Cu ratio 5 and 8 are shown in Fig.4.31 & 4.32 respectively.

There was no change in the binding energy values of different elements in these samples. XPS depth profile showing the binding energy values of different elements for the sample prepared from the sulfur rich solution (S/Cu = 8) is shown in Fig.4.33

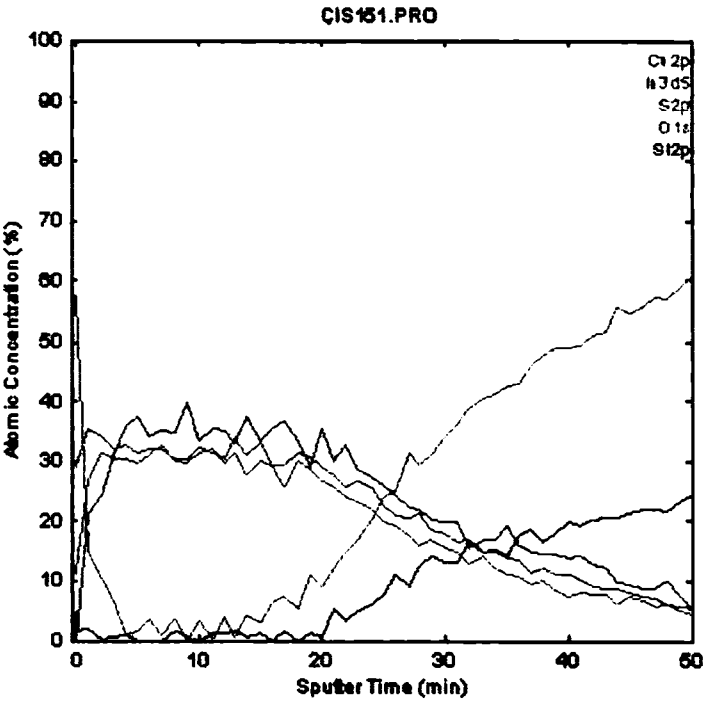

Fig.4.31 Atomic conc.% versus sputter time graph of sample prepared from solution with S/Cu ratio 5

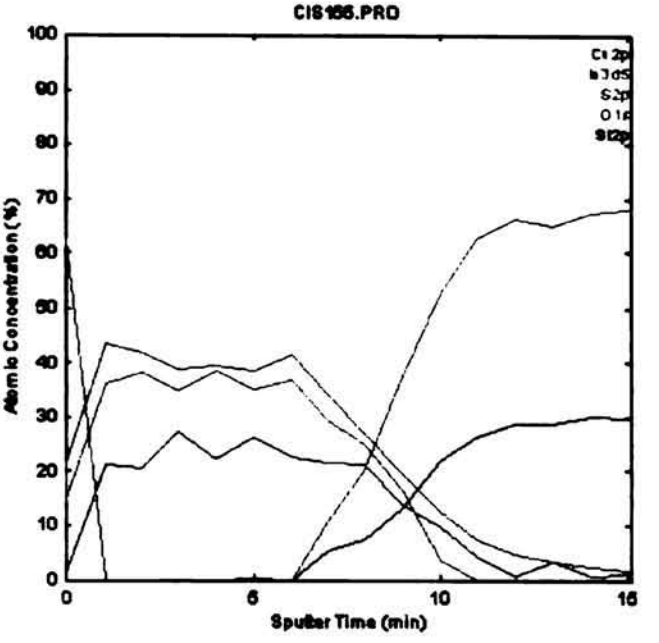

Fig.4.32 Atomic conc.% versus sputter time graph of sample prepared from solution with S/Cu ratio 8

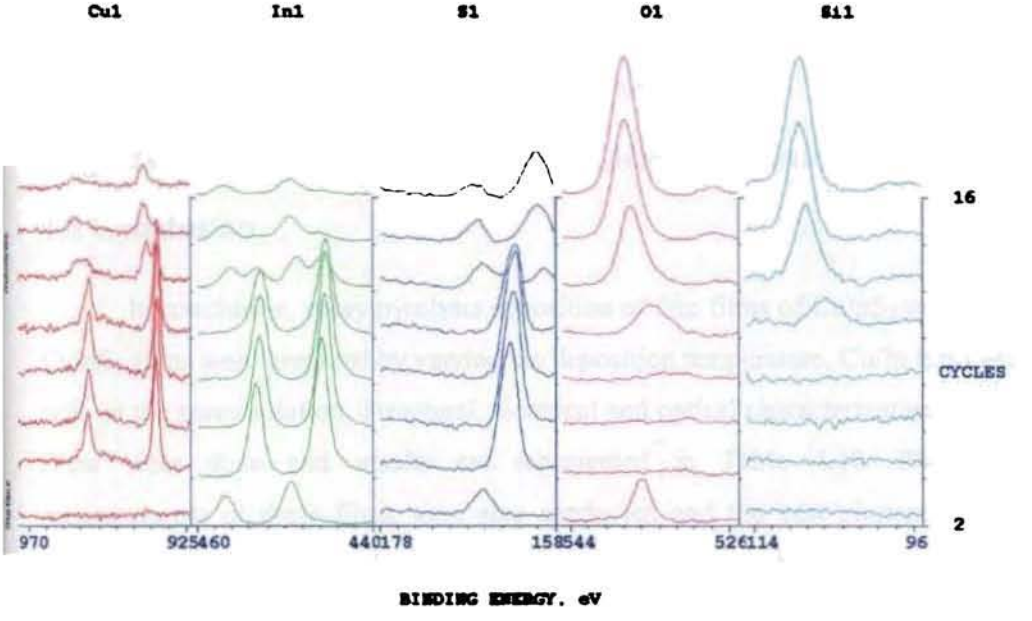

Fig.4.33 XPS depth profile of sample prepared from solution with S/Cu ratio 8

4.7.4 Photosensitivity

Photosensitivity of these samples is shown in Fig.4.34. It increases with increase in S/Cu ratio, reaches high values for S/Cu = 5 &6 and then decreases with increase in S/Cu ratio. Photosensitivity is maximum for samples prepared using the solution containing S/Cu ratio = 5.

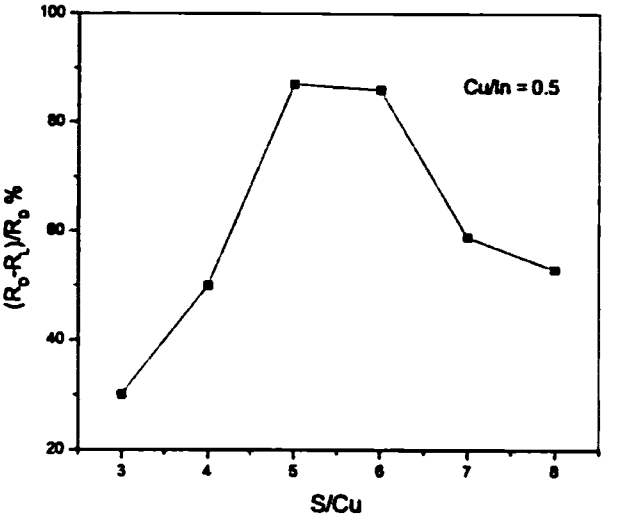

Fig.4.34 Photosensitivity of samples prepared from solution with different S/Cu ratio

4.8 Conclusion

In conclusion, spray pyrolysis deposition of thin films of $CuInS_2$ was successful. $CuInS_2$ films were prepared by varying the deposition temperature, Cu/In ratio and S/Cu ratio in the spray solution. Structural, electrical and optical characterizations of all these films were done and results are represented in Table 4.10. Photosensitivity measurements of these films were also conducted and the best photosensitivity was observed for a film prepared from the solution containing Cu/In ratio 0.5 and S/Cu ratio 5 and this sample was selected as the absorber layer for fabricating junction with CdS.

Table-4.10

Summary of properties of different samples prepared

I. Varaition of Cu/In at 400^{0}C, keeping S/Cu = 4

Cu/In	XRD	Grain size (nm)	Energy Band gap (eV)	Photo sensi-tivity %	Electrical property		XPS			
					ρ (Ω-cm)	μ (cm^2/Vs)	Cu%	In%	S%	Cu/In
0.9	Good crystallinity with preferred orientation along (112) plane	23	1.42	13.8	70	4.73	44	24	27	1.83
1.0		30	1.40	14.2	1.21	2.24	44	24	28	1.83
1.1		16	1.42	27.8	60	103	40	25	31	1.60

I. Varaition of deposition temparature (Cu/In - 1.0, S/Cu - 4)

Deposition Temp.	XRD	Grain size (nm)	Energy Band gap (eV)	Photo Sensi-tivity %	Electrical property		Remarks
					ρ (Ω-cm)	μ (cm^2/ Vs)	
200°C	Good Crysta-llinity At deposition temp. between 300°C and 400°C	-	1.46	43	-	-	Cryrstallinity were better of films Prep. At 350°C, but photosensitivity was higher for samples prepared at 300°C. Hence deposition temp was fixed at 300°C
250°C		-	1.41	38	1.21	0.285	
300°C		22	1.41	45	34.9	7.19	
350°C		48	1.39	13	3.04	4.06	
380°C		38	1.43	12.3	0.219	6.5	
400°C		30	1.42	14.2	1.21	2.24	

III. *Varaition of (Cu+In)/S , keeping Cu/In =1*

S/Cu	XRD	Grain size (nm)	Energy Band gap (eV)	Photo sensi-tivity %	Sheet resistance (KΩ)
2	As S/Cu increased deteriorat ion in crysatalli nity	33	1.51	18.05	13.6
3		25	1.45	1.06	2.2
4		20	1.42	4.49	143.5
5		-	1.43	3.55	39.8
6		-	1.47	1.14	80

IV. *Varaition in Cu/In at 300^{0}C keeping S/In = 4*

Cu/In	XRD	Grain size (nm)	Energy Band gap(eV)	Sheet resistance (Ohms)	Photo-sensitivity %	XPS			
						Cu%	In%	S%	Cu/In
0.5	XRD Pattern	-	1.52	3009M	71	34	33	26	1.03
0.6	Improved With	-	1.50	1118M	62				
0.7	Increase In Cu/In	-	1.44	459M	57				
0.8	ratio	4.2	1.47	50M	53				
0.9		14	1.44	120M	48				
1.0		15	1.42	5.86M	18	42	24	29	1.8
1.1		22	1.41	1.4M	15				
1.2		43	1.47	5.73K	1.57				
1.3		58	1.30	1.99K	2.01				
1.4		51	1.43	901	1.6				
1.5		51	1.42	345	2.0	52	18	27	2.8
1.7		-	-	486	1.75	50	17	27	2.9

V.*Varaition in S/Cu ratio, keeping Cu/In = 0.5*

S/Cu	XRD	Energy Band gap (eV)	Sheet resistance (Ohms)	Photo Sensi-tivity %	XPS			
					Cu%	In%	S%	Cu/In
4	Crysatllinity is not good	1.55	4444M	50	34	33	26	1.03
5		1.50	3.49M	87	35	31	31	1.12
6		1.51	3500M	86	38	29	29	1.31
7		1.51	4523M	59	-	-	-	-
8		1.54	4377M	53	24	37	39	0.65

References

[1] R.R. Chamberlin and J.S. Skarman, *J. Electrochem. Soc.*, 113 (1966) 86

[2] B. Pamplin, and R.S. Feigelson, *Thin Solid Films*, 60 (1979) 141

[3] M. Gorska, R. Beaulieu, J.J. Loferski, and B. Roessler, *Solar Energy Materials*, 1 (1979) 313

[4] J. Gonzalez-Hernandez, P.M. Gorley, P.P. Horley, O.M. Vartsabyuk, Yu.V.Vorobiev, *Thin Solid Films*, 403/404 (2002) 471

[5] S. Marsillac, M.C. Zouaghi, J.C. Bernede, T. Ben Nasrallah, S. Belgacem, *Sol. Energy Mater. Sol. Cells*, (article in press)

[6] M. Krunks, O. Kijatkina, H. rebane, I.Oja, V. Mikli, A. Mere, *Thin Solid Films*, 403-404, (2002) 71

[7] Mauricio Ortega-Lopez, Arturo Morales-Acevedo, *Thin Solid Films*, 330 (1998) 96

[8] P. Raja Ram, R. Thangaraj, A. K. Sharma, A. Raza and O.P Agnihotri, *Thin Solid Films*, 100 (1983) 111,

[9] H. Bihri, M.Abd-Lefdil, *Thin Solid Films*, 354 (1999) 5

[10] M.C.Zouaghi, T.Ben nasrallah, S. Marsillac, J.C. Bernede, and S. Belgacem, *Thin Solid Films*, 382 (2001) 39

[11] A.N. Tiwari, D. K. Pandya, and K. L. Chopra, *Thin Solid Films*, 130 (1985) 217

[12] Hirde J. P and Tembhurkar Y. D, *Indian J. Pure Appl. Phys.*, 28, (1990) 583

[13] H.Y. Ueng, H. L. Hwang, *J. Phys. Chem. Solids*, 50 (1989) 1297

[14] J. L. Shay, J. H. Wernick, Ternary chalcopyrite semiconductors: Growth, Electronic properties, and Applications, Pergamon Press, New York, 1975

[15] H.L.Hwang, C. L. Cheng, L.M. Linu, Y. C. Lin and C.Y. Sun, *Thin Solid Films*, 67 (1980) 83

Chapter 5

FABRICATION AND CHARACTERIZATION OF ALL-SPRAYED $CuInS_2$/CdS SOLAR CELLS

5.1 Introduction 193
5.2 Device Fabrication 193
5.2.1 Substrate cleaning 194
5.2.2.Deposition of SnO_2 layer 194
5.2.3 Deposition of $CuInS_2$ (absorber) layer 198
5.2.4 Deposition of CdS (window) layer 198
5.2.5 Annealing 201
5.2.6 Electrode deposition 201
5.2.7 Measurement of J-V characteristics 202
5.3 Results and Discussions 203
5.3.1 Cells using low resistance $CuInS_2$ films 209
5.3.2 Junctions with bilayer structure for $CuInS_2$ 210
5.3.3 Cells using low resistance CdS 212
5.3.4 Series resistance analysis of the cells 213
5.4 Conclusions 215
References 216

Chapter 5

FABRICATION AND CHARACTERIZATION OF ALL-SPRAYED $CuInS_2$/CdS SOLAR CELLS

5.1 Introduction

Although there has been considerable interest for developing $CuInS_2$ thin films using various techniques, no single technique has been chosen yet as the most favored one for the fabrication of solar cells using this film. It is felt that chemical spray pyrolysis (CSP) technique is much suitable for solar cell production, because of the following reasons: 1) Large- area deposition of thin films with low-cost is possible, 2) This technique is ideally suited for the deposition of films with controlled dopant profiles, 3) Possibility of varying stoichiometric composition as well as doping profile along thickness of sample and 4) Easy deposition of multi layer films with large area in a continuous process. These points made us to think about the usage of this technique for depositing thin films of important compound semiconductors and hence try the fabrication of an all-sprayed solar cell. This chapter describes the preliminary results of our attempt to fabricate an 'all-sprayed' $CuInS_2$ thin film solar cell.

5.2 Device Fabrication

Fabrication of a thin film solar cell involves several sequential steps. Fig 5.1 shows schematic diagram of the flow chart of process for the preparation of the present 'all-sprayed' $CuInS_2$/ CdS solar cell. Each of these steps will be briefly described in the following section.

5.2.1 Substrate cleaning

Before any substrate can be used, it must be adequately cleaned using proper cleaning techniques, which depend on nature of the substrate, nature of the contaminants and degree of cleanliness required. Ordinary soda lime glass slides cut to an area of (37.5mm × 12.5mm × 1.25mm) by scribing with a diamond point, were used as the substrate. These slides were washed thoroughly first using soap solution and then using chromic acid. Finally these were rinsed in distilled water. Microscopic impurities were removed through ultrasonic cleaning. Cleaned slides were then dried in hot air oven.

5.2.2.Deposition of SnO_2 layer

Several types of transparent conducting oxides (TCOs) are commercially produced to be used as a front/back contact of solar cells. The most commonly available TCOs are tin oxide (SnO_2), doped tin oxide such as SnO_2: F, indium tin oxide (ITO), and sometimes the combination of a tin oxide layer and indium tin oxide layer (ITO/SnO_2). Typically, these films should have low resistance, high optical transmission, and should be thermally stable during the subsequent processing steps of cell fabrication [1].

SnO_2 is a wide band gap material with an energy gap of 3.5 – 4 eV and refractive index 1.9 [2]. Techniques such as chemical vapor deposition (CVD)[3], reactive sputtering [4] and reactive evaporation [5] have been used for the deposition of thin films of this important material. Properties of transparent conducting oxide films prepared using various methods are presented in detail in the reference [6]. There are many papers on the preparation of SnO_2 thin films using spray pyrolysis and it is reported that films prepared using this technique have better electrical and optical properties [7-9].

Several important parameters linked with preparation of good quality SnO_2:F films using CSP had been already optimized in our lab, and these films were fully characterized [10,11].

In the present work, although we used spray pyrolysed SnO_2: F thin films as well as commercially available ITO films as the bottom electrode, performance of cells prepared using ITO films as electrode was rather poor and hence use of ITO was discarded for later preparations. Also it is reported that $CuInS_2$ thin films prepared on SnO_2:F coated glass substrates have good adherence, which is due to the surface roughness of the SnO_2:F films. The pyramidal shape of the SnO_2:F crystallites induces micro roughness at the surface of the substrates which behave as anchorage sites for the growing films. High density of the anchorage sites allows growth of continuous films with good adherence without cracks or pinholes [12].

For the preparation of the spray solution, 33gms of hydrated stannic chloride ($SnCl_4.5H_2O$) was dissolved in 33ml methanol and 33ml distilled water. 2gms of ammonium fluoride (~6% by weight) was added to this solution for doping. Temperature of the substrate was kept constant at 450^0C and the solution was sprayed at a rate of 10ml per minute. 30ml of the solution was used at a time for spraying. Films thus prepared had good adherence and had good transparency.

Fig.5.2 shows the transmission spectrum of the SnO_2:F films. Transmission of the films is around 70%. Structure of the film was analyzed using XRD. Samples showed good crystallinity with preferred orientation along (200) plane. XRD spectrum of the film is shown in Fig.5.3 and the corresponding d values are listed in Table-5.1.

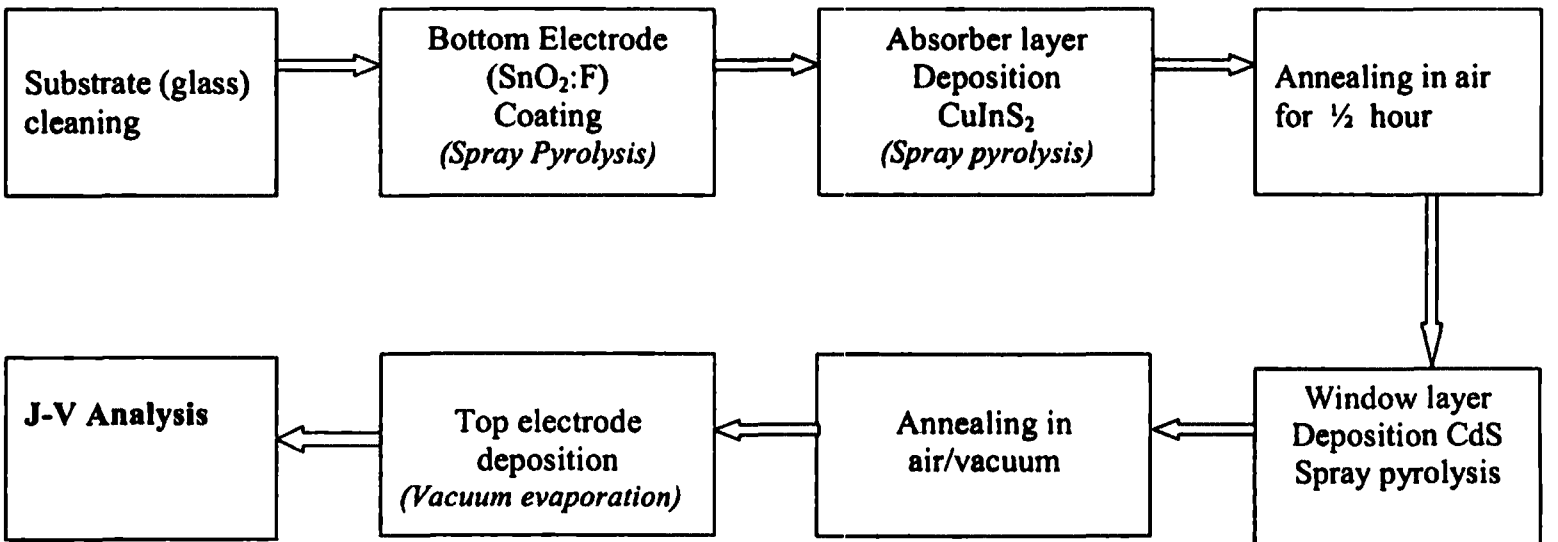

Fig. 5.1 Flow chart of the process of fabrication of $CuInS_2$/CdS solar cells

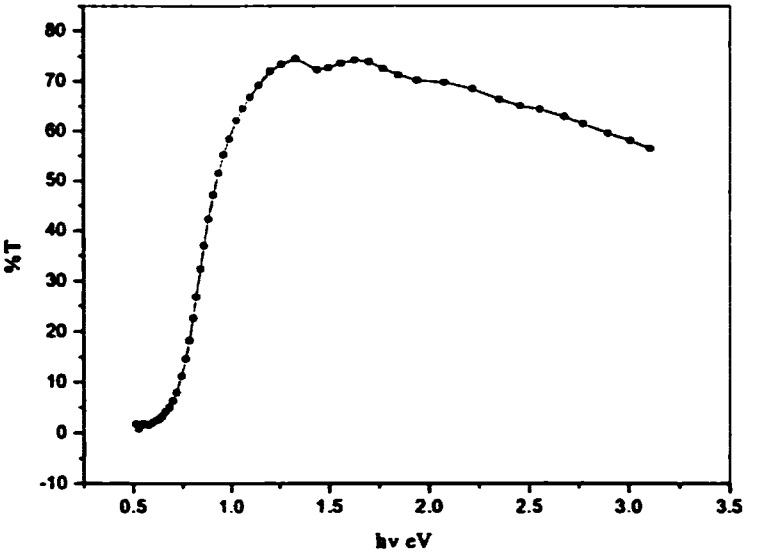

Fig.5.2 Transmission spectrum of SnO_2:F

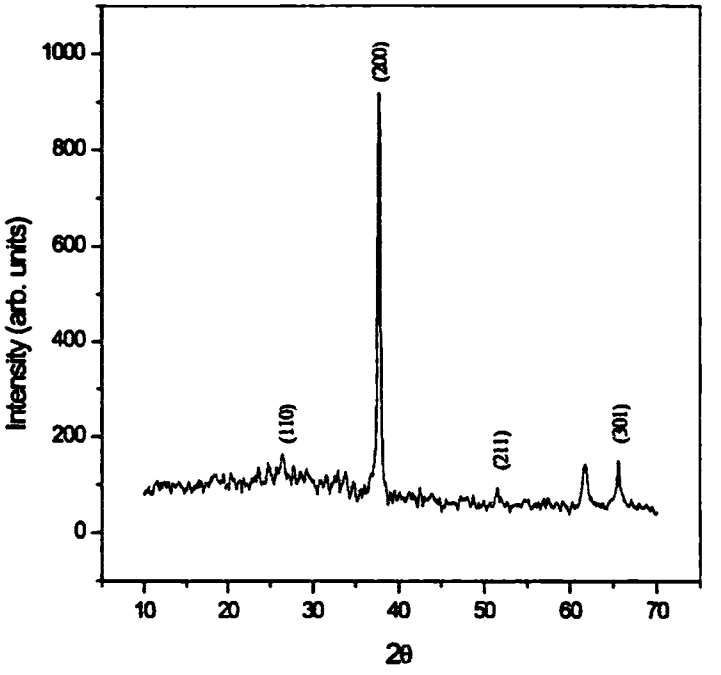

Fig.5.3 XRD spectrum of SnO_2:F film

Table-5.1
XRD analysis of SnO_2 film

Peak	2θ	d space Å		plane
		observed	standard	
1	26.55	3.354	3.351	(110)
2	37.94	2.369	2.369	(200)
3	51.59	1.770	1.765	(211)
4	61.85	1.498	1.498	(310)
5	65.6	1.421	1.415	(301)

5.2.3 Deposition of $CuInS_2$ (absorber) layer

In the former chapter, variation of photosensitivity of $CuInS_2$ films with composition in the spray solution has been described. Samples prepared from solution having Cu/In ratio 0.5 and S/Cu ratio 5 were having highest photosensitivity and these were selected for device fabrication. The composition of the spray solution was $CuCl_2.2½\ H_2O$- 0.0125 M (100ml), $InCl_3$ - 0.025M (100ml), and $CS(NH_2)_2$ - 0.0625M (100ml). pH of the solution was 2.5. This solution was sprayed onto SnO2:F films kept at a temperature of 300 ± 5^{0}C. Spray rate was 15ml/minute. After deposition, these films were kept at the same temperature for ½ hour. Films were then masked using glass plates to select better area for CdS deposition. CdS layer was deposited at the same temperature, in the same manner.

5.2.4 Deposition of CdS (window) layer

Characterization of CdS films prepared using CSP technique was already carried out in our lab, and CdS homojunction was fabricated using this CdS film [11]. Aqueous solutions of cadmium chloride ($CdCl_2$) and thiourea ($CS(NH_2)_2$) were used for the deposition of CdS films. Cd: S ratio in the solution was 1:1. This solution was sprayed

onto $CuInS_2$ film kept at a temperature of 300°C, at the rate of 15ml/minute. Chemical reaction can be represented as,

$$CdCl_2 + CS(NH_2)_2 + 2H_2O \rightarrow CdS + 2NH_4Cl + CO_2$$

After deposition of window layer, the samples were allowed to cool at a rate of 6^0C/minute. Details of characterization of CdS films are given in Ref. [10]. However in the present study, structural and optical properties of CdS films prepared on glass substrate were again done to confirm the quality. XRD pattern of CdS sample is is given in Fig.5.4. It is evident that the films are crystalline with preferred orientation along (002) plane and the peaks closely match with those corresponding to hexagonal structure. Observed d-values and standard JCPDS values are listed in Table-5.2.

Fig.5.5 and Fig.5.6 depict the absorption and transmission spectra of CdS sample. $(\alpha h\nu)^2$ vs. hν plot is shown in the inset of absorption spectrum and band gap value obtained from this plot is 2.4eV.

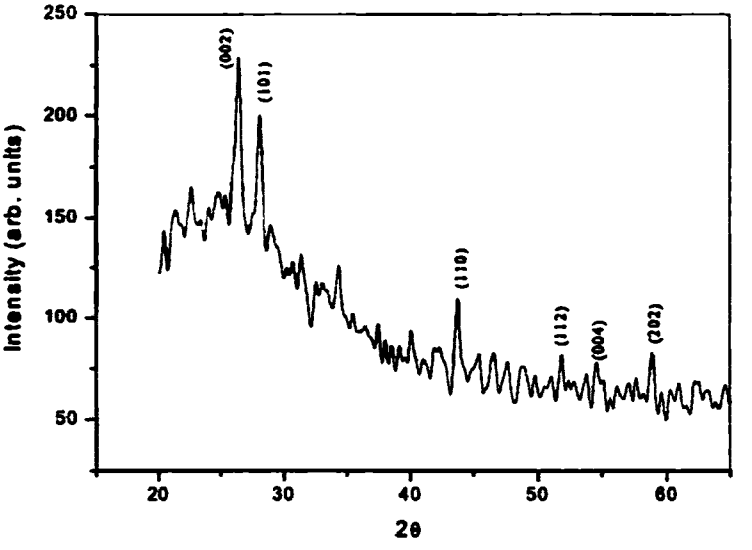

Fig.5.4 XRD spectrum of CdS

Table-5.2
X-ray analysis of CdS film

Peak	2θ	d space Å		plane
		observed	standard	
1	26.45	3.366	3.367	(002)
2	28.2	3.161	3.161	(101)
3	43.75	2.067	2.068	(110)
4	51.85	1.761	1.761	(112)
5	54.55	1.680	1.679	(004)
6	58.85	1.567	1.581	(202)

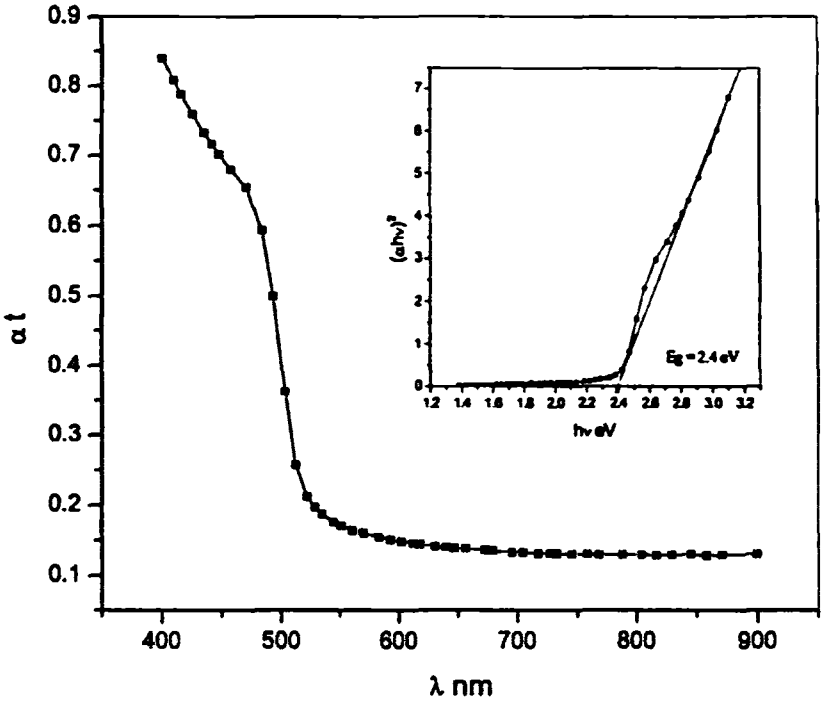

Fig.5.5 Absorption spectrum of CdS

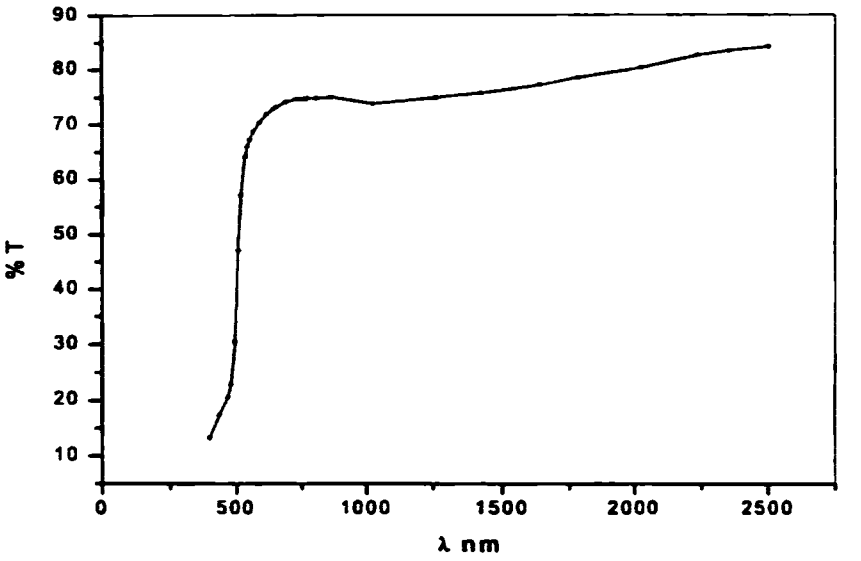

Fig.5.6 Transmission spectrum of CdS

5.2.5 Annealing

Annealing of the junctions is an inevitable step in the device fabrication. Here we annealed the junction in air as well as in vacuum. Result of vacuum annealing was not encouraging. For air annealing, a hot air oven with temperature control was used. Results of these annealing processes will be discussed in the following sections.

5.2.6 Electrode deposition

In the present case, we tried Silver (Ag) and Indium (In) as top electrodes. In was deposited using vacuum evaporation and silver paint was used for Ag electrode. Comb-structures as well as grid-structure were tried for In electrodes. However, in all these cases, it was found that after indium deposition, the bilayer structure got shorted. This was not the case with silver. Hence we selected Ag paint as the top electrode for the cells. Light was allowed to fall through substrate side and Ag paste was painted over

required area ($0.04cm^2$) on CdS layer. This area was separated from other portions of the cell by scribing using diamond cutter. In all these cases, contact between the film and the electrode was found to be ohmic. Structure of the cell fabricated is shown schematically in Fig 5.7.

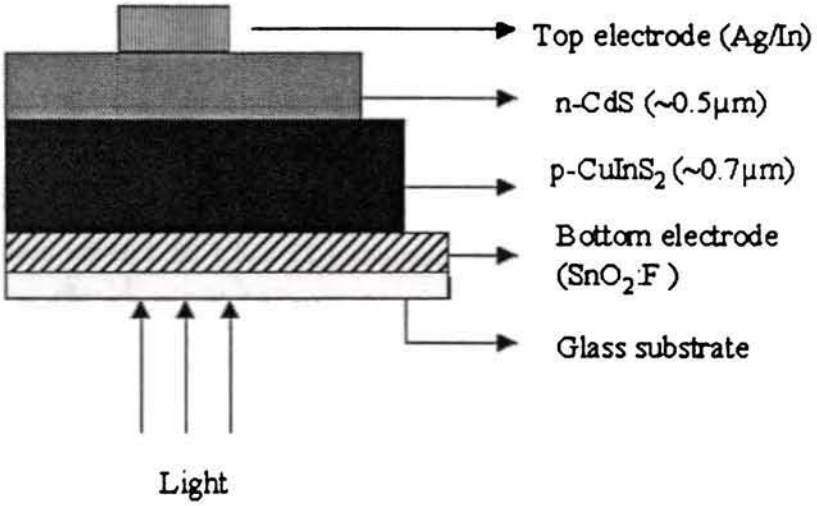

Fig.5.7 Schematic diagram of the structure of $CuInS_2$/CdS solar cell

5.2.7 Measurement of J-V characteristics

Dark and illuminated J-V characteristics of the cell were measured using Keitheley's Source Measure Unit (SMU, KI236) and Metric's interactive software (ICS version 3.4.1). Cell was illuminated using 250 W tungsten halogen lamp so as to have an intensity of $60mW/cm^2$ on the substrate surface. In the present case, since light is entering the cell through SnO_2 side, it suffers a loss in intensity, as transmission of SnO_2 is only around 70%. Hence actual intensity falling on the cell was still less, and was only $42mW/cm^2$. Input power was measured using a "suryamapi" (A-136 model of

CEL). An infrared filter along with water jacket was used to remove heat content in the incident light and to ensure that there is no increase in the temperature of the cell during measurement. Sample was masked in such a way that no light falls at portions other than the required area, especially on the electrode. Distance between cell and source was ~ 10 cm. Dark characteristics of the cell were measured after keeping the sample in darkness for at least 24 hours.

Series resistance (R_s) and shunt resistance (R_{sh}) can be calculated from the dark J-V characteristics of the cell. Inverse of the Slope of far forward characteristics (in the first quadrant), where J-V curve becomes linear gives R_s. And R_{sh} can be found from the inverse of the slope of the J-V curve in the third quadrant [13].

Solar cell parameters V_{oc} and J_{sc} were determined from illuminated J-V curve and FF and η were calculated using equations 1.27 and 1.28. For the best cell, diode quality factor was calculated from the slope of voltage vs. ln J graph [14].

5.3 Results and Discussions

Variation of solar cell parameters with thickness (in terms of volume of solution used for spraying) of $CuInS_2$ layer is shown in Table-5.3. Here thickness of the CdS layer was approximately 0.5μm (vol. of the spray solution = 250ml). Open circuit voltage is maximum (415mV) when the volume of the spray solution is 525 ml. However, the short circuit current density is only 1.1 mA/cm^2, and the efficiency is only 0.18%. When thickness of the $CuInS_2$ layer increases, films have a tendency to peel off from the substrate and also, pin holes are developed in the film. This is the reason for the observed low value of the short circuit current density when 525 ml solution was used for spraying. When 450ml solution was used for spraying, short circuit current density and efficiency are maximum, although there is a slight decrease in the open circuit voltage of the cell (J_{sc} = 10.8mA/cm^2, Voc = 331 mV and η = 1.3%). Hence for

later preparations, volume of the spray solution was fixed at 450ml, which corresponds to an absorber layer thickness of ~ 0.7μm.

Table-5.4 represents variation of cell parameters with thickness of the CdS (window) layer. Here, maximum efficiency is obtained when the thickness of the CdS layer is 0.5 μm.

Variation in diode quality factor (A) and series resistance (R_s) with thickness of absorber layer is illustrated in Fig.5.8. From the figure, it follows that Rs and A are low for the cell prepared using 450ml $CuInS_2$ solution.

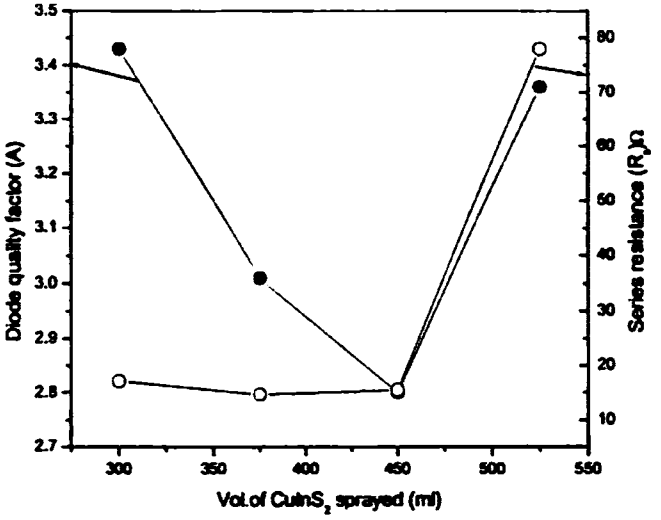

Fig.5.8 Variation in 'A' and 'R_s' with thickness of absorber layer

For the illuminated J-V curve of the best cell fabricated (Fig.5.10), open circuit voltage and short circuit current density are good, but over all performance is limited by the low value of the fill factor (FF= 0.21). This reduction in the fill factor may be due to large series resistance of the cell [15].

R_s calculated from dark forward characteristics of the cell, shown in Fig.5.9, was 15.49Ω. Shunt resistance of the cell was found to be 11.4 Ω. Diode quality factor (A) calculated from the dark forward characteristics of the cell, by plotting ln J vs. V graph (inset of Fig.5.9) was 2.8, which indicates that the generation – recombination process dominates. Such higher values have been reported earlier. For the n,p-$CuInS_2$ homojunction device, diode quality factor of 2.3 was reported by Kzmerski et al., and the values reported were 2.34 and 2.5 respectively for a InP/CdS device and a Si solar cell respectively [15,16]. For poor devices, values of diode quality factor reached 3 or even 4 [14]. Absorption spectrum of SnO_2/CuInS2/CdS structure is represented in Fig.5.10.

Table-5.3

Variation of cell parameters with thickness of $CuInS_2$ layer

Thickness of CdS layer– 0.5μm

Volume of Solution sprayed ml	Open circuit Voltage(Voc) Volts	Short circuit current Density (Jsc)mA/cm^2	Fill factor ff	Efficiency η%
300	0.220	4.7	0.22	0.38
375	0.200	1.3	0.23	0.1
450	0.331	10.8	0.21	1.3
525	0.415	1.1	0.24	0.18

Table-5.4

Variation of cell parameters with thickness of CdS layer

Thickness of $CuInS_2$ layer ~ 0.7μm (450ml)

Volume of Solution sprayed ml	Open circuit Voltage(Voc) Volts	Short circuit current Density (Jsc) mA/cm^2	Fill factor ff	Efficiency η%
100	0.053	4.1	0.24	0.09
150	0.167	3.6	0.21	0.21
200	0.113	0.92	0.21	0.04
250	0.331	10.8	0.21	1.30
350	0.133	4.6	0.23	0.23
450	0.133	3.3	0.21	0.10

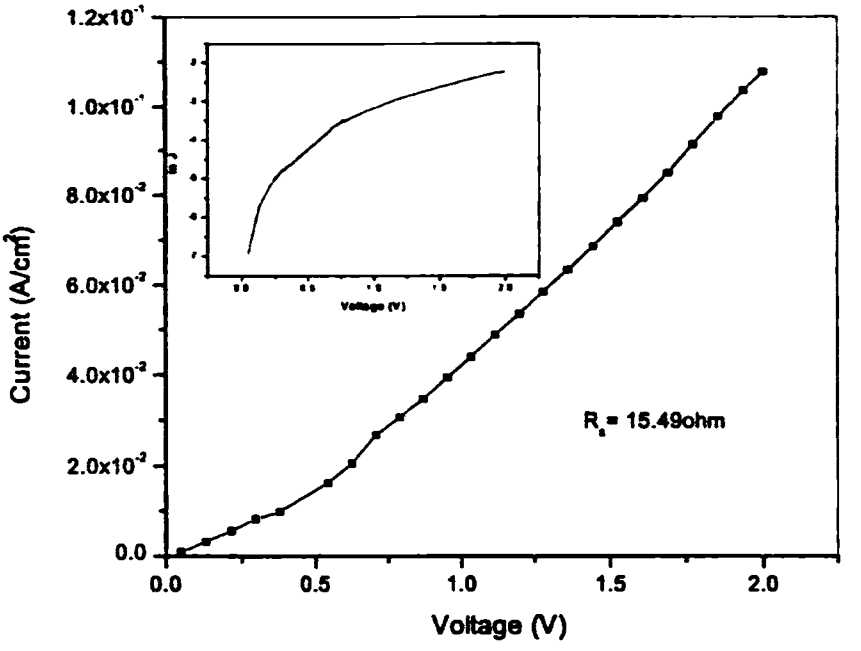

Fig.5.9 Dark forward characteristics of the cell

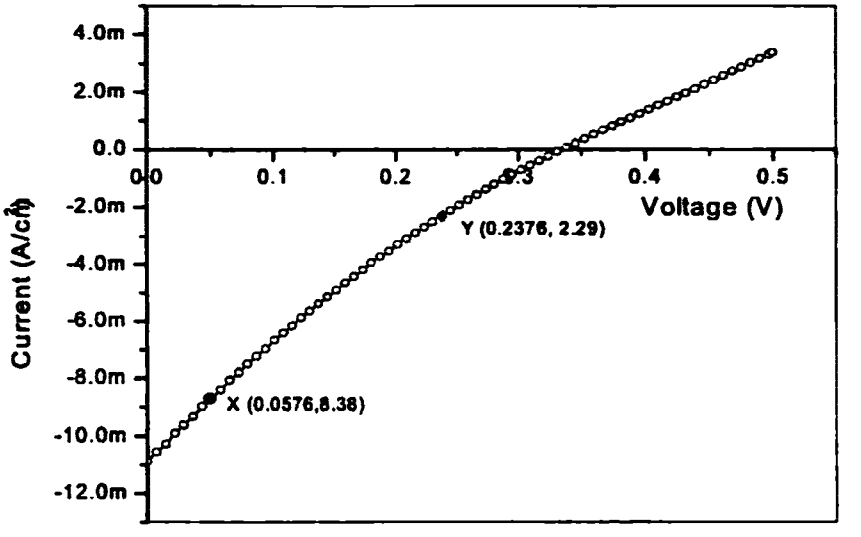

Fig.5.10.Illuminated J-V characteristics of the cell

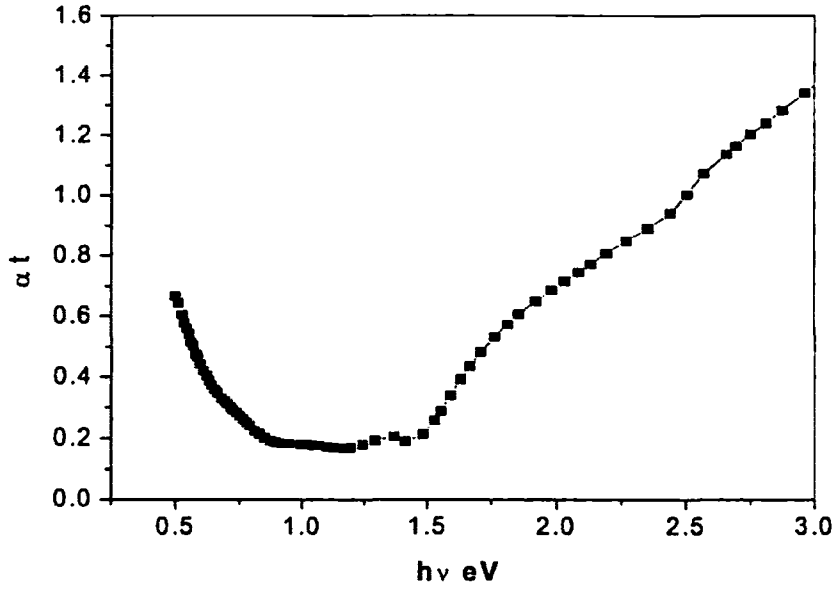

Fig.5.11 Absorption spectrum of SnO_2/$CuInS_2$/CdS cell structure

These devices, when annealed in vacuum (in a pressure of 10^{-5} torr, 100-200^{0}C, 1-2½ hours) showed no significant increase in performance as reported for several heterostructures [17,18]. For devices annealed in air, there was a drastic degradation in the cell performance.

In order to reduce series resistance of the cell, attempts were made to fabricate devices with low resistivity $CuInS_2$ thin films. When we use low resistance films, a compromise has to be made with photosensitivity. In the former case, we used $CuInS_2$ thin films deposited from a solution in which the Cu/In ratio was maintained at 0.5 and S/Cu ratio at 5. These films had a resistivity of 254 Ω-cm (sheet resistance of ~3009MΩ/□) and photosensitivity s = 87%. When the Cu/In ratio is increased to 0.8, the resistivity became 8.46 Ω-cm (sheet resistance is 50 MΩ/□), but the photo sensitivity (S

= 53%) is less. Films having still lower resistivity can be prepared using solution containing Cu/In = 1.1. In this case, even though the resistivity is only 0.184 Ω-cm (resistance is 1.39 MΩ/□), photosensitivity is only 15%.

5.3.1 Cells using low resistance $CuInS_2$ films

SnO_2:F/ $CuInS_2$/ CdS solar cell was fabricated using $CuInS_2$ films prepared from a spray solution containing Cu/In ratio 0.8, keeping all other conditions same as in the previous case. Fig.5.11 represents the J-V characteristics of the cell in the dark, under illumination and after annealing in air at 100°C for 1 hour. For the as prepared device, open circuit voltage (V_{oc} = 400mV) is slightly higher than that in the previous case (V_{oc} = 331mV), but short circuit current density (J_{sc}=0.93mA/cm^2) is very much less than that in the former case (J_{sc}=10.8mA/cm^2) and calculated efficiency is only 0.09%. When these devices were annealed in air for 30 minutes to 2 hours, it was found that there is considerable increase in the short circuit current density even though the voltage decreased. The best result was obtained for samples annealed at 100°C for 1 hour. In this case, V_{oc} = 0.297 V, J_{sc} = 9 mA/cm^2 with an overall efficiency of 1%. The cell parameters are tabulated in Table-5.5

Table-5.5

Out put parameters of the cell

	Voc mV	Jsc mA/cm^2	η
As-prepared	400	0.93	0.09
After air annealing	279	9.0	1.0

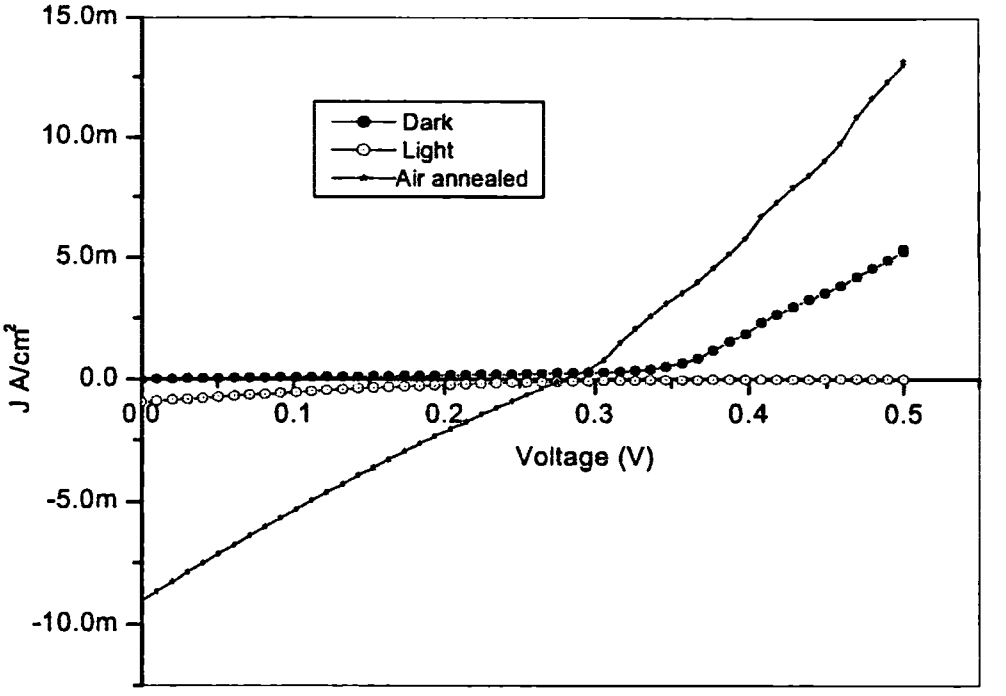

Fig.5.12 J-V characteristics of the cell

Devices prepared using still lower resistance $CuInS_2$ films (Cu/In = 1.1 in the spray solution) showed no photo activity. After air annealing also, there was no improvement in the device performance.

5.3.2 Junctions with bilayer structure for $CuInS_2$

$CdS/CuInS_2$ heterojunctions were prepared using a bilayer structure for the $CuInS_2$. Preparation procedure of the junction is as follows. SnO_2: F films were first deposited on glass substrates using CSP technique. Over this, $CuInS_2$ layer was deposited in two stages. First, a layer of low resistance $CuInS_2$ was deposited by maintaining the Cu/In ratio in the spray solution as 0.8. Next, the ratio was changed to 0.5 to get a layer of high resistance and this was deposited over the low resistance layer.

The thickness of these two layers were varied by changing their respective volumes as 300ml & 150ml and vice versa. However, the total volume used for spraying was kept constant at 450ml. Finally, CdS layer was deposited over this layer using chemical spray pyrolysis. Of these two types of devices, better result was obtained for the device in which thickness of the low resistance film was higher. Parameters of the cell are as follows:

V_{oc} = 0.5V; J_{sc} = 8.9mA/cm2; FF = 0.13; η = 1.0%. Even though there is an increase in the Voc, the fill factor is small and again efficiency is only 1%. In this case also, series resistance is high and shunt resistance is low as indicated by the low fill factor. Low shunt resistance could be due to recombination along the grains and the defects, which are in large numbers in sprayed films [19].

Table-5.6

	Voc mV	Jsc(mA/cm^2)	FF	η
(Cu/In=0.8,300ml + Cu/In=0.5,150ml + 250ml CdS)	500	8.9	0.13	1.0%
(Cu/In=0.8,150ml + Cu/In=0.5,300ml + 250ml CdS)	248	1.6	0.22	0.09%

5.3.3 Cells using low resistance CdS

Attempts were then made to reduce resistance of CdS layer. For this, Cd/S ratio in the spray solution was kept at 2. The resistivity of the films obtained is nearly 140 Ω-cm. This low resistance CdS film was deposited over the bilayer $CuInS_2$ layer. There was a large increase in the short circuit current density. In this case, the efficiency is 1.7%. When correction is applied for the transmission losses at the SnO_2 film, the device efficiency becomes 2.4%

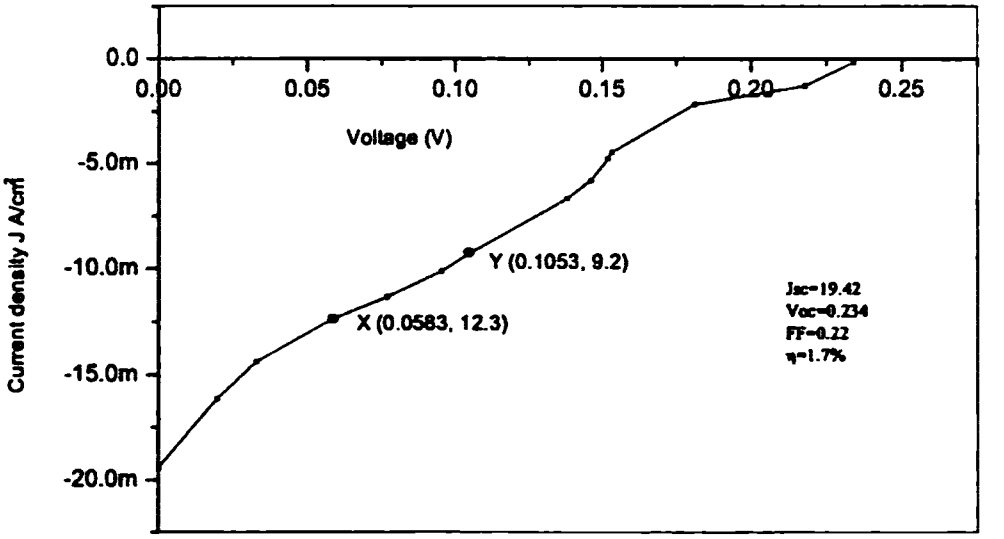

Fig.5.13 J-V Characteristics of the best cell prepared

Experimental measurements of the electrical properties of single crystals indicated that p-$CuInS_2$ samples are heavily self-compensated. This would seriously reduce minority carrier life times and limit the junction and photovoltaic characteristics [15].

5.3.4 Series resistance analysis of the cells

Recently, there was a report on a new method to determine the solar cell series resistance (R_s) from a single I-V characteristic curve by Adawi et al. [20]. They have obtained a simple relation for R_s which makes it possible to utilize a single I-V curve to evaluate R_s. The equation is,

$$R_s = \frac{1}{\lambda}\frac{1}{(I_2 - I_1)}\ln\left[\frac{I_{ph} - I_2}{I_{ph} - I_1}\right] - \left(\frac{V_2 - V_1}{I_2 - I_1}\right) \quad \text{.....(5.1)}$$

where, $\lambda = \frac{q}{AkT}$; A is diode quality factor, $\frac{kT}{q}$ is thermal voltage,

I_{ph} is the light generated current density, V_1, I_1, V_2 & I_2 are the voltage and current density values at any two points on the I-V characteristics curve.

Using the above equation, R_s was calculated for the cell with 1.3% efficiency and also for the cell fabricated using low resistance CdS films. From Fig.5.8, the diode quality factor for the first cell is 2.8. Two points X and Y are chosen on the illuminated I-V curve as shown in fig.5.9. Here, V_1 = 57.6mV, I_1 = 8.38 mA,

V_2 = 237.6mV, I_2 = 2.29 mA,

I_{ph} = 10.8mA, A = 2.8, T = 300K, kT/q = 0.025

Substituting all these values in equation 5.1, we get the value R_s as 15.10Ω. This is in close agreement with the R_s value of 15.49 Ω obtained from the slope of dark forward characteristics of the cell.

Rs was calculated also for the cell fabricated using the low resistive CdS films. In this case, diode quality factor determined from the lnJ vs Voltage graph is 1.51. (Fig.5.13) Here also, T= 300K, kT/q = 0.025 and

V_1 = 58.3mV, I_1 = 12.3 mA,

V_2 = 105.3mV, I_2 = 9.2 mA, I_{ph} = 19.42 mA

Series resistance value obtained is 10.76Ω.

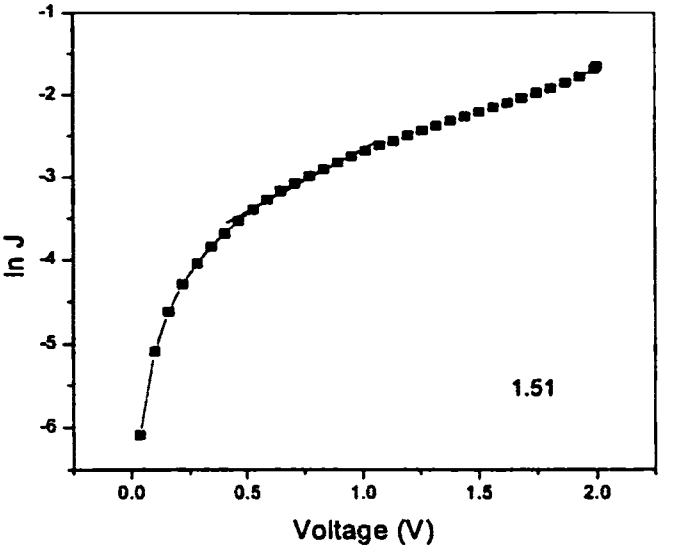

Fig.5.14 ln J versus V graph for the cell with 1.7% efficiency

Here we can see that there is an improvement in the diode quality factor and a reduction in the series resistance when the low resistive CdS is used as the window layer. However, the series resistance of the cell is still very high. It has been demonstrated that a series resistance of 1 Ω for a $1cm^2$ device drops the efficiency by 15 for Si and 0.6% for GaAs. As the photocurrent increases, the effect of series resistance also increases, and the efficiency drops very rapidly for resistances of several ohms or more [14].

Small value of FF obtained for the cells is another factor, and this is the major cause for low efficiency. For good FFs, forward dark currents, diode quality factor and the series resistance have to be low. Value of Rs should be less than 1 Ω for a $1cm^2$ area. Hence efforts are to be made to further reduce the series resistance of the cell.

5.4 Conclusions

An 'all- sprayed' $CuInS_2$/CdS solar cell has been fabricated with an efficiency of 1.3% (1.9% after transmission loss correction). The efficiency increased to 1.7% (2.4% after correction) by using a bilayer structure for the absorber layer and low resistivity CdS films. There is also an improvement in the diode quality factor. Fill factor of the cell fabricated was found to be low. Series resistance of the cell was estimated to be 10.76Ω. This high series resistance is one of the reasons for the reduction in FF.

References

[1] Saleh N. Alamri, *Jpn. J. Appl. Phys.*, 41(10A), (2002) 1052

[2] K. L. Chopra, S. Major and D. K. Pandya, *Thin Solid Films*, 102, (1983) 1

[3] A. K. Saxena, R. Thankaraj, S. P. Singh, and O.P. Agnihotri, *Thin Solid Films*, 131 (1985) 121

[4] G. Beensh Marchwicka, L. K. Stephiewska, and A. Misiuk, *Thin Solid Films*, 113 (1984) 215

[5] H. Demiryont and N. Tezey, *Thin Solid Films*, 101 (1983) 345

[6] K. L. Chopra and S. R. Das, Thin Film Solar Cells, Plenum press, New York, (1983), p-326]

[7] A. K. Abass and M. T. Mohammed, *J. Appl. Phys.*, 59 (1986) 1641

[8] J. C. Manifacier, *Thin Solid Films*, 90 (1982) 297

[9] W. Siefart, *Thin Solid Films*, 121 (1984) 275

[10] P. K .Vidyadharan Pillai, Ph.D Thesis, (1997), Cochin University of Science and Technology, Kochi.

[11] K. P. Varkey, Ph.D Thesis, (1999), Cochin University of Science and Technology, Kochi.

[12] M. C. Zouaghi, T. Ben Nasrallah, S. Marsillac, J. C. Bernede, and S. Belgacem, *Thin Solid Films*, 382 (2001) 39

[13] K.L Chopra and S.R Das, Thin Film Solar Cells, Plenum press, New York, (1983); p-159

[14] Harold J. Hovel, Semiconductors and semimetals; Vol-II, Solar cells, Academic press, New York, 1975

[15] L. L. Kazmerski and G. A. Sanborn, *J. Appl. Phys.*, 48 (1977) 3178

[16] Wolf M, Rauschenbach H, Adv. Energy Conversion, 3 (1963) 455

[17] L.L.Kazmerski, F.R.White, and G.K.Morgan , *Appl. Phys. Lett.*, 29 (1976) 268

[18] L.L. Kazmerski, F.R.White, M.S.Ayyagari, Y.J. Juang, and R.P.Patterson, *J. Vac. Sci. Technol*, 14 (1977) 65

[19] Poola Raja Ram, R. Thangaraj, A K Sharma and O P Agnihotri, *Solar Cells*, 14 (1985) 123

[20] M.K. El-Adawi, I.A.Al-Nuaim, *Vacuum*, 64 (2002) 33

Chapter-6

SUMMARY AND CONCLUSIONS

This chapter presents brief summary of the work done for the preparation and characterization of $CuInS_2$ thin films using chemical methods and fabrication of $CuInS_2$/CdS solar cells. Some of the environmental and safety aspects of the material and its preparation technique are also included.

Main objective of present work was to prepare $CuInS_2$ thin films using low cost techniques and fabricate $CuInS_2$/CdS solar cell using this film. Two new methods were developed for preparing $CuInS_2$ films: starting from i) CBD Cu_xS and ii)CBD CdS. In addition to these, another well-known chemical method (viz., chemical spray pyrolysis) was also used for preparing device quality $CuInS_2$ thin films.

In the first method, $CuInS_2$ was prepared through thermal diffusion of In into Cu_xS films. Here Cu_xS films were prepared using simple and low cost chemical bath deposition technique at room temperature. Best result was obtained by evaporating indium layer of thickness 400Å over Cu_xS and subsequent annealing of the bilayer film in vacuum (~10^{-5} torr) at 300°C for 2 hours. XRD analysis of sample showed crystalline nature with preferred orientation along (112) plane and grain size calculated using Scherer's formula was 32nm. From the plot of $(\alpha th\nu)^2$ versus hν, optical bandgap of 1.41eV was obtained. Electrical resistivity, mobility and carrier density were investigated using Hall measurement and the values obtained were 2.56×10^{-3} Ω-cm, 5.1cm^2/Vs and $4.77\times10^{20}cm^{-3}$ respectively. XPS depth profile of the sample showed presence of Cu, In and S almost uniformly through out the thickness. Cu/In ratio in the film was 1.29. However, sample showed deficiency of sulfur.

In order to increase S content in the films, samples were annealed in sulfur vapor in an open tube at 200°C for 0.5 to 2 hours. An increase in grain size and band gap was

observed with annealing time. Photosensitivity was high for samples annealed in sulfur atmosphere for 30 to 60 minutes, compared to the as-prepared ones. When samples were annealed for 1 hour, there was an improvement in sulfur content in the film. (increased from 21% to 33%). However, no further increase in S content was observed on increasing the annealing time.

In the second method used for the preparation of $CuInS_2$, Cu_xS films were first prepared from CBD CdS films using Clevite process. Then indium was evaporated over this film and the bilayer was annealed at 300°C for 2 hours.

We tried to fabricate $CuInS_2$/ CdS solar cells using $CuInS_2$ films prepared using these two methods and could fabricate solar cell by converting top layer of a sufficiently thick CdS into Cu_xS. Although open circuit voltage was quite measurable, current was very feeble. Hence we tried to fabricate an 'all-sprayed' $CuInS_2$/CdS cell, in which the back electrode (SnO_2), absorber layer ($CuInS_2$) and window layer (CdS) were deposited using CSP. For this, we had to characterize $CuInS_2$ films prepared using CSP.

Films were prepared by varying deposition temperature, copper to indium ratio and sulfur to copper ratio in a wide range. All these films were characterized and photosensitivity of samples was measured. Since photosensitivity was good for films prepared at 300°C, deposition temperature was fixed at that value. XPS analysis revealed that when Cu/In ratio in the spray solution was 0.5, that in film was ~1. Best photosensitivity was obtained for the sample prepared from a solution containing Cu/In ratio 0.5 and S/Cu ratio 5. Hence this film was selected for fabricating an 'all-sprayed' solar cell with CSP CdS. These films had a resistivity of 254 Ω-cm (sheet resistance of ~3009 MΩ/□) and photosensitivity s = 87%

Comparison of $CuInS_2$ films prepared using the above three techniques are given in Table-6.1.

Preparation Technique	Properties/ Results	Remarks
1.Starting from CBD CuxS Evaporation of In over CBD CuxS and subsequent annealing of bilayer in vacuum at 300°C for 2 hours. Sulfur annealing	Best film was obtained by evaporating 400Å over CuxS and subsequent annealing. XRD- Good crystallinity, grain size ~32 nm Band gap = 1.41 eV P = $2.56\times10^{-3}\Omega$-cm, μ = 5.1cm^2/V-s, n= 4.77×10^{20} cm XPS- presence of Cu, In & S through out the depth, cu/in ratio in film = 1.29 Photosensitivity was low ~5% An increase in grain size and band gap with annealing time. Photosensitivity was high for samples annealed for 30-60 minutes (31-33%).	Sample prepared using this technique showed deficiency of sulfur. Hence these samples were annealed in sulfur vapor in an open tube at 200°C to 0.5 to 2 hours. Sulfur content could not be increased above 33% even after increasing annealing time.
2. Preparation starting from CBD CDS: Preparation of CuxS from CBD CdS using Clevite process and conversion of CuxS into CuInS2 by thermal diffusion of indium.	Good samples were obtained by diffusing 600Å In . XRD peaks showed good crystallinity XPS showed presence of Cu,In & S , B.E matched well with that of $CuInS_2$	$CuInS_2$/ CdS junction was fabricated by converting top layer of a thick CdS film into CuInS2. Open circuit voltage was quite measurable, but current was very feeble. In this method, there is greater chance of shorting between the layers during

Preparation Technique	Properties/ Results	Remarks
3. Preparation using CSP CuInS2 thin films were prepared by varying the deposition temperature, Cu/in ratio and S/Cu ratio in a wide range. *I)Variation of Cu/In at 400 °C, keeping S/Cu = 4* Cu/In ratio in the spray solution was varied as 0.9,1.0, &1.1 (sample A,B & C respectively), by keeping molarity of CuCl2.2H2O at 0.125 and S/cu ratio 4. *II) Variation of deposition temperature [Cu/In = 1.0, S/Cu = 4]* Deposition temperature was varied from 200°C to 400°C *III) Variation of S/Cu ratio, keeping Cu/In = 1* S/Cu ratio was varied from 2 to 6 *IV) Variation of Cu/in at 3000C, keeping S/Cu = 4* Cu/In ratio in spray solution was varied from 0.5 to 1.5	XRD showed good crystallinity with preferred orientation along (112) plane. Grain size was high for B (30nm) Resistivity was low for sample B(1.21Ω-cm) XPS analysis showed Cu/in ratio in the film as 1.83 Photosensitivity was 14.2% for sample B XRD showed good crystallinity at temperatures between 300°C & 400°C Grain size increased with deposition temperature and electrical resistivity decreased with deposition temperature. Photosensitivity was best for the sample prepared at 300°C As S/cu increased, deterioration in crystallinity was observed. As S/Cu increased from 2 to 6, sheet resistance increased from 13.6k to 80k Photosensitivity was poor for all these films XRD pattern improved with increase in Cu/in ratio. Also grain size increased with Cu/In ratio Sheet resistance decreased from 3009M Ω to 345Ω With increase in Cu/In Photosensitivity decreased from 70% to 2 % XPS analysis showed Cu/In ratio in the film as 1.03 when Cu/In ratio in the solution is 0.5	- Crystallinity was better for films prepared at 350°C, but photosensitivity was maximum for the film prepared at 300°C. Hence for later preparations, temperature was fixed at 300°C Cu/In ratio in solution was fixed at 0.5 for later preparations

Preparation Technique	Properties/ Results	Remarks
V. *Variation in S/Cu ratio , keeping Cu/In = 0.5* S/Cu ratio was varied from 4 to 8	Crystallinity was not good for these samples Energy band gap was greater than 1.5 in all cases Sheet resistance increased from 3.49MΩ to 35000 MΩ with increase in S/cu ratio from 4 to 8 Photosensitivity was high for the sample with S/cu ratio 5 (87%)	Sample prepared from solution containing Cu/in ratio 0.5 and S/cu ratio 5 showed best photoresponse and this film was selected for fabricating Solar cell .

Glass/SnO_2:F/$CuInS_2$/CdS structure was fabricated and thickness of the absorber layer and window layer were optimized.1.3% (~ 1.9% when corrected for transmission losses at SnO_2) efficiency was obtained for a cell with an absorber layer thickness of ~ 0.7μm (vol. of spray solution = 450ml) and window layer thickness ~0.5 μm (vol. of spray solution 250ml). Cell parameters of the cell are given below: Jsc = 10.8mA/cm^2, Voc = 331 mV and η = 1.3%. Diode quality factor and series resistance of the cell were calculated from the forward J-V characteristics and the values were 2.8 and 15.49 Ω respectively.

On increasing Cu/In ratio in spray solution to 0.8, resistivity of the film reduced to 8.46 Ω-cm and there was a reduction in sensitivity (s = 53%) also. When this low resistive $CuInS_2$ was used to fabricate devices, open circuit voltage (V_{oc} = 400 mV) was slightly higher than that in the previous case (V_{oc} = 331 mV), but short circuit current density (J_{sc}=0.93 mA/cm^2) was very much less than that in the former case (J_{sc}=10.8 mA/cm^2) and calculated efficiency was only 0.09%. On annealing the device at 100^{0}C for 1 hour, there was considerable increase in the short circuit current density even though the voltage decreased. The cell parameters were, V_{oc} = 0.297 V, J_{sc} = 9 mA/cm^2 with an overall efficiency of 1%. No photoactivity was observed when cells were fabricated using still lower resistivity $CuInS_2$ films (Cu/In = 1.1 in solution, resistivity 0.184 Ω-cm & photosensitivity 15%).

Attempts were made to reduce the resistance of CdS layer by keeping Cd/S ratio in the spray solution at 2. Resistivity of the films obtained was nearly 140 Ω-cm. There was a large increase in short circuit current density when this low resistive layer was used as window layer. Cell parameters were J_{sc}=19.42 mA/cm^2,V_{oc}= 0.234 V, & FF=0.22. In that case, efficiency was 1.7% and when correction was applied for transmission losses at the SnO_2 film, efficiency was 2.4%. Diode quality factor and

series resistance were 1.51 and 10.76 Ω respectively. Thus a decrease in series resistance was observed when low resistive CdS film was used as the window layer.

Occupational health and safety

There is only limited information on the toxicity of $CuInS_2$. However, since its constituents are non-toxic, from the environmental point of view this is much better than the other ternary chalcopyrites like $CuInSe_2$.

Environmental and health hazards presented by CdS are severe, as cadmium, one of the constituents of CdS is a highly toxic material. Cd compounds have higher absorption efficiency through lung than through gastrointestinal tract. However, absorption through skin is not observed [1]. Primary chronic adverse health effects from inhalation of Cd are lung cancer and kidney damage. However, occupational health hazards presented by this compound generally depend on its preparation method and its physical state.

In the present work, CdS films were prepared using two techniques: chemical bath deposition and chemical spray pyrolysis. In CBD, there is no emission of toxic gases since it is a low temperature wet chemical process. Unreacted chemicals and by-products can be easily disposed since they remain in the bath itself. These chemicals can be removed by chemical treatment before allowing to flow to the environment. In the case of CSP, a large quantity of by-products, including Cd containing wastes may be produced. Since most of these will be in gaseous form, they can be removed by powerful exhaust stream. Even though in CSP very low concentration of chemicals is needed, special precautions must be taken to prevent health hazards from fumes that could be accidentally released from spray pyrolysis unit.

In our lab, entire CSP unit is placed inside a fume hood provided with an exhaust and gaseous by-products are thrown out of the room through long pipes by the powerful airflow. Hence chance for contamination inside the room is minimum. Also

proper masks and gloves were used while spraying. While preparing Cu_xS and CdS films using CBD, even though no gaseous by-products were produced, deposition was always carried out inside the fume hood. Also, particular sets of beakers were used for preparing each compound.

Reference

1. V.M. Fthenakis and P.D. Moskowitz, Progress in photovoltaics; Research and applications, 3, (1995); p-295]
